

POLITECNICO DI TORINO

**Corso di Laurea Magistrale
in Ingegneria Biomedica**

Tesi di Laurea Magistrale

**Centrifugal microfluidic platform for optical monitoring of
bacterial biofilms**



Relatore

Prof. Danilo Demarchi

Candidato

Giaele Severini

Luglio 2018



This project was developed at Micro and Nanotechnology department of Technical University of Denmark, under the supervision of the Senior Researcher Kinga Zor and PhD Student Laura Seriola.

Contents

Abstract	13
Chapter 1	15
Introduction	15
1.1 Motivation and aim.....	15
1.2 From Petri dishes to centrifugal microfluidic devices	17
Chapter 2	24
Materials and methods	24
2.1 Materials for polymer-based microfluidic chips.....	24
2.2 Methods	26
2.2.1 CO_2 laser ablation	26
2.2.2 Micro-milling.....	27
2.2.3 Bonding of the fluidic system.....	29
2.2.4 Injection molding.....	33
2.3 Optical Spin Stand and image analysis.....	33
2.4 Sterilization methods.....	36
2.4.1 A brief description	36
2.4.2 Sterilization method for the centrifugal microfluidic platform	39
Chapter 3	40
Designs, fabrication and tests	40
3.1 First prototype	40

3.1.1 Description of the design	40
3.1.2 Fabrication	42
3.1.3 Flow rate evaluation	46
3.2 Second prototype design of the cell culture on disc device	49
3.2.1 Description of the second design	49
3.2.2 Fabrication	50
3.2.3 Evaluation of flow rate	51
3.3 Problem with first and second prototype design.....	55
3.4 Solution: design on the third prototype	59
3.4.1 Description of design	59
3.4.2 Fabrication technique.....	61
3.4.3 Fluidic tests.....	63
Chapter 4.....	66
Lab-on-a-disc for long-term cell culture	66
4.1 Design and fabrication.....	66
4.1.1 Fabrication with milling machine, CO ₂ laser ablation and thermal bonding	66
4.2 Fluidic tests.....	68
4.3 Theoretical calculations of the flow rates and estimation of shear stress inside the cell culture chamber	74
4.4 Lab-on-a-disc for long term cell culture, additional optimization.....	78
4.6 Lab-on-a-disc for long term cell culture: implantation of <i>Pseudomonas aeruginosa</i> bacterial cells. ...	80
4.6.1 <i>Pseudomonas aeruginosa</i> bacterial cells	80

4.6.2 <i>Pseudomonas aeruginosa</i> culture in the developed lab-on-a-disc device.....	81
Conclusion	83
Appendix	84
References	87

List of figures

1.1 Image of Staphylococcus aerus biofilm with confocal microscope [1].....	15
1.2 Scheme of biofilm formation [2]	16
1.3 Equipment for cell cultures in microfluidic device.....	19
1.4 Centrifugal microfluidic device for separation of plasma from whole blood [3].....	20
1.5 Structure implemented in the LOD to separate plasma from whole blood [4].....	21
1.6 LOD for extraction of nucleic acid of Food-Borne Pathogens [42].....	22
1.7 Centrifugal microfluidic device for enzyme linked immunosorbent assays [45].....	22
1.8 Centrifugal microfluidic device for Pichia Pastoris cultures [31].....	23
2.1 Luers connectors in Topas that are used to hold filters.....	26
2.2 CO2 laser used for rapid prototyping at DTU Nanotech.....	26
2.3 (A)Micro-milling machine at DTU Nanotech (B) Micro-milling process[59].....	28
2.4 The temperature and pressure assisted bonding press in the microfabrication lab at DTU Nanotech.....	29
2.5 The different layers were joined through PSA layers and pressed with the bonding press.....	30
2.6 Thermal bonding.....	31
2.7 Photographs of the PC discs exposed to different temperatures and forces during thermal bonding.....	32
2.8 Photographs of bonded lab-on-disc system with the breakage in the top layer (A). Successful thermal bonding (B).....	32
2.9 Schematic procedure for injection molding [66].....	33
2.10 Custom optical spin stand in the Centrifugal lab at DTU Nanotech.....	34
2.11 Photo of the liquid in the channel (left) and the created reservoir's mask (right).....	35

2.12	Photograph of the portable spin stand with the cell culture device in the incubator room at DTU Biosustain.....	36
2.13	Sterilization methods based on paper [70].....	37
2.14	Autoclave for steam sterilization at DTU Biosustain.....	39
3.1	Photograph of the first prototype fabricated with CO ₂ laser ablation (A) and with micro-milling and thermal bonding (B).....	40
3.2	CAD drawing of the first prototype.....	41
3.3	(A) Top PMMA layer, (B) top PSA layer, (C) layer in PMMA with loading, waste, cell culture chambers and micro-channels, (D) layer in PSA with loading and waste chambers (E) bottom layer in PMMA (F) Assembly.....	42
3.4	The disc's layers were fabricated with CO ₂ laser ablation, then they were joined through PSA layers and pressed with bonding press.....	44
3.5	(A) Top PMMA layer, (B) PMMA layer with loading, waste and cell culture chambers and micro-channels, (C) Fully assembled system.....	44
3.6	The disc's layers were fabricated with both CO ₂ laser ablation and milling machine, then were bonded with thermal bonding.....	45
3.7	(A) results obtained testing the disc at a rotational frequency of 1.5 Hz, with “ultrapure” water plus food dye for eight hours and leaving it to spin overnight. (B) Results obtained testing the disc at rotational frequency of 1.5 Hz, with only “ultrapure” water for six hours and leaving it to spin overnight.....	46
3.8	(A) results obtained testing the disc at rotational frequency of 1.25 Hz, with “ultrapure” water for ten hours and leaving it to spin overnight. (B) Results obtained testing the disc at rotational frequency of 1.25 Hz, with “ultrapure” water for about six hours and leaving it to spin overnight.....	48
3.9	Second prototype design.....	49

3.10	(A) Top layer with inlet and venting holes. (B) layer with loading, waste, cell culture chambers and micro-channels. (C) Fully assembled prototype.....	50
3.11	The disc's layers were fabricated with both CO2 laser and milling machine and then they were joined with thermal bonding.....	51
3.12	(A) Flow rate during the fluidic test and its average value. (B) Flow rate during the fluidic test and its average value. (C) Flow rate during the fluidic test and its average value. (D) Flow rate during the fluidic test and its average value. (E) Flow rate during the fluidic test and its average value.....	54
3.13	In both experiments done at low rotational frequency (2Hz), we can see that the flow rate assumed higher values when the fluid was in the first channel of loading chamber. The flow rate started to decrease during the passage from the first channel to the second one.....	55
3.14	CAD design with differential centrifugal pressures.....	57
3.15	CAD design with the differential centrifugal pressure.....	58
3.16	Photograph of the third design.....	59
3.17	(A) The loading channel had a width of 8mm. (B) The loading channel had a depth of 5.5 mm. (C) The loading channel had a depth of 5mm.....	60
3.18	A good fluid front (left) can be achieved if the channel has an appropriate width. If the channel is too large the fluid moves as reported on the right side.....	60
3.19	CAD drawing of the third prototype with differential centrifugal pressure between loading and waste chamber.....	61
3.20	(A) Top layer with inlet and venting holes. (B) PSA layer with inlet and venting holes. (C) PMMA layer with loading, cell culture, waste chambers and micro-channels. (D) PSA layer with loading and waste chambers. (E) PMMA layer. (F) Fully assembled prototype.....	62

3.21 (A)-(F): flow rates and their average values obtained testing the disc at different rotational frequencies.....	64
3.22 Dependency between the flow rate and the rotational frequency.....	65
4.1 (A) Top PMMA layer with inlet and venting holes. (B) PMMA layer with loading, cell culture, waste chambers. (C) Fully assembled system.....	67
4.2 Photograph of the disc with filters in inlet and venting holes.....	68
4.3 Sterile filters.....	69
4.4 Graphs show the flow rate over time at different rotational frequencies.....	70
4.5 Dependency between the flow rate and rotational frequency.....	71
4.6 (A) Flow rate and average value for the first two experiments (B) Flow rate and its average value in red.....	73
4.7 Flow rate and its average value in red.....	74
4.8 (A) Theoretical flow rate. (B) Theoretical and experimental flow rate for each rotational frequency.....	76
4.9 (A) CAD drawing of the third prototype (B) The new positions of inlet and venting holes.....	78
4.10 (A) Top PC layer with loading and venting holes. (B) PC layer with loading, cell culture and waste chambers. (C) Fully assembled system.....	79
4.11 Photograph PC layer cut using CO ₂ laser ablation.....	80
4.12 (A) Confocal microscopy images of bacterial cells at day 1 (B) and day 2.....	81
4.13 (A) CAD drawings of the design used to cultivate <i>Pseudomonas aeruginosa</i> . The micro-channels had a width of 0.4 mm. (B) CAD drawings of the design with modified micro-channel to inoculate bacterial cells. The micro-channels had a width of 0.7 mm and it was closer to cell culture chamber.....	82
4.14 Final design with new micro-channel to inoculate bacterial cells.....	82

A.1 Forces that arise from disc rotation [86].....84

List of tables

1. Table 1: Average flow rate, standard deviation (STD) and number of sample used to calculate STD for each frequency.....65
2. Table 2: Average flow rate, standard deviation (STD) and number of sample used to calculate STD for each frequency.....71
3. Table 3: Component of M9 medium.....71
4. Table 4: Values of parameters used to calculate flow rate with equation.....75
5. Table 5: Theoretical values of flow rate for each rotational frequency.....76
6. Table 6: Values of parameters used to estimate the shear stress inside the cell culture chamber.....77

To my fantastic parents

Abstract

Most bacteria can adhere to various surfaces, included human tissues, developing a complex 3D structure called biofilm[5], which has high resistance to disinfectant chemicals and antibiotics[6].

Commonly in hospitals, the analysis of antibiotics resistance is carried out using static bacterial cultures in Petri dishes, which are time and resource consuming and then they do not mimic the *in vivo* like conditions.

In the last few decades in research laboratories, bacterial cultures are also carried out in microfluidic systems where bacterias are cultured in flow fluids mimicking, in this way, more *in vivo* like conditions. However, most of the pumps used to move liquid in the microfluidic systems are complex and bulky, often requiring large amount of reagents and culture medium[7].

Centrifugal microfluidic platforms, “also referred to as lab-on-a-disc (LOD)”, have a simple fluid actuation module to pump and handle the fluid inside the platforms. These systems require a simple motor to rotate the disc in order to exploit the forces which arise from rotation to manipulate the fluid [8]. These systems without auxiliary pumps and tubing require low sample volumes and could potentially decrease of the possibility of contaminations.

The aim of this project was to create a LOD system which was enabled low flow rates (few hundreds nl/min), suitable for perfusion culture. The system was fabricated in Polycarbonate (PC), which is biocompatible material and can resist the commonly used sterilization methods. The final disc was composed of two PC layers. One layer presented the inlet, outlet reservoirs, cell culture chamber and micro-channels and the second layer, containing the inlet and venting holes, was used as a lid to have a closed system. The structures in bottom layer were fabricated with micromilling, while the inlet and venting holes on the lid were done with a drill. The two layers were bonded with thermal bonding. The flow rate were measured optically and calculated with an image analysis through a Matlab code. The flow rate were evaluated at different rotational frequencies ranged from 1.125 Hz to 0.375 Hz.

The lowest rotational frequency (0.375 Hz), in according to study [9] has permitted to obtain a centrifugal force that it was in the range which didn't cause harmful effects on cells and a flow rate (~500 nl/min) which involved low shear stress inside the cell culture chamber. The flow rate achieved at 0.375 Hz permits to cultivate bacterial cells for about 5 days without change culture medium. The system was used for culturing *Pseudomonas aeruginosa* at 30°C and at a flow rate of 400 nl/min. The bacterial culture was observed for two days using a confocal microscope. From the results obtained the platform needs an additional optimization in order to have a better bacterial cells inoculation. After this optimization, the biofilm and the effects of antibiotics will study.

Chapter 1

Introduction

1.1 Motivation and aim

In nature bacterias, in most cases, appear in form of biofilm[1][2][6] and according to National Institutes of Health, biofilms cause about 65% of all microbial infections and 80% of all chronic infections, because they have an high resistance both to antibiotics and to components of human immune system [6][2][10].

Bacterial biofilm is an aggregation of microorganisms in which the bacterias are close to each other within the matrix of extracellular polymeric substance (EPS) produced by the cells themselves on living or no-living surfaces [2][11] (Figure 1.1).

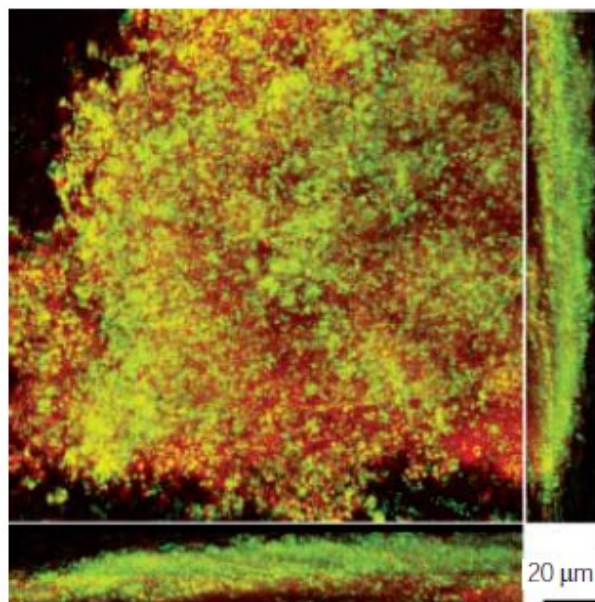


Figure 1.1: image of *Staphylococcus aerus* biofilm with confocal microscope [1].

Since the last century, several methods have been developed to identify and quantify the EPS's components [12]. From the results obtained, it can be said that the matrix is composed by water (97%), the main component which allows the flow of nutrients inside the biofilm matrix, proteins

(<2%, including enzymes), polysaccharides (<2%) which give stability and protection to biofilm, RNA (<1%) and DNA (<1%) [6][2][13][14], which plays a significant role in gene transfer [15][16][17][18][19][20][21][22][23][24][25][26].

Several imaging techniques enable investigation of biofilm formation and architecture. This complex architecture suggests that biofilm formation is a multi-step process (Figure 1.2) in which bacteria are subjected to certain changes [2][1].

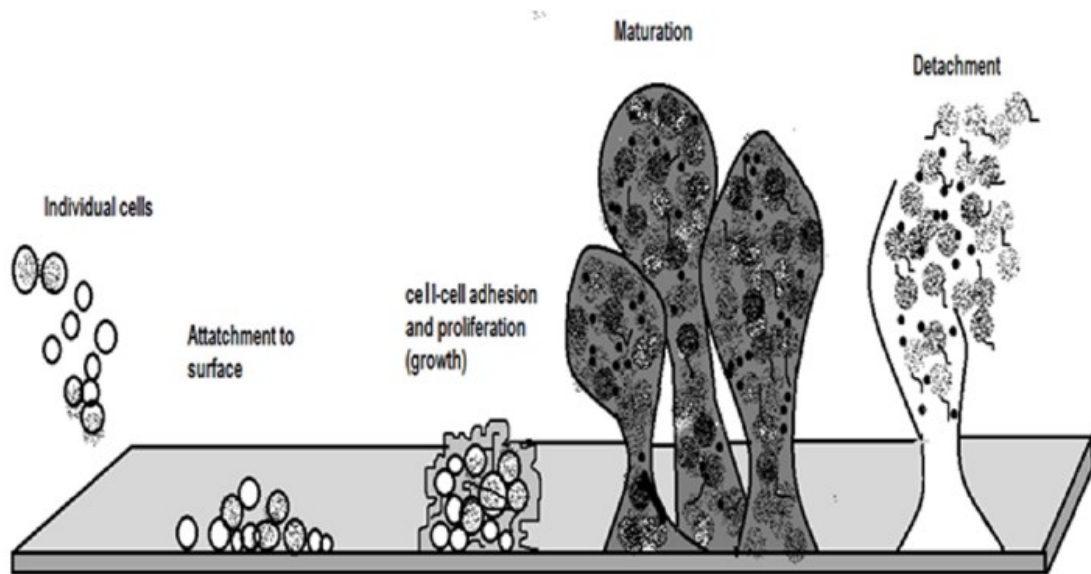


Figure 1.2 scheme of the biofilm formation [2].

The formation of a biofilm starts with singular bacterial cells, which come close to a surface and make a reversibly attach to it [2]. At this stage, the cells are still sensitive to antibiotics [6]. After this first attachment, if the surface and the environment have suitable characteristics (e.g. hydrophilic, coated, rough surface and a certain flow velocity and nutrient concentrations) the bacteria form an irreversible binding to the surface and thanks to chemical signals they start the formation of micro colonies [2][10]. After this step the bacteria start to produce the EPS matrix and the channels for fluid transport inside the biofilm itself generating a three dimensional structure [2][24]. The final structure has an high resistance to antibiotics due to [6][2] [25][26]:

- the nature of EPS matrix that prevent antibiotics to go inside biofilm,

- the presence of neutralizing enzymes which degrade the antibiotics before they have effect,
- several efflux pumps that take out unknown substances present inside the biofilm,
- heterogeneous nature of biofilm itself: the deeper layers have limited availability of nutrients and oxygen so this reduces the sensitivity to antibiotics,
- the system, called quorum sensing, that bacterial cells use to communicate with each other.

The purpose of this work was to develop a centrifugal microfluidic device for a long-term (5-6 days) bacteria culture that enables growth of biofilms and can be used for evaluation and testing of antibiotics in research and development phase.

Most bacteria, to create a biofilm need a stable flow rate at few hundreds nl/min [9][27]. Higher flow rate cause high shear stress that brings to the cells detachment. Therefore, stable flow rate at a specific value is set as a goal in order to create an adequate environment for bacteria and to permit a good formation of biofilm.

1.2 From Petri dishes to centrifugal microfluidic devices

Over the past decades, *in vitro* cell cultures enabled basic researches as well as clinical studies which led to in depth knowledge about cell structure, function and how cells respond to precise stimuli [28]. In *in vitro* cell cultures, cells are grown in artificial environment such as Petri dishes, outside of their natural environment.

The first platforms that have been implemented for cell culture were 2D systems (e.g. Petri dishes, flasks and plates) [29], where cells were grown in static condition and the culture medium needed to be changed regularly, every 2-3 days [29]. Static cell culture is well established and commonly used in research and development as well as in clinics, although they mimic poorly the natural cell microenvironment.

In vivo, cells grown in environment with specific biochemical, physicochemical properties and where chemical gradients are present [28]. Furthermore, most cells are surrounded by a complex structure,

the extracellular matrix (ECM), which is composed by protein and proteoglycans, and they receive continuously nutrients through vascular perfusion [28].

In the last few decades, culturing cells in microfluidics provided to be suitable for cell biology research [28][30].

“Microfluidics refers to the science and technology of systems that manipulate small amounts of fluids in devices with characteristic length scales at microscale” [8][31]. Working in microfluidics offers many advantages: reduction of samples/reagents used to carry out biochemical analysis, low fabrication cost, fast analysis, high integration of multiplexing functions on a single chip and low power consumption [8][31][32]. Related to cell culture, microfluidic platforms are able to mimic cell’s microenvironment, creating continuous perfusion and chemical gradients that are important for cellular functions. Furthermore, these platforms permit to manipulate few cells and this is an advantage, for example, to study the complex cellular behavior and cell migration process [33]. In the case of bacterial cells, microfluidics permits to cultivate them giving the possibility to form biofilms and to study how specific features of environment (e.g. flow rate, shear stress, presence of antibiotics...) can affect the biofilms[27][34][35][36].

Despite of these advantages, most microfluidic cell culture devices require a large auxiliary equipment such as incubator and peristaltic pump, which are bulky and expensive [28][31] (Figure 1.3).



Figure 1.3: Equipment for cell cultures in microfluidic devices.

In this project we aimed to develop a centrifugal microfluidic system for bacterial cells culture, since centrifugal microfluidic platforms proved to be a promising and valid alternative to conventional ones, providing simple and easy to use liquid handling solution.

Centrifugal microfluidic system, “also referred to as lab-on-a-disc or lab-on-a-CD (LoD)”, started in the late of 1960s [37], is based on polymer disc, which is used to manipulate the fluid through microfluidic channels. A simple motor is used to rotate the disc in order to exploit the forces which are generated by rotation to move and handle the fluid [38]. In a centrifugal microfluidic platform, the fluids are pumped thanks to centrifugal force and manipulated exploiting Coriolis force and capillary action (see Appendix).

Due to the relative liquid handling approach, this technology permits the precise control of small volumes of fluids only with the forces that arise from the rotation, without pumps and actuators. Centrifugal pump requires a simple motor and therefore centrifugal pumping can be implemented in a wide range of channel sizes (from $5\mu\text{m}$ to 1mm) [39].

In addition, centrifugal microfluidics enables a high degree of parallelization. The disc can be designed in order that all the fluidic modules are exposed to the same forces so this allows the

implementation of the same assay multiple times on the same device [38]. Another benefits of Lab-on-a-disc is that permits to use simple and low-cost fabrication techniques [38].

On the other hand, there are also certain disadvantages of these platforms. The fact that whole disc rotates at the same frequencies, enabling the implantation of the same assay multiple times as described above, can be a drawback in case the assays and processes on the platform require different frequencies. In addition the liquid can move only in one direction: from the center radially outward [8].

During the years, several LoD systems has been developed for diagnostics, which implemented all assay steps, from sample pretreatment to detection.

In diagnostics blood analysis is very important. A key step in blood analysis, which was implemented on disc, was the separation of plasma from whole blood achieved easily exploiting centrifugal microfluidics principles. For example, the first lab on a disc, which has been realized, processed 90 μl of whole blood and separated the plasma into 12 different chambers [3] (Figure 1.4).

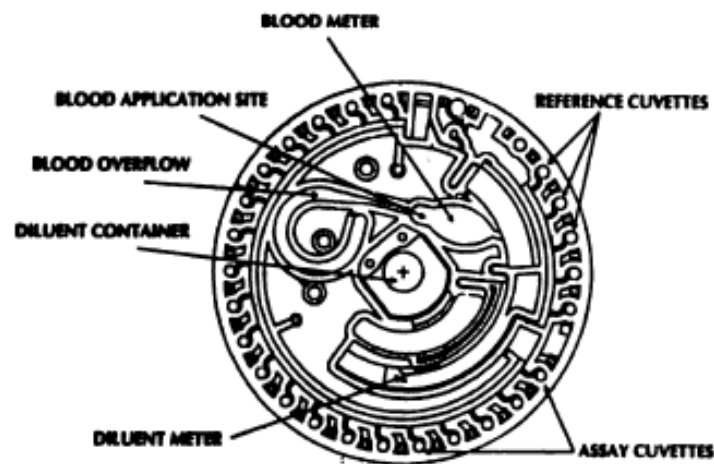


Figure 1.4: Centrifugal microfluidic system for separation of plasma from blood [3].

Additionally another centrifugal microfluidic device was implemented, using even lower sample volume, 5 μl of whole blood to obtain 2 μl of plasma. The disc included a metering structure which

was connected, through a microchannel, to two chambers; one chamber retained the cells and other chamber received the plasma [4] (Figure 1.5).

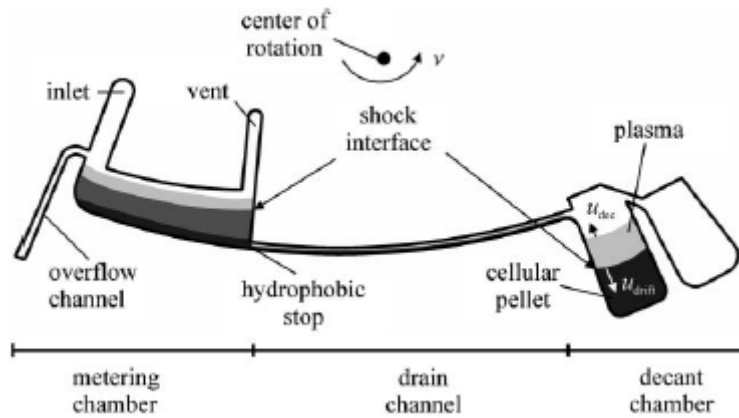


Figure 1.5: Structure implemented in the LOD to separate plasma from whole blood [4].

Another main step in biological assay, often used in diagnostics, is cell lysis. The sample lysis in centrifugal microfluidic devices can be obtained with chemical, biological or mechanical methods. The simplest lysis method exploited the forces created during the disc rotation to break the cells membranes [40]. It has also been implemented a method which uses magnets placed under the disc and zirconia beads. During the CD rotation, each chamber is subjected to a magnetic field that causes the beads movement and their collision with the sample [41]. On the other hand, chemical methods use alkaline buffers to decompose cells or thermoelectric techniques to denature proteins [37].

In addition, lab-on-a-disc systems have been also used for extraction of nucleic acid from various samples, such as clinical samples, human or environmental and food samples [8][41][42][43][44](Figure 1.6).

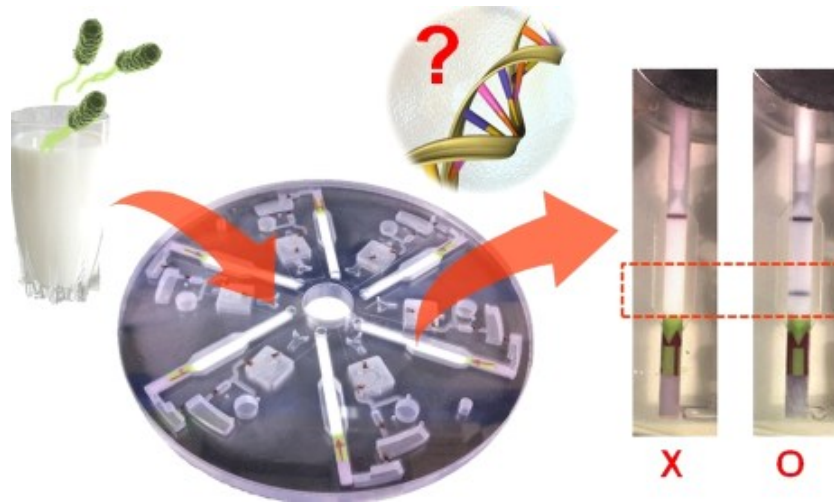


Figure 1.6: LOD for extraction of nucleic acid of Food-Borne Pathogens [42].

Beside, the above mentioned sample pretreatment approaches, various detection methods has been also adapted to LoD devices, to enable a complete assay. By integrating immunoassays into microfluidics devices, reagents consumption and diagnosis times can be drastically reduced [37]. For example, a centrifugal microfluidic device has been realized to execute an enzyme-linked immunosorbent assay (ELISA) for rat IgG, where the system was composed of 24 sets of assays [45] (figure 1.7).

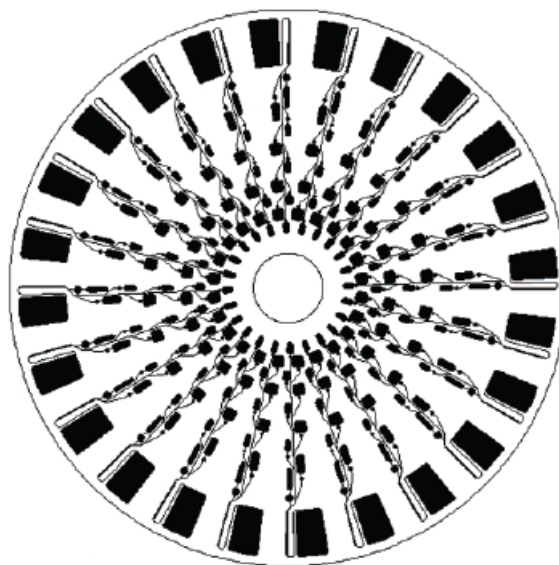


Figure 1.7: Centrifugal microfluidic device for enzyme linked immunosorbent assays [45].

Immunoassays has been implemented on lab on disc for example to extract biomarkers of infection diseases [46] or protein biomarkers present in various samples [39][47].

Beside their applicability in biological assays and diagnostics, centrifugal platforms have been proposed for cell culture and cell-based assay [31][37][48] (Figure 1.8). During the last years experiments were done to investigate the centrifugal force's effects on cells [37][49]. The cells tested were shown to support high values of forces, much larger than the forces needed to move liquids inside a centrifugal microfluidic platform [37][49]. Only a few platforms have been developed with the purpose of creating a suitable environment for cells [31][37][48], however long term perfusion culture was not yet established. An example is reported in Figure 1.9 where *Pichia Pastoris* cells are cultivated in three different chambers connected to micro-channels that contain the medium.

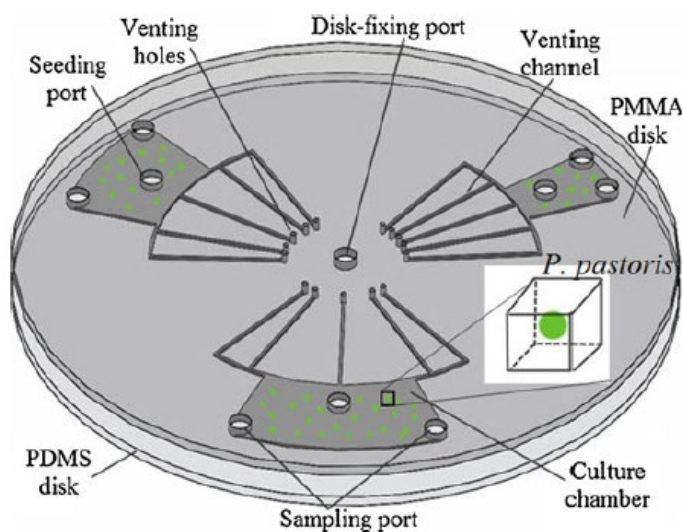


Figure 1.9: Centrifugal microfluidic device for *Pichia Pastoris* cultures [31].

Chapter 2

Materials and methods

For the fabrication of microfluidic systems different types of materials can be used, such as glass, silicon and polymers [50]. Glass and silicon were the first materials to have been implemented, since they are suitable for capillary electrophoresis and compatible with solvent-involved applications. However, glass and silicon are not suitable for long-term cell cultures due to their gas-im-permeability and their surface characteristics (especially silicon) [50][32]. Furthermore, glass and silicon require expensive and time-consuming microfabrication techniques to be processed [32].

Today, polymers are the most used for microfluidic devices [50][51]. Their variety permits to choose the suitable materials for a specific application, they are low cost and they can be also processed with simple and rapid prototyping techniques [50][51].

2.1 Materials for polymer-based microfluidic chips

Poly(dimethylsiloxane) (PDMS) was the first polymer to be used in microfluidics [50][52]. It is an elastomer with physical and mechanical properties that make it suitable for a wide range of application [52]. The fabrication process of PDMS-based microfluidic chips is divided in two parts: the fabrication of master in silicon or glass and the fabrication of PDMS chip. The master is realized with lithography while the final microfluidic chip in PDMS is obtained pouring the PDMS liquid pre-polymer on the master and causing the polymerization reaction to take place at a defined temperature [50][51]. For several years, PDMS has been the most used polymeric material in microfluidics. However, it has also some limitations such as its hydrophobic nature, resulting in the absorption of small hydrophobic molecules (like drugs). In addition even after surface treatments PDMS returns to hydrophobic state [50][52].

Recently, thermoplastic polymers, such as Poly(methyl metacrilate) (PMMA), Polycarbonate (PC), Polystyrene (PS) and cyclic olefin copolymer (COC) have become alternatives to PDMS.

In this project, three thermoplastic materials were used: PMMA, PC and COC.

PMMA was the first material used to develop the first prototype of the centrifugal microfluidic platform for perfusion cell culture. It is low cost with good mechanical properties and optical transparency [53][54]; unfortunately, it has a low solvent resistance and a glass transition temperature of 110°C, so sterilization methods which use solvents, such as ethanol (EtOH), or temperature above 110°C can't be used. For these reasons, the final device was fabricated in PC. This material has the same characteristics of PMMA but an higher resistance to solvents than PMMA and a glass transition temperature of about 145°C, thus PC disc can be sterilized using steam autoclaving, EtOH and irradiation[55].

PMMA and PC are both compatible with cells but they are hydrophobic materials so they need to be subjected to surface treatments. There are two common surface treatments that can be used to make the surfaces more hydrophilic: UV and plasma oxidation. UV-ozone treatment is preferred over the other one because the surfaces retain the hydrophilicity longer but it can't be used with PMMA due to the formation of peroxides groups on its surface that are harmful for cells viability [52]. However, for mammalian cell cultures, it is preferred to coat the surfaces, without any surface treatment, directly with protein of extracellular matrix (e.g. collagen, fibronectina) to improve the adhesion between cells and the surface.

Finally, the third thermoplastic material used was Topas 5013-L10. It was used to fabricate the luers, small connectors that were located above inlet and venting holes to hold the filters (Figure 2.1).

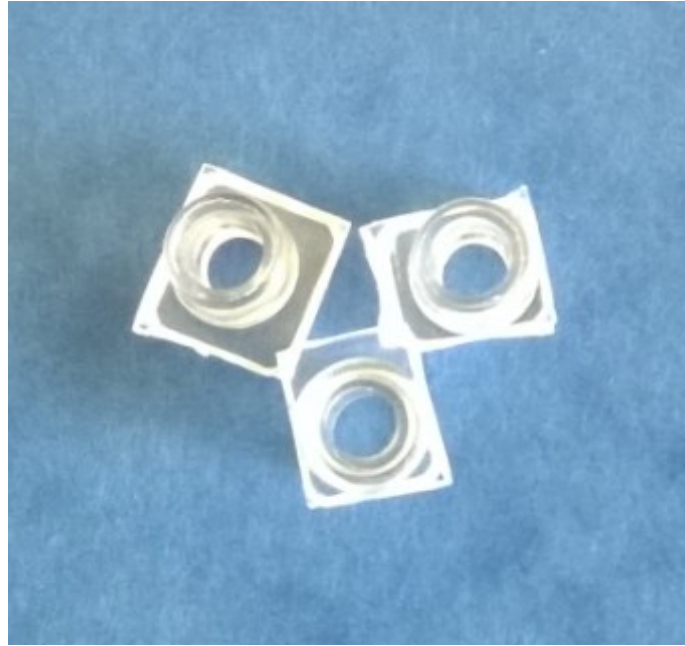


Figure 2.1: Luers in Topas that are used to hold filters.

Topas 5013-L10 is a cyclic olefin copolymer (COC); it has good mechanical properties, easy fabrication, and good biocompatibility. Furthermore, it has a good resistance to acids and alkalis and a glass transition temperature of about 130°C, so it can be sterilized using heat steam, ethylene oxide or ethanol [56].

2.2 Methods

2.2.1 CO₂ laser ablation

CO₂ laser ablation (Figure 2.2) was used to cut or engrave the PMMA substrates[57][58]. It is a rapid prototyping method, which allows the fabrication of the desired design in a short time.



Figure 2.2: CO₂ laser used for rapid prototyping at DTU Nanotech.

The CO_2 laser operating principle is very simple: an invisible infrared beam is generated exciting the CO_2 gas, which is inside a tube, with radiofrequency energy. The beam can be used for cutting or engraving the workpiece.

The two important parameters that the user must set carefully are the power and the speed of the gas flow that permits to cut the material or to generate structures, inside it, with a specific depth.

For the fabrication of the fluidic system, all the 2D design was realized with *SolidworksTM*, then it was saved in a *.Dxf* format and imported in *CorelDRAW*.

To cut the PMMA substrate and to create through-parts, the vector function was chosen and the following values for speed and power gas flow were set:

- Speed = 5%
- Power = 100%

To create the engraved parts, the raster function was chosen and the following parameters for speed and power gas flow were set:

- Speed = 20%
- Power = 50%

2.2.2 Micro-milling

In comparison with laser ablation, with micro-milling we are able to obtain smoother surfaces with higher resolution.

Micro-milling is a technique that uses tools, such as drills to remove materials from a surface (Figure 2.3 (A), Figure 2.3(B)). There are several tools with different geometry, sizes and coatings, which can be used for different applications (drill, ball cutter, end mill, etc...).

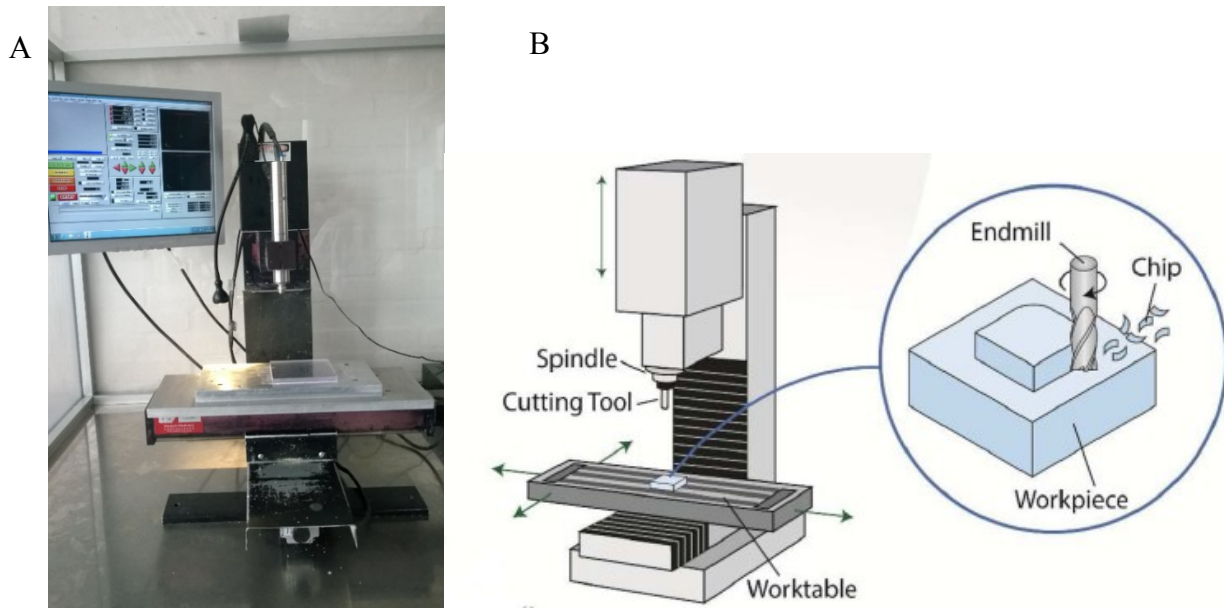


Figure 2.3: (A) Micro-milling machine at DTU Nanotech. (B) Micro-milling process[59].

For creating micro-milled structures, we need to create a working code, compatible for the micro-milling machine. To create this working code, first of all, the device's design has been made in *SolidworksTM* and imported into *CimatronE*. This software allows the user to introduce the parameters of the used cutting tool and the machining parameters, such as speed. The software permits also to choose the tolerance parameters and which surface's parts must be cut with the chosen tool. To fabricate the cell on a disc were used two different end mill cutters:

- end mill with a 3 mm diameter to mill the reservoirs,
- end mill with a 0.3 mm diameter to mill the finer parts, such as the cell culture culture chamber and micro-channels that connect the cell culture culture chamber to the reservoirs and to hole used to inoculate bacterial cells.

The *CimatronE* generated a G-code which contained cutting movements along x,y and z directions. Before milling, as a final step the G-code has been loaded in second software: *Mach3 loader* that controls the milling machine's operations and allows the user to choose the values of two parameters: the cutting speed and feed rate. The cutting speed is the velocity between the cutting tool and the work piece, while the feed rate is the velocity at which the tool advances along the surface.

2.2.3 Bonding of the fluidic system

Two different methods were used to join the different layers of the fabricated device. In both techniques, a bonding press was used, which is a tool with two plates. The devices which need to be bonded are placed between the two metallic plates, and a specific pressure and temperature are applied (Figure 2.4).



Figure 2.4: The temperature and pressure assisted bonding press in the microfabrication lab at DTU Nanotech.

In the initial phase of development, we used a pressure sensitive layer (PSA) to bind the fabricated parts of the fluidic system. The plastic layers with the PSA were placed in the bonding press for a few minutes at a low pressure, in order to create a strong bond between substrates.

First, the different layers were cleaned to avoid particles to be trapped in the fluidic channels and then the disc was assembled by placing the fabricated polymer structures and the PSA tape in a defined order. The assembled layers were placed between the metallic plates of the bonding press and a force of 12 kN was applied for five minutes[60] (Figure 2.5).

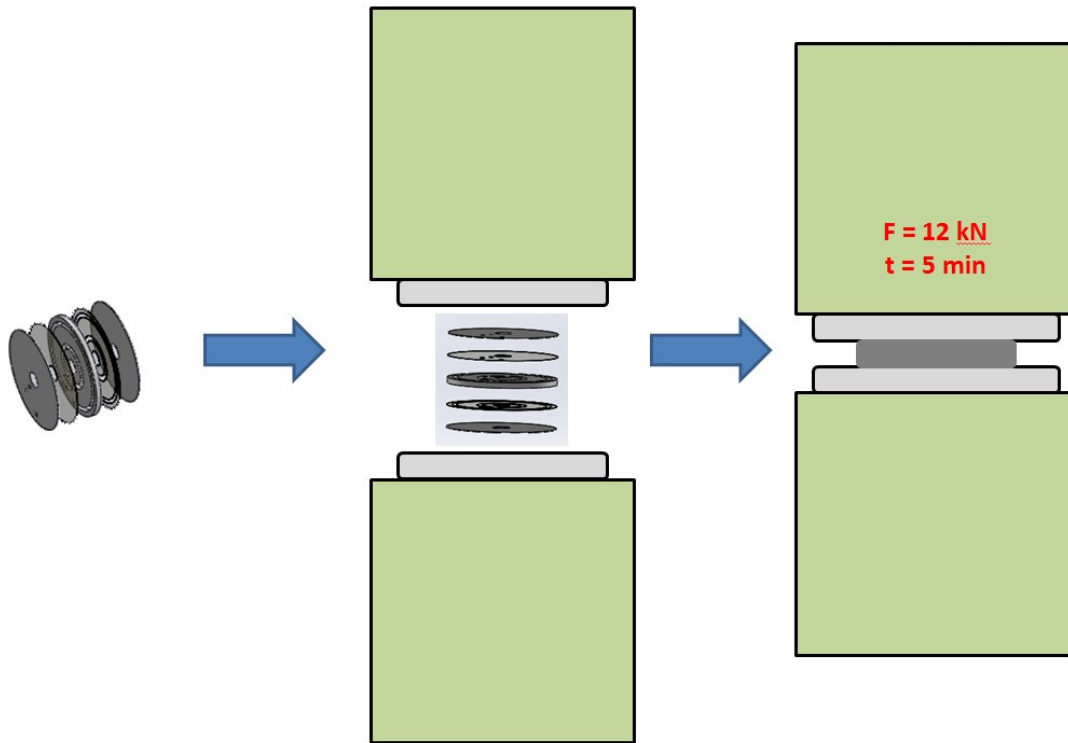


Figure 2.5: The different layers were joined through PSA and pressed with the bonding press.

However, this method presents some limits: the adhesive layers can change the wetting characteristics of channel sidewalls[61] and if the force applied is too high a little bit of PSA can enter inside the channels and can affect the fluid flow, thus a second bonding method was introduced.

Thermal bonding doesn't use any kind of adhesive layers but only temperature and pressure to attach different polymeric parts. The combination of temperature and pressure creates the interdiffusion of polymer chains between the surfaces forming a strong bond. To reach an adequate bond strength and uniformity and to avoid the distortion of structures on chip, the temperature that was chosen for PMMA thermal bonding was 90°C both for lower and upper plate of the bonding press and the force applied is 12 kN for ten minutes[60][62][53]. After ten minutes, the disc was left to cool until 50°C (Figure 2.6).

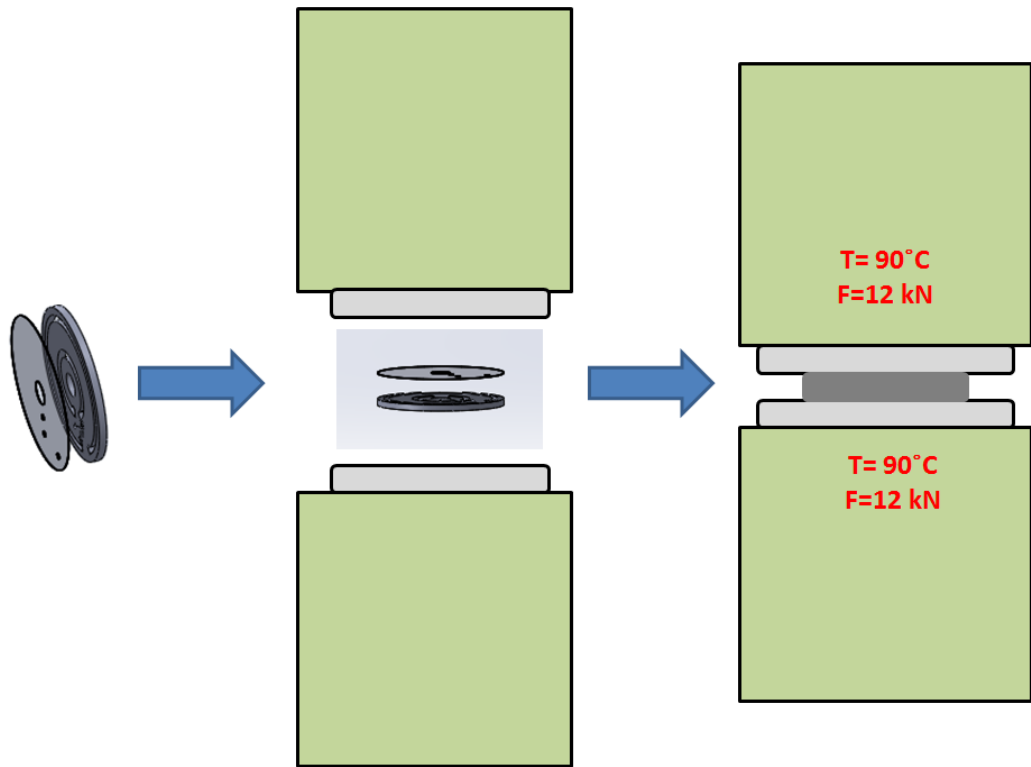
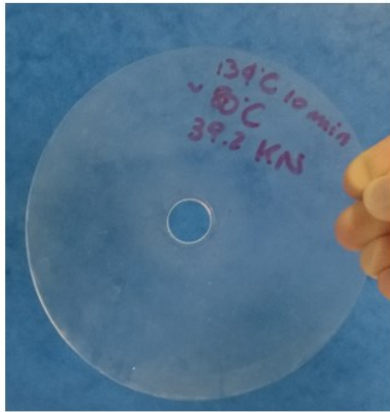


Figure 2.6: Thermal bonding process.

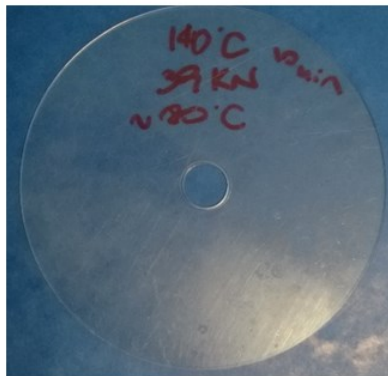
In the case of PC the thermal bonding needed to be optimized. Three different temperature, taken from literature, 134°C , 135°C , 140°C were tested using two 0.6 mm thick discs of PC [63][64]. The results obtained are reported in Figure 2.7.



T=134°C and F= 39 kN for ten minutes



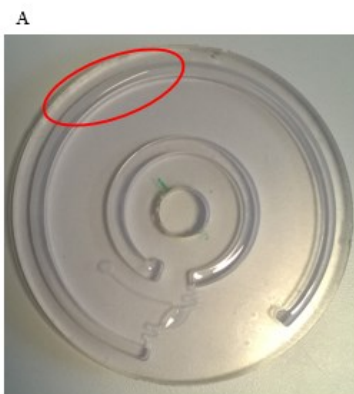
T=134°C and F=30 kN for ten minutes



T=140°C and F=39 kN for ten minutes

Figure 2.7 Photographs of the PC discs exposed to different temperatures and forces during thermal bonding.

A suitable bond was obtained when maintaining the PC layers at 140°C, applying a force of 39 kN for ten minutes and leaving them to cool until 80°C. When channels and reservoirs are present in the plastic structures, a lower force (10 kN) has to be used to avoid the breakage of top layer (Figure 2.8).



T=140°C and F=39 kN for ten minutes



T= 140°C and F= 10/12 kN for ten minutes

Figure 2.8: Photographs of the bonded lab-on-disc system with the breakage in the top layer(A). Successful thermal bonding (B).

2.2.4 Injection molding

Injection molding is a fabrication process that consists of injection, under a high pressure, of melted polymers into a master which has the desired design[53][65][66]. The injection molding process was used to fabricate the luer connectors. Firstly, the material used, Topas 5013-L10, was introduced in granular form inside the injection molding machine and it was melted in a cylinder. Afterwards, the molten polymer was injected, under a high pressure, in a cavity where a metal mold, with the negative of desired structures, was located. Finally, when the polymer had filled the master, the temperature and the pressure, in the cavity, were rapid decremented in order to permit the solidification of Topas and to demold it from the master. A schematic procedure is reported in Figure 2.9.

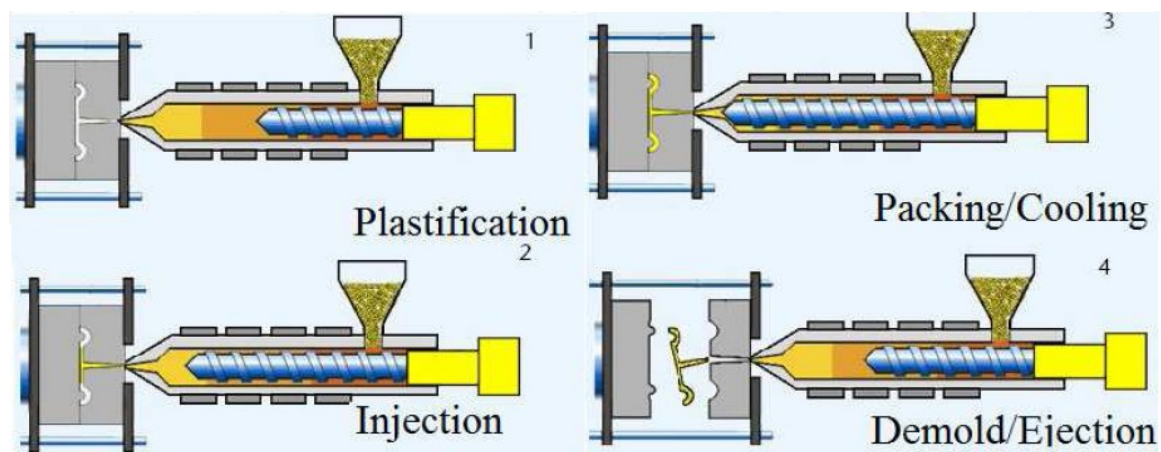


Figure 2.9: Schematic procedure for injection molding [66].

2.3 Optical Spin Stand and image analysis

The optical spin stand was used to measure the fluid flows and calculate the flow rates in the cell-on-a-disc platform (figure 2.10).

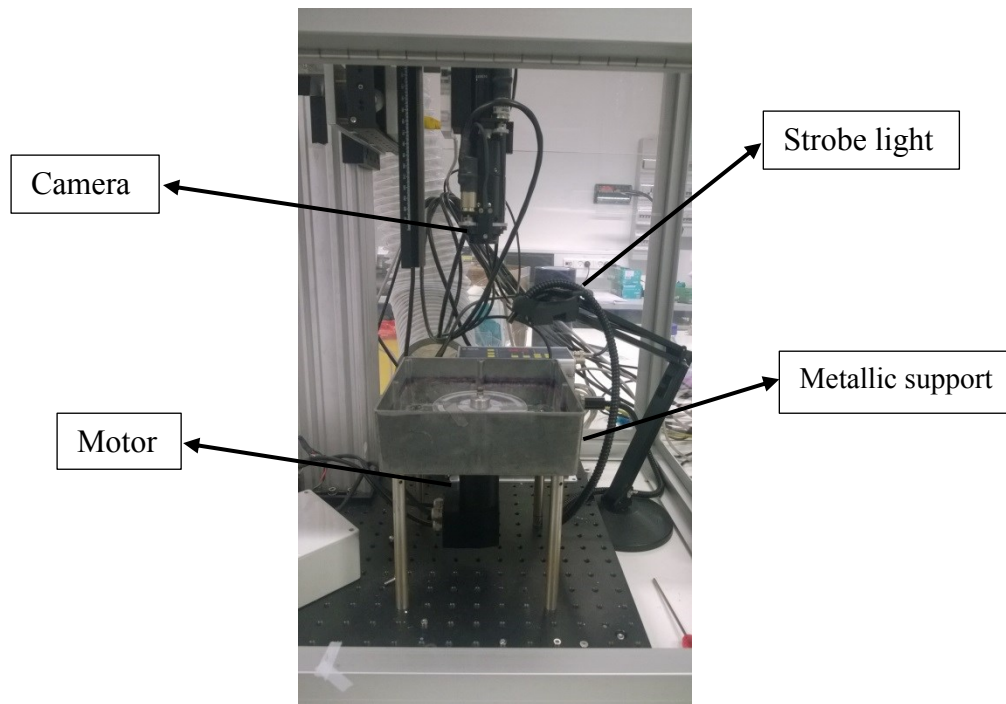


Figure 2.10: Custom optical spin stand in the centrifugal lab at DTU nanotech.

The optical spin stand consists of spin-stand that is used to spin the disc and a system for visualization that is used to observe the fluid flow inside the channels [45][67]

The optical spin stand (Figure 2.10) is composed of a metallic enclosure with a support for placing the disc. The metallic support is connected to the motor positioned below the metallic enclosure, controlled by a control unit. In addition, the stand is equipped with a camera and a strobe light. When the camera visualizes the same position of rotating disc, the strobe light is triggered and the user can observe that position through a software.

To select the speed and acceleration of rotation the WinMotion software was used, while controlling the movement of the disc was achieved by an Arduino based software and the images were captured with CamWare64.

To calculate the flow rates a Matlab code was used. This code permits to measure the fluid volume inside a reservoir. First of all, the image of reservoir was loaded into Matlab. After that, a mask around

the fluid present inside the reservoir was drawn. The pixels inside the mask were converted in black pixels, while the pixels that didn't belong to the mask were converted in white pixels (Figure 2.11).

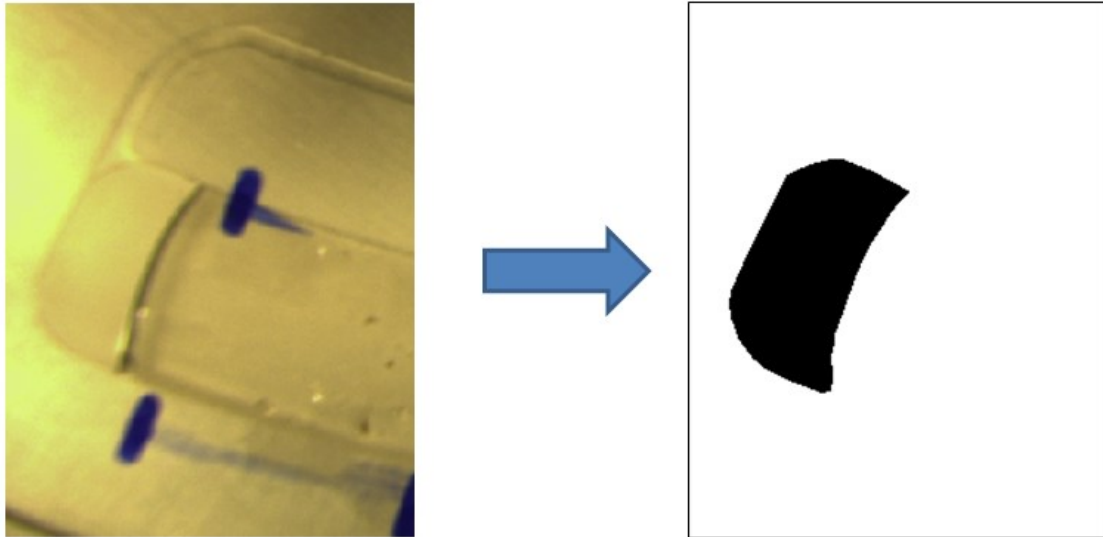


Figure 2.11: Photo of the liquid in the channel (left) and the created reservoir's mask (right).

To calculate the area of the mask the dimension of a pixel must be known, so the Matlab function *Improfile()* was used. This function provides the user with the number of pixels on a line drawn on the image. The line was drawn between two points of the image where the distance in mm was known. After that, the dimension of a pixel was calculated. Subsequently, the number of black pixels was obtained subtracting to the total number of pixels the number of white pixels. To calculate the mask's area the number of black pixels was multiplied with the dimension of a single pixel, while the volume was obtained multiplying the area with the depth of reservoir.

Finally, the flow rate was calculated dividing the volume with the time spent since the beginning of the fluidic test:

$$Q = \frac{V}{t} \quad (1)$$

Once the frequency that permitted the optimum flow rate (below $1\mu\text{l}/\text{min}$) for bacterial cells was found, the disc was used for bacterial culture. Bacterial cells culture was performed in an incubator

room where the temperature was about 30 °C. The system was very simple and portable; it was composed of a motor and a software that permitted to control the disc's rotation velocity (Figure 2.12).

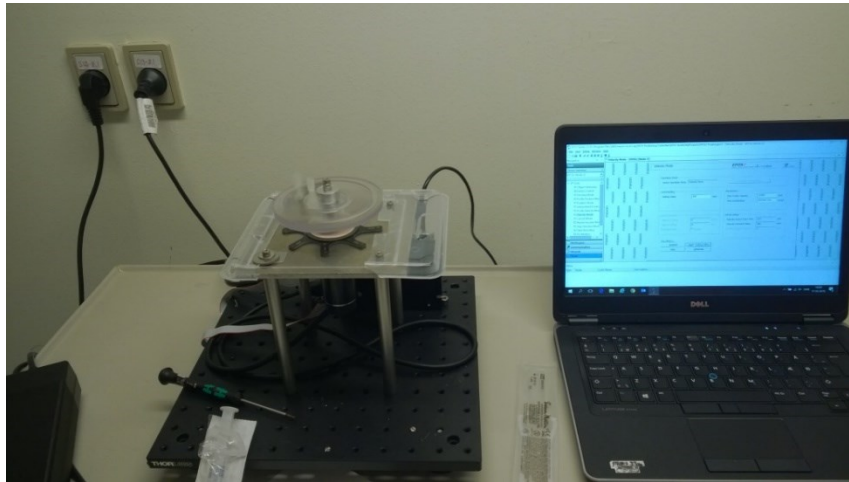


Figure 2.12: Photograph of the portable spin stand with the cell culture device in the incubator room at DTU Biosustain.

2.4 Sterilization methods

Before bacteria cells were inoculated in the device, the disc has to be sterilized. The sterilization is that process which allows the elimination all forms of microbial organisms such as viruses, spores and fungi[68][69].

2.4.1 A brief description

There are several methods (Figure 2.13) of sterilization that can be divided according to agents or materials that are used: heat sterilization, chemical sterilization, radiation sterilization and mechanical sterilization.

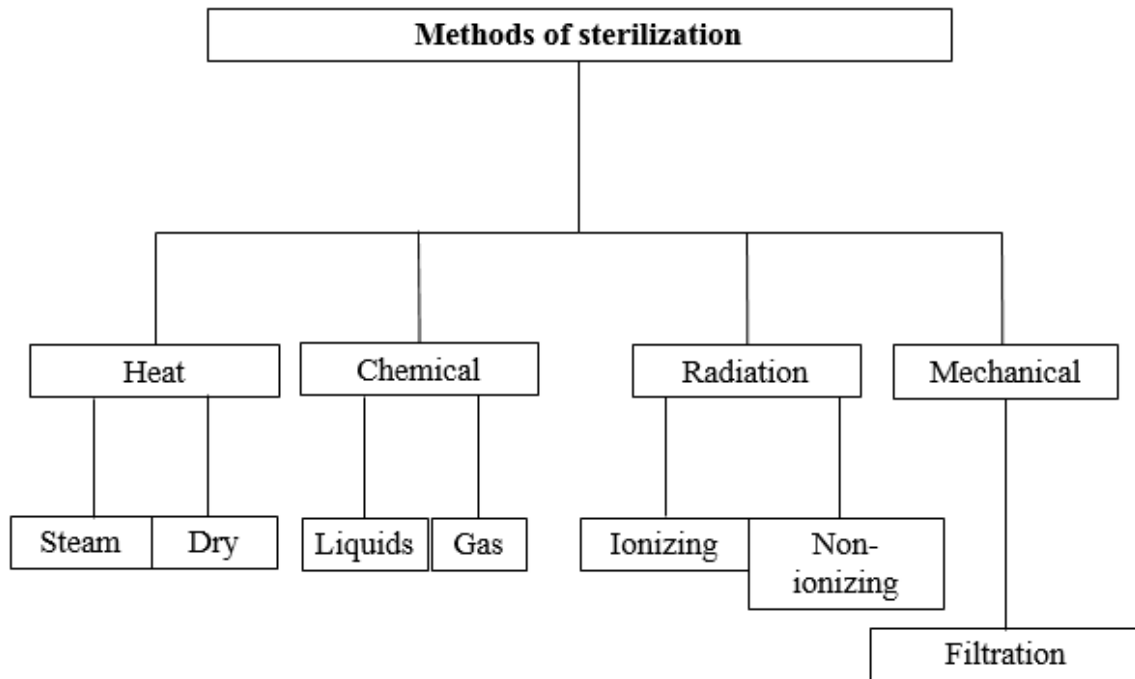


Figure 2.13: Sterilization methods based on paper[70].

Heat sterilization

- Steam sterilization: it is the first method that was introduced. It consists of exposing material to a steam in an autoclave. The steam has to be saturated and without air. The temperature inside the autoclave is 121°C-124°C and the entire process requires about two hours. These conditions lead to the denaturation of cell components such as proteins, enzymes, DNA and RNA chains. It is possible to use higher temperature but lower exposition times. This method is very simple, economic, fast, and no toxic but it can't be used with those materials such as liquids, electrical devices, polymers that are sensitive to high temperatures [69][71][70][72][73][74].
- Dry heat sterilization: this process takes place inside a chamber where the material is exposed to high temperatures, 160°C-170°C for a long time. It is a simple method, non-toxic but it is not adequate for those polymers that have a glass transition temperature below 160°C [69][70][72][75].

Chemical sterilization

- Ethylene oxide (EtO) sterilization: EtO is an alkylating agent, so this means that it is able to introduce alkyl groups (C_nH_{2n+1}) inside cellular constituents, such as proteins, enzymes, DNA chains, causing their denaturation. This method doesn't require high temperature, so it is suitable for those materials which can't be sterilized in autoclave or with dry heat sterilization. However, it presents some disadvantages: the compound used is toxic, it can react with others elements, present on the material's surface, producing others toxic residues which have to be eliminated, extending, in this way, the duration of the entire process and it can't be used with those materials sensitive to chemical agents such as PMMA[69][72][74][76].
- Ethanol (EtOH) sterilization: EtOH is an alcohol that is used to do liquid washes and so to sterilize the materials. It is able to disrupt membranes and to inactivate enzymes[70]. The sterilization with EtOH and with heat steam are the most common used methods.

Radiation sterilization

- Non ionizing radiations: UV and infrared radiations are used to sterilize only surfaces because of their low power of penetration. Infrared radiations during the interaction with the material, generates heat that kills microorganisms present on the surface while UV light causes chemical reactions with cell components[69][72][75].

- Ionizing radiation: there are two types of ionizing radiations that are used to sterilize objects: E-beams and Gamma rays.

E-beam sterilization uses e-beams generated by an accelerator, it doesn't require high temperatures and it doesn't leave any residues after process. The disadvantage is that an expensive instrumentation is needed to generate e-beams[69].

On the contrary, gamma rays are photon with high energy (1keV-10keV) produced by the decay of Cobalt-60 or Cesium-137 and they have a higher power of penetration than e-beams [69][72][75].

Mechanical sterilization

- Filtration: this method uses filters made of plastic material. It is a method suitable only for aqueous solutions [72].

2.4.2 Sterilization method for the centrifugal microfluidic platform

In this project the heat steam sterilization was chosen to sterilize the disc, the luer connectors and filters. Firstly, the disc, luers and filters were covered with aluminum foils, then they were placed inside an autoclave chamber (Figure 2.14) and they were subjected to high-pressure steam at about 125°C. The entire process, which was composed by sterilization part and cooling part, required about two hours.



Figure 2.14: Autoclave for steam sterilization at DTU Biosustain.

Chapter 3

Designs, fabrication and tests

3.1 First prototype

This section presents the first design that was made, its fabrication, fluidic tests and the results obtained.

3.1.1 Description of the design

The design of the first prototype enabled two different cell cultures on the same disc, which had an external diameter of 100 mm and an internal diameter of 15.25 mm, in the same time. Each part was composed by a loading, a cell culture and a waste chamber as well as three micro-channels. One of the channels, connected the loading chamber to cell chamber, the second, linked the culture chamber to the waste chamber while the third one connected the cell chamber to an opening that was used to avoid the formation of air bubbles and it allowed the introduction of the cells inside the chamber (Figure 3.1 (A), Figure 3.1 (B)).



Figure 3.1: Photograph of the first prototype fabricated with CO2 laser (A) and with micro-milling and thermal bonding (B).

The loading chamber meant to be used to store the cell culture medium, which was perfused in the cell culture channel. In the design presented in Figure 3.2, loading chamber was composed by three channels, each of them having a width of 3.5 mm and a depth of 2 mm with a total volume of about 1000 mm³.

The waste chamber is the reservoir which will contain the cell culture medium that flown through the cell culture chamber and contains the waste products from the cells. It was composed by a channel with a width of 5 mm and a depth of 2 mm with a volume of about 1000 mm³ (Figure 3.2).

The cell culture chamber is the area where the bacterial cells will be located; it had an oval shape, a depth of 0.5 mm in order to permit the formation of biofilm (thickness about 50 μm [6]), and a volume of about 14 mm³ (Figure 3.2).

In addition, the micro-channels, which connected the reservoirs (inlet and waste) to the cell culture chamber, had a width of 0.5 mm and a depth of 0.3 mm (Figure 3.2).

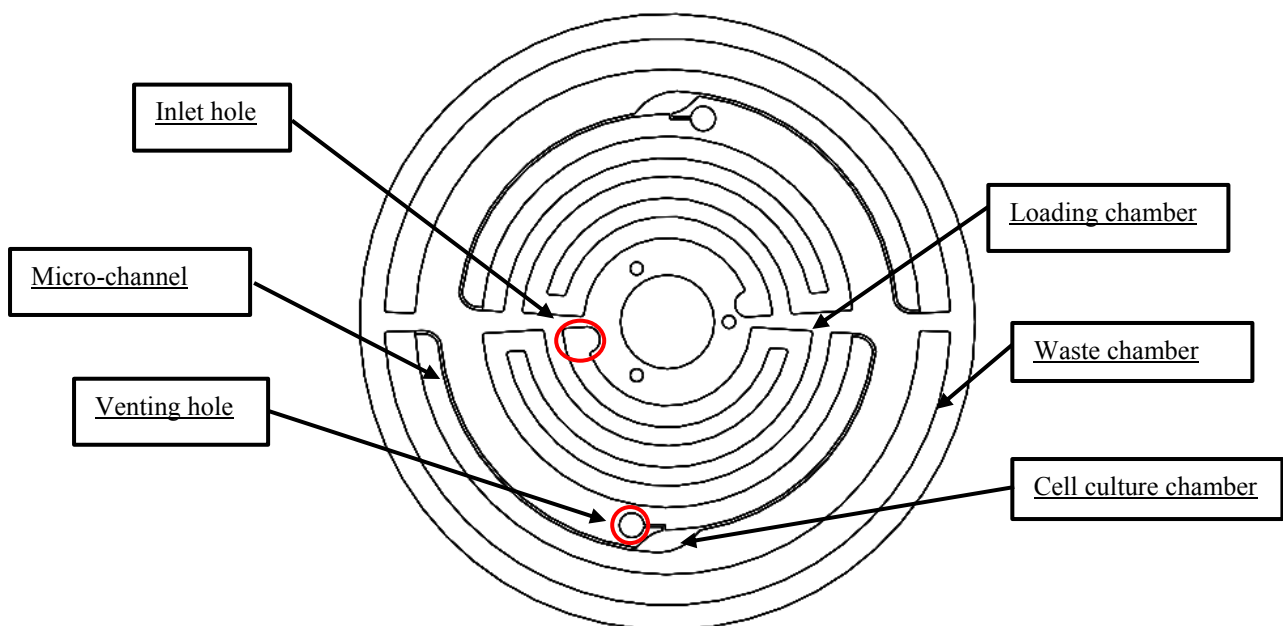


Figure 3.2 First prototype features.

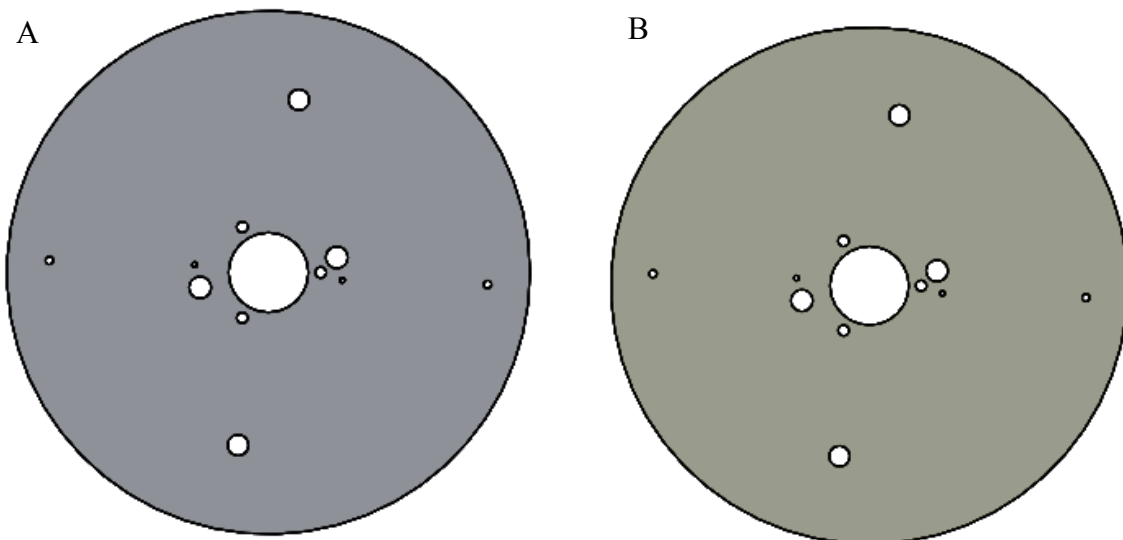
3.1.2 Fabrication

As mentioned earlier, the first prototype was fabricated using two different fabrication methods: CO₂ laser ablation and micro-milling.

3.1.2.1 Fabrication with CO₂ laser and bonding press

In this case, five different layers composed the disc (Figure 3.3 (A), 3.3 (B), 3.3 (C), 3.3 (D), 3.3 (E), 3.3 (F)):

- A. 2 mm thick PMMA layer with loading, venting and alignment holes,
- B. 0.150 mm thick PSA layer with loading, venting and alignment holes,
- C. 2 mm thick PMMA layer with loading chamber, waste chamber, cell chamber, micro-channels and alignment holes,
- D. 0.150 mm thick PSA layer with loading chamber, waste chamber and alignment holes,
- E. 2 mm thick PMMA layer.



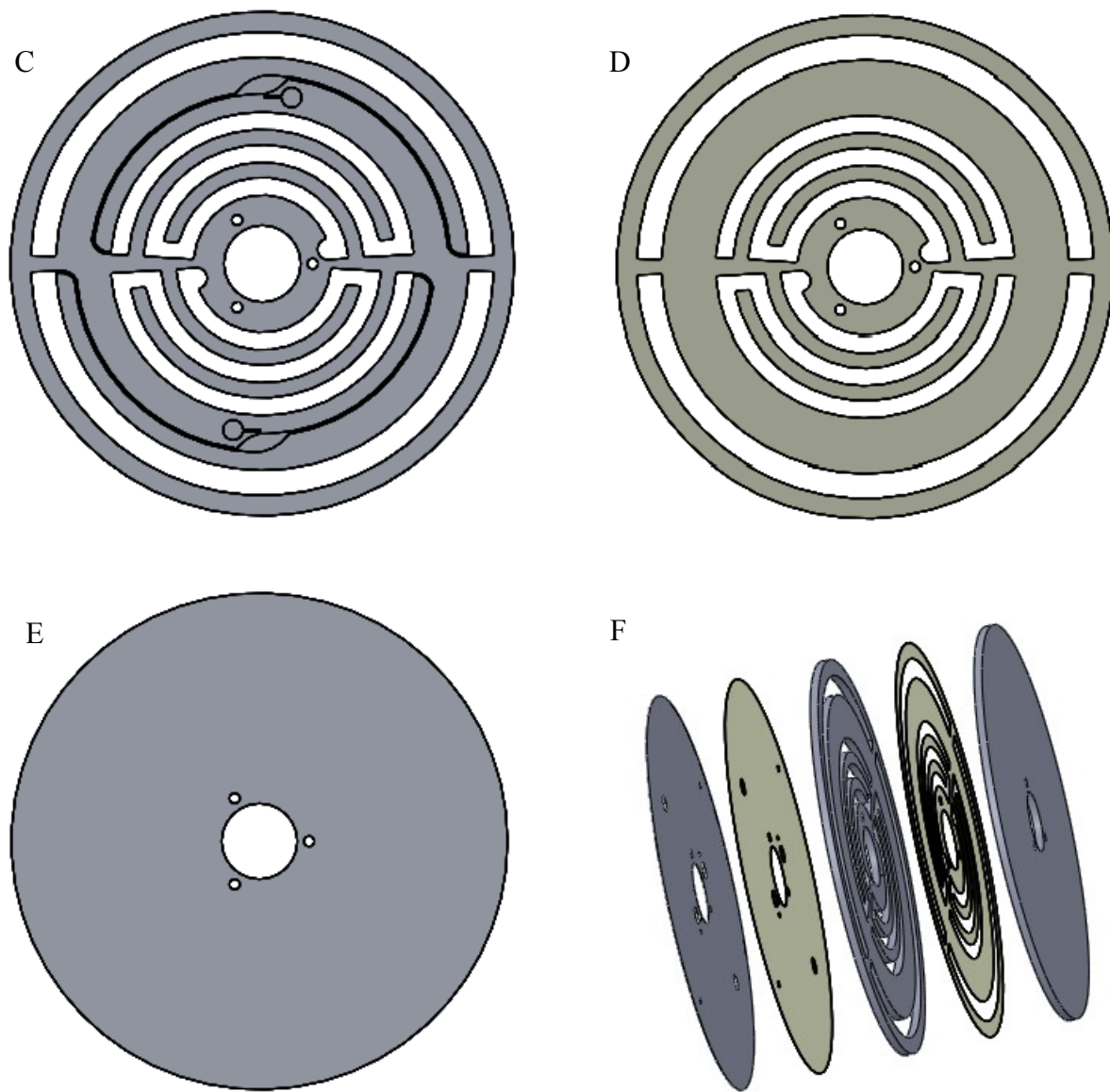


Figure 3.3: (A) top PMMA layer, (B) top PSA layer, (C) layer in PMMA with loading, waste, cell chambers and micro-channels, (D) layer in PSA with loading and waste chambers (E) bottom layer in PMMA (F) Assembly.

The parameters of CO₂ laser ablation that were used to cut and to engrave the structures are reported in the second chapter “Materials and methods”. After the fabrication, the layers were joined together and pressed with a force of 12 kN for five minutes using the bonding press (Figure 3.4).

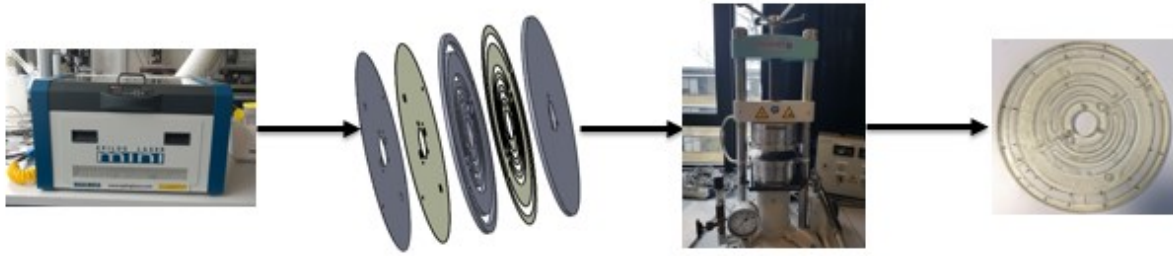
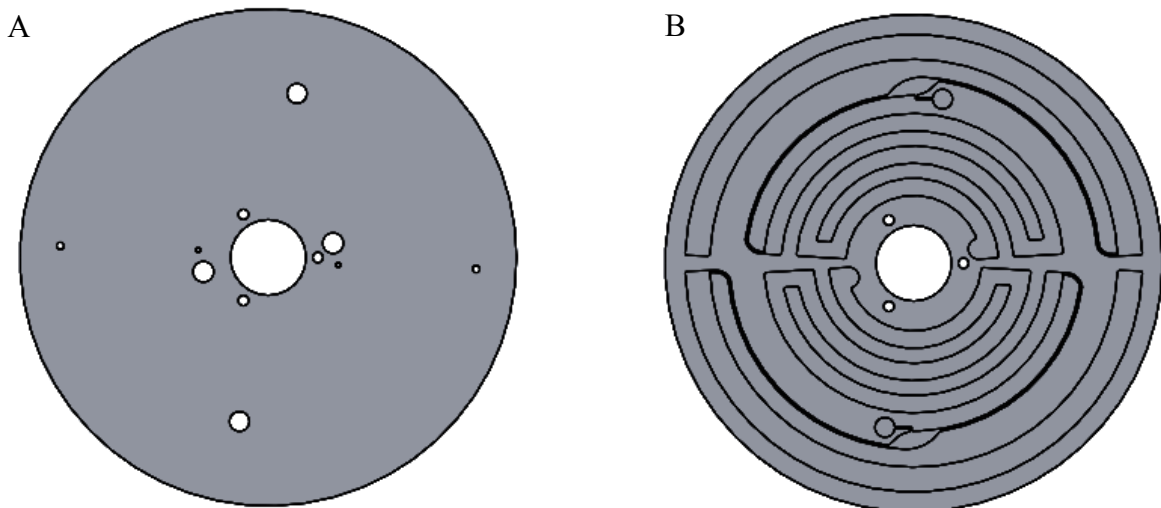


Figure 3.4: Disc's layers were fabricated with CO₂ laser ablation, then they were joined through PSA layers and pressed with bonding press.

3.1.2.2 Fabrication with micro-milling, CO₂ laser and thermal bonding

In this case, only two layers composed the disc (Figure 3.5 (A), Figure 3.5 (B) and Figure 3.5 (C)):

- A. 0.6 mm thick PMMA layer with inlet, venting and alignment holes,
- B. 3 mm thick PMMA layer with loading, waste, cell culture chambers, micro-channels and alignment holes.



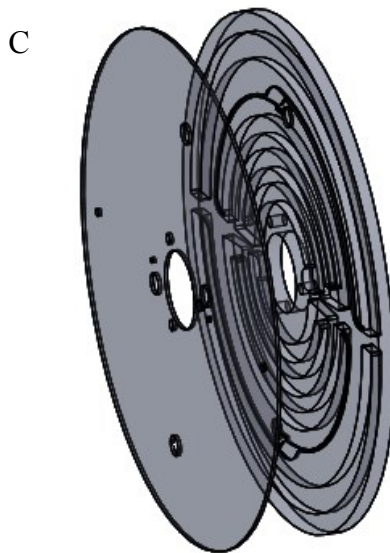


Figure 3.5: (A) Top PMMA layer, (B) PMMA layer with loading, waste, cell culture chambers and micro-channels, (C) Fully assembled system.

The inlet, venting and alignment holes on the top layer (Figure 3.5 (A)) were fabricated with CO₂ laser ablation, while the structures on the second layer (Figure 3.5 (B)) were made with micro-milling. After the fabrication, the two layers were bonded together with thermal bonding. The parameters used for ablation, milling and thermal bonding are reported in the second chapter: “Materials and methods” (Figure 3.6).

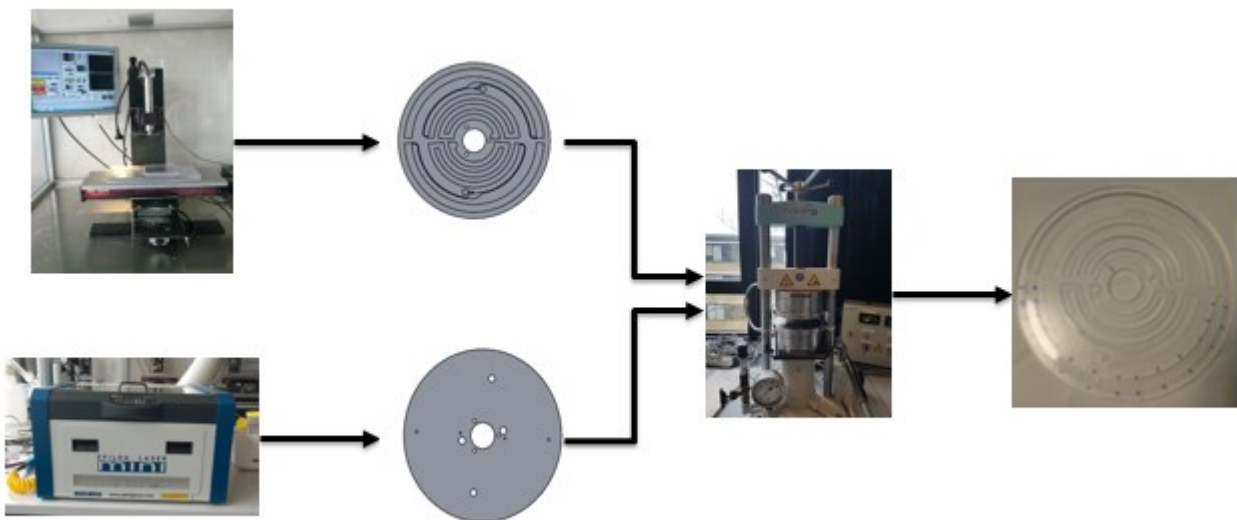


Figure 3.6: The disc layers fabricated with both laser ablation and micro-milling and bonded with thermal bonding.

3.1.3 Flow rate evaluation

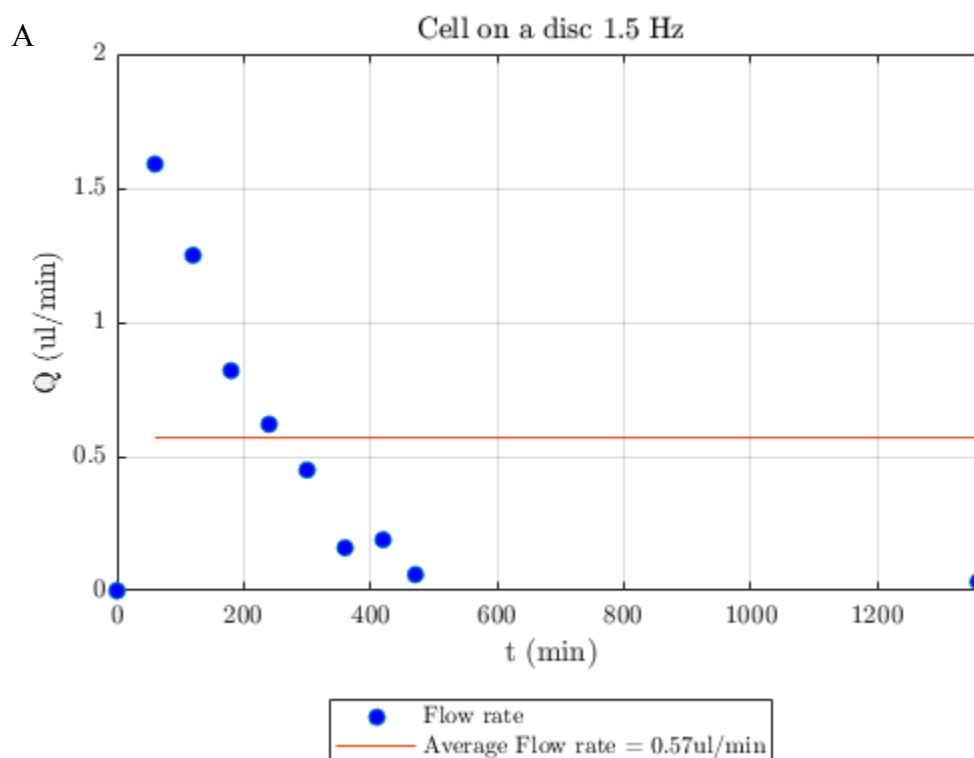
As mentioned in chapter one is important to create a suitable environment for the cells, so it is necessary that we achieve a stable flow rate.

3.1.3.1 Fluidic tests of first prototype, fabricated with CO₂ laser ablation

The disc fabricated with CO₂ laser was tested two times with a rotational frequency of 1.5 Hz, spinning the disc counterclockwise and using both high-purity water with and without food dye.

High-purity water or “ultrapure water” was obtained with several step of filtration, through resin filters, and deionization[77].

To calculate the flow rate in the way it was reported in the second chapter, a picture of waste chamber was taken every hour for eight hours in the first experiment and six hours in the second experiment. In both experiments then the disc was left to spin overnight. The results obtained are reported in two different graphs, where the flow rate is represented over time (Figure 3.7 (A), 3.7(B)).



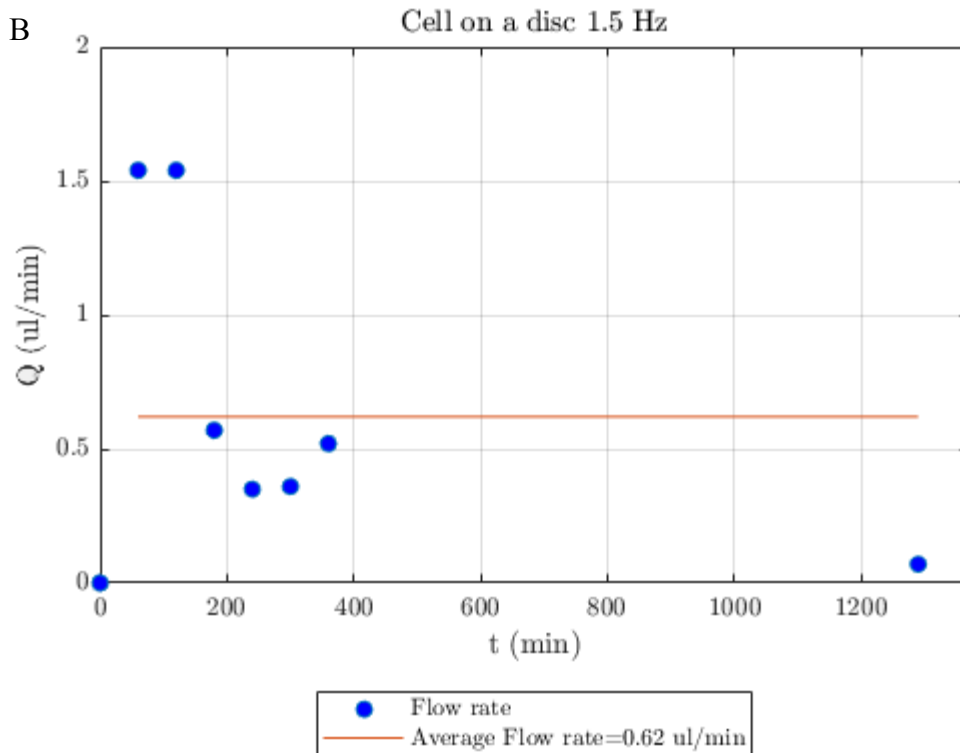


Figure 3.7: (A) Results obtained testing the disc at a rotational frequency of 1.5 Hz, with “ultrapure” water plus food dye for eight hours and leaving it to spin overnight. (B) Results obtained testing the disc at rotational frequency of 1.5 Hz, with only “ultrapure” water for six hours and leaving it to spin overnight.

The results show that the average flow rate was similar in the both experiments (0.57 $\mu\text{l}/\text{min}$ in the first one and 0.62 $\mu\text{l}/\text{min}$ in the second one). However, the flow rate decremented from a value of about 1.6 $\mu\text{l}/\text{min}$ to a value of 0.03 $\mu\text{l}/\text{min}$ during the first test and from a value of about 1.5 $\mu\text{l}/\text{min}$ to 0.07 $\mu\text{l}/\text{min}$ in the second test.

3.1.3.2 Fluidic tests of the first prototype fabricated with micro-milling

Since the previously obtained results suggested that there is no relevant flow rate difference between the test carried out with ultrapure water in the presence or absence of food dye, this tests were carried out only with ultrapure water as previously described. The test was performed two times at a rotational frequency of 1.25 Hz. The results obtained are reported in Figure 3.8 (A) and 3.8 (B).

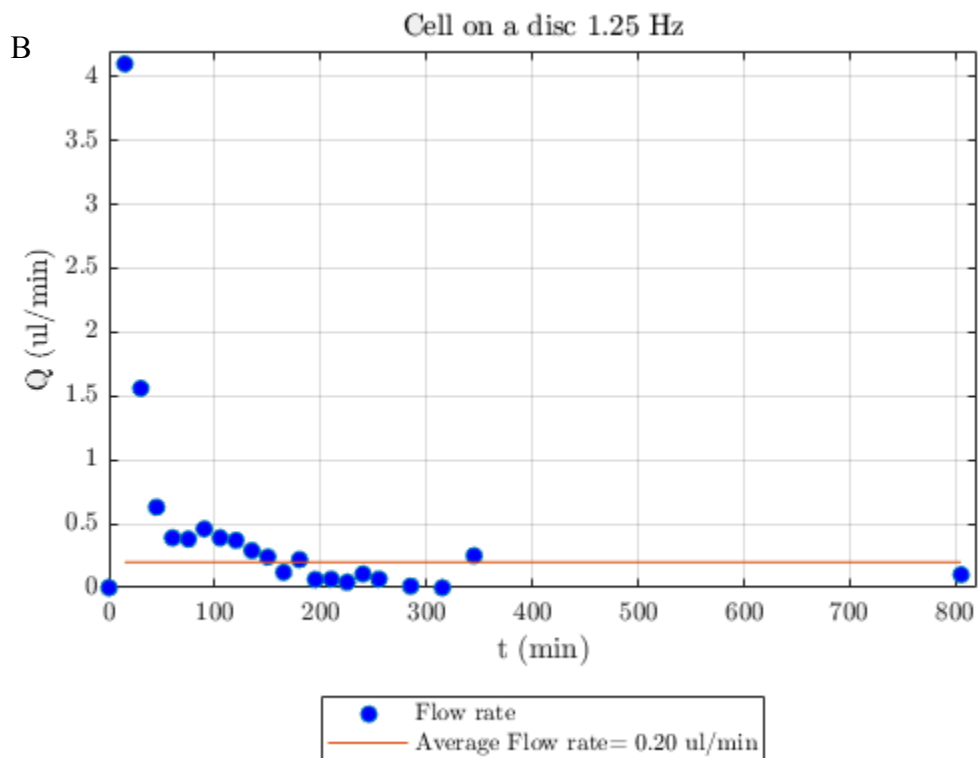
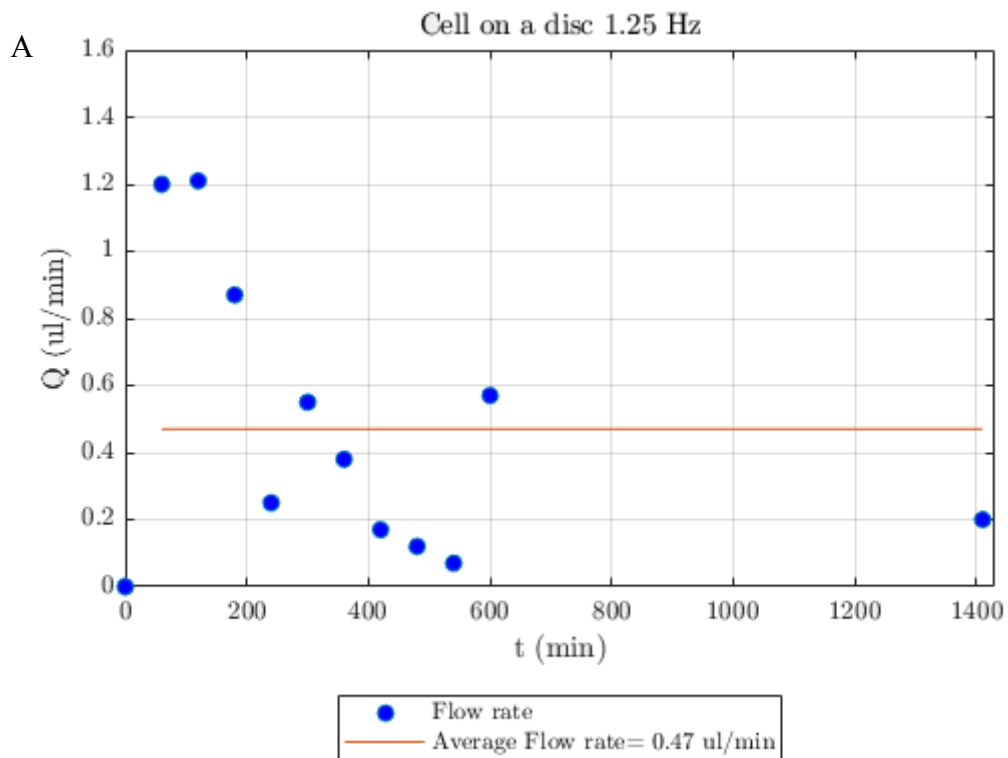


Figure 3.8: (A) Results obtained testing the disc at rotational frequency of 1.25 Hz, with “ultrapure” water for ten hours and leaving it to spin overnight. (B) Results obtained testing the disc at rotational frequency of 1.25 Hz, with “ultrapure” water for about six hours and leaving it overnight.

The results show that the flow rates obtained were not stable: they decremented during the first hour, then there were picks where the flow rates took higher values and after these picks, they started to decrement again. Furthermore, the average flow rates were different: $0.47\mu\text{l}/\text{min}$ for the first experiment and $0.20\mu\text{l}/\text{min}$ for the second experiment.

3.2 Second prototype design of the cell culture on disc device

This section presents the second design, its fabrication, fluidic test and the results obtained.

3.2.1 Description of the second design

The second design was similar to the first one; the only difference is that the loading chamber was modified in order to have a more stable flow rate. It was composed by two channels very close each other, to avoid the possible pressure difference between the channels, as it will be explained in detailed in the section 3.3 first and second prototype design problem'. In this design each channel had a width of 4.40 mm and a depth of 1.5 mm (Figure 3.9)

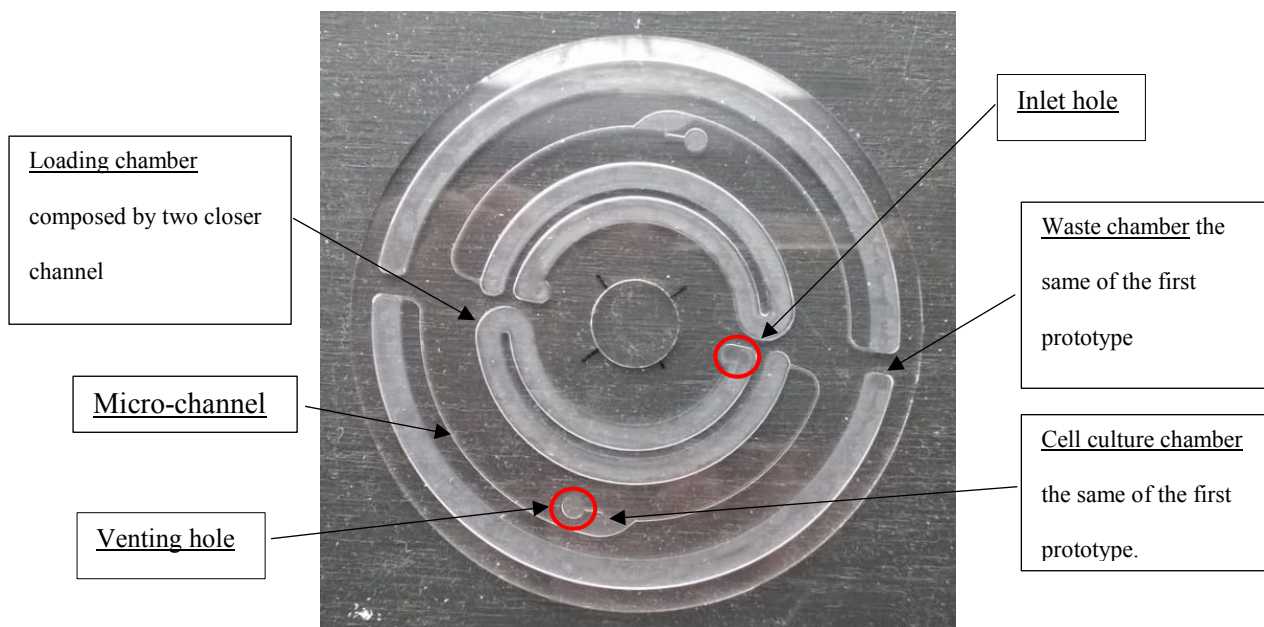


Figure 3.9: Second prototype design.

3.2.2 Fabrication

Two layers composed the disc (Figure 3.10 (A), Figure 3.10 (B) and Figure 3.10(C)):

- A. a 0.6 mm thick PMMA layer with inlet and venting holes,
- B. a 2 mm thick PMMA layer with loading, waste, cell chambers and micro-channels

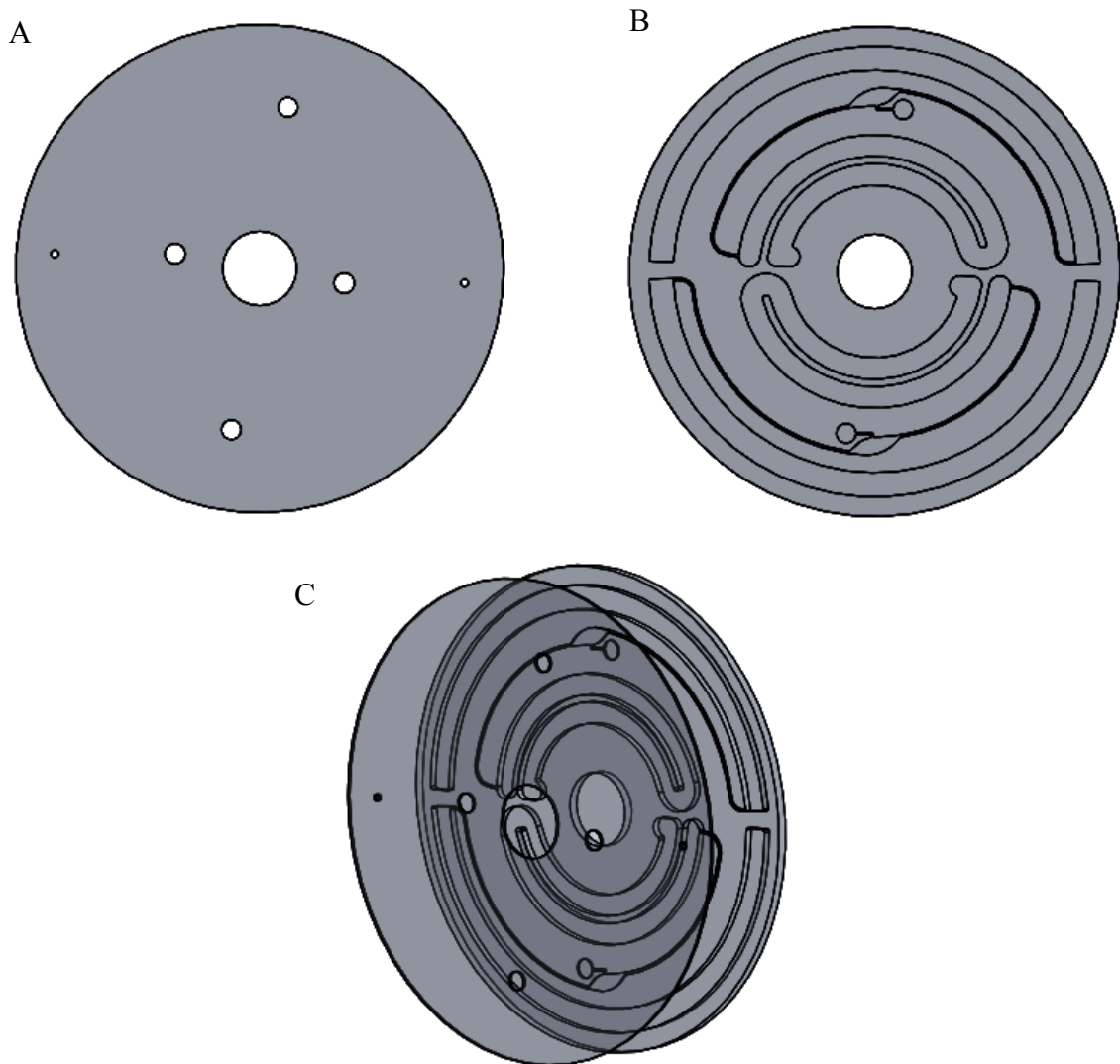


Figure 3.10: (A) Top layer with inlet and venting holes. (B) layer with loading, waste, cell chambers and micro-channels. (C) Fully assembled prototype.

The inlet and venting holes on the top layer were realized with CO₂ laser, while the structures on the second layer were fabricated with milling machine. After the fabrication, the two layers were bonded with thermal bonding to avoid the adhesive layers that could affect the fluid flow inside the

disc. The parameters for CO₂ laser ablation, micro-milling and thermal bonding are reported in the second chapter “Materials and methods” (Figure 3.11).

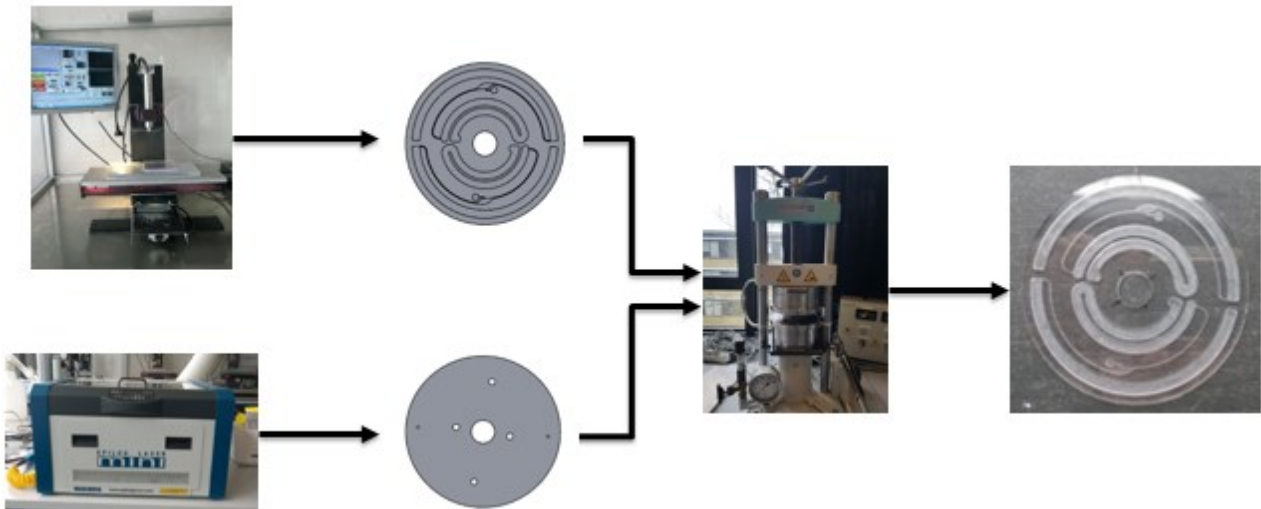


Figure 3.11: The disc's layers were fabricated with both CO₂ laser ablation and micro-milling and joined with thermal bonding.

3.2.3 Evaluation of flow rate

The cell culture on disc system was tested at different rotational frequencies: 3.5Hz, 3Hz, 2.5Hz and 2 Hz, spinning it counterclockwise and using only “ultrapure” water. During the tests, photos of waste and loading chambers were taken. We took images of loading chamber to be able to correlate the position of liquid with the changes in the flow rate, as we observed previously. The results obtained are reported in Figure 3.12 (A), Figure 3.12 (B), Figure 3.12 (C), Figure 3.12 (D) and Figure 3.12 (E).

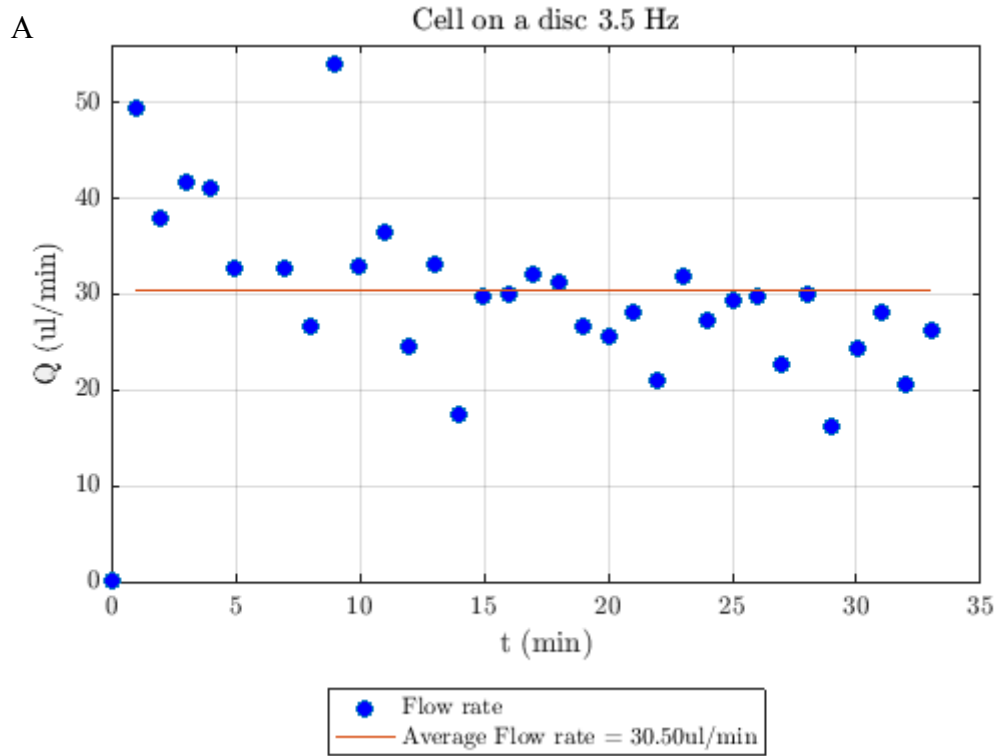


Figure 3.12 (A): Flow rate during the fluidic test and its average value.

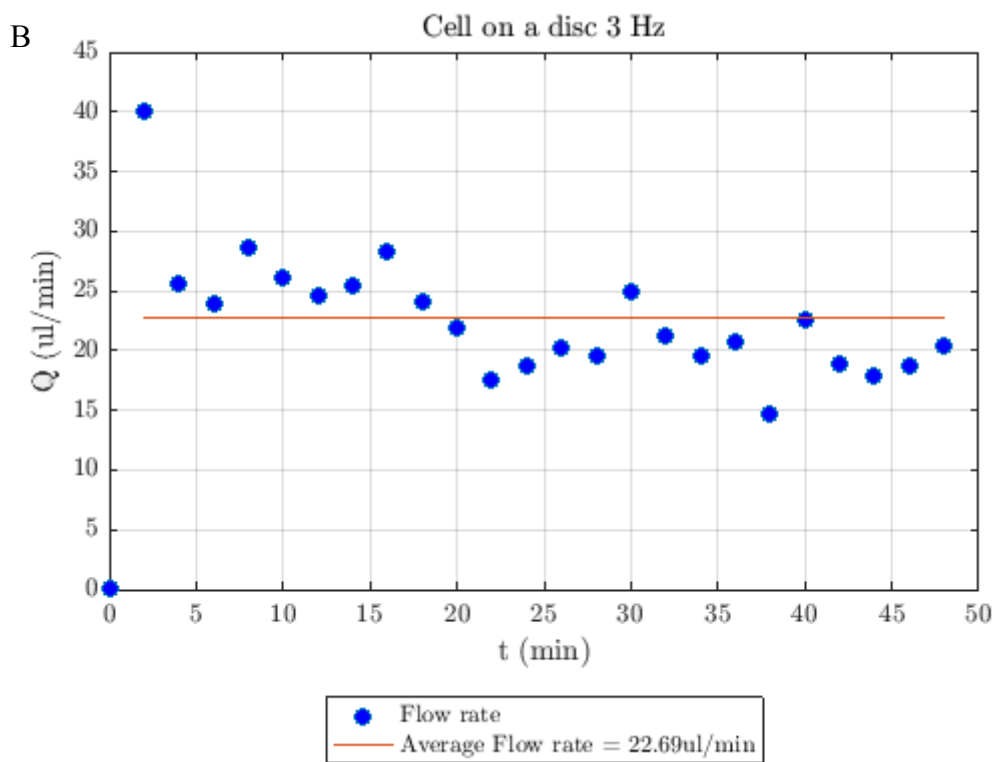


Figure 3.12 (B): Flow rate during the fluidic test and its average value.

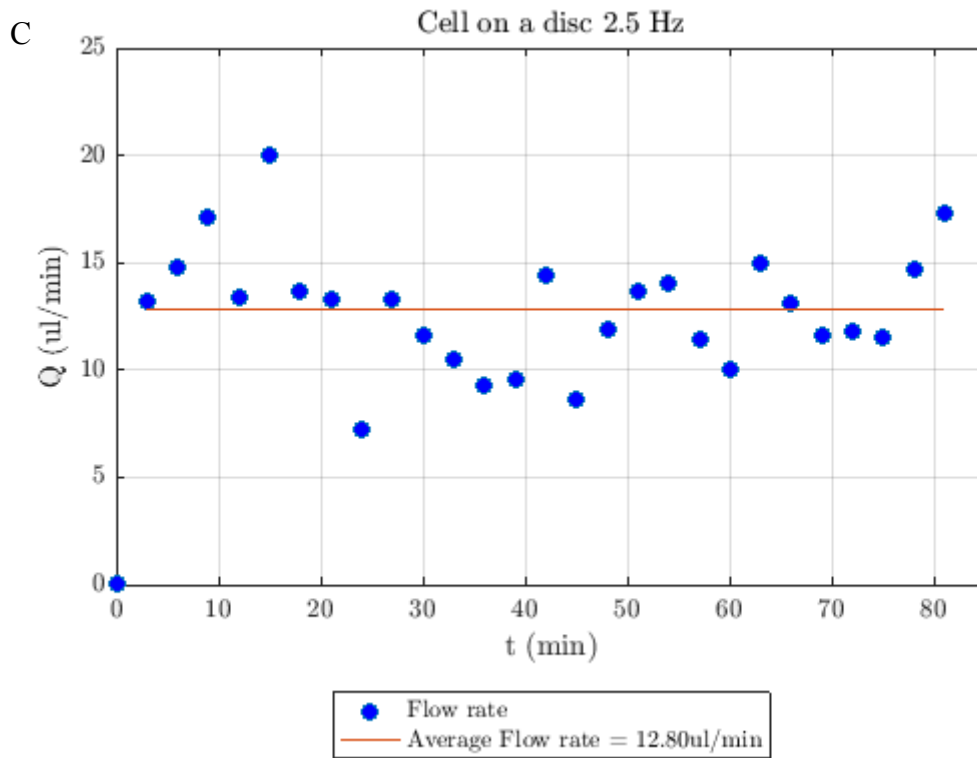


Figure 3.12 (C): Flow rate during the fluidic test and its average value.

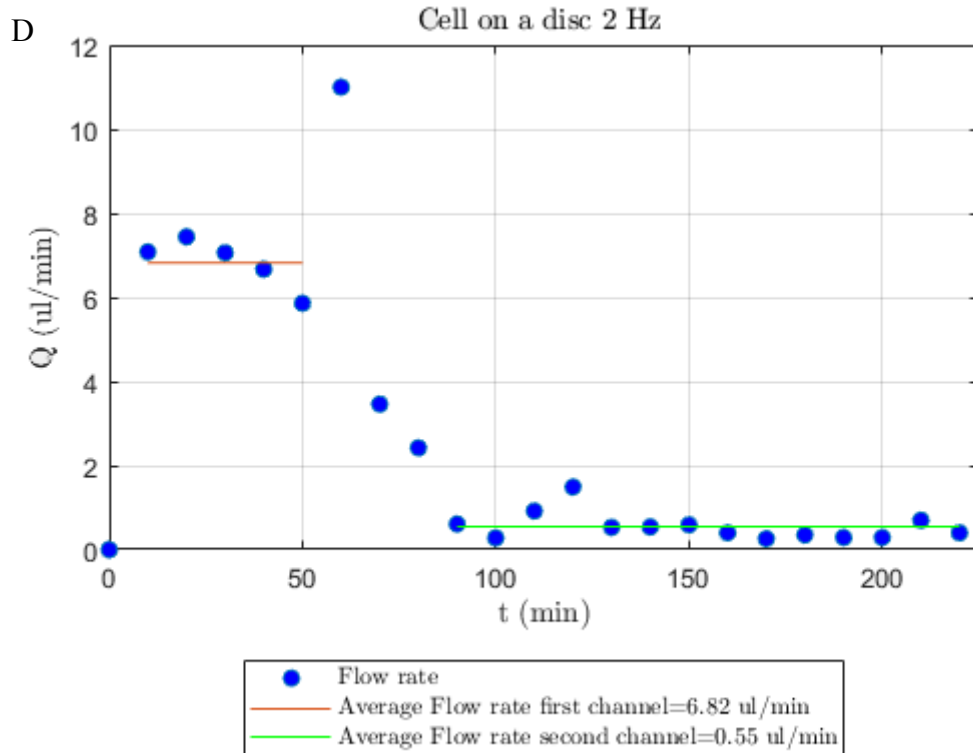


Figure 3.12 (D): Flow rate during the fluidic test and its average value.

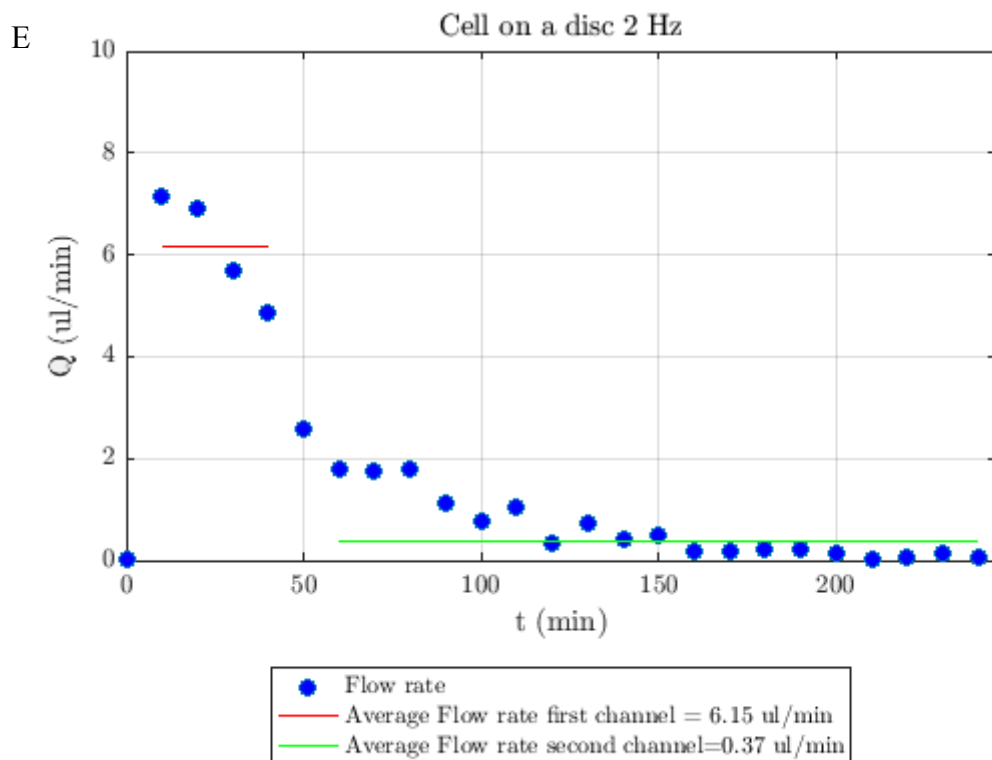


Figure 3.12 (E): Flow rate during the fluidic test and its average value.

The results in Figure 3.12 (A), Figure 3.12 (B), Figure 3.12 (C) show that the flow rate was not stable, while in Figure 3.12 (D) and Figure 3.12 (E), both obtained spinning the disc at a rotational frequency of 2 Hz, we noticed that there is a correlation between the location of the liquid in the inlet reservoir channel and the changes in flow rate (Figure 3.13). When the fluid was in the first channel of reservoir, the flow rate assumed higher values than those assumed in the second channel, which means that probably there still a significant difference in pressure between the channels, which effect can be observed at low rotational frequencies.

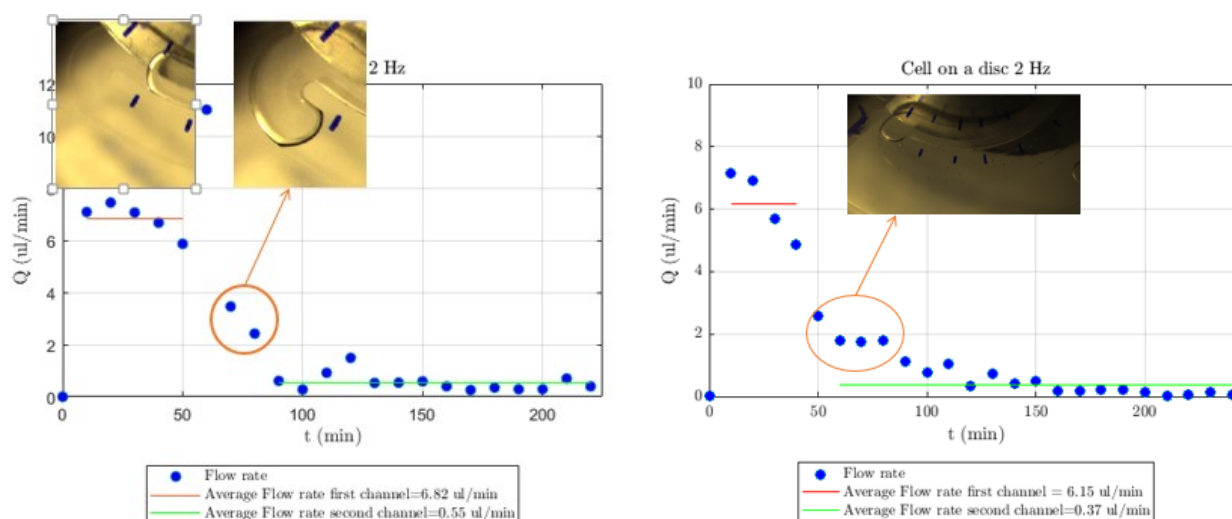


Figure 3.13: In both experiments done at low rotational frequency (2Hz) we can see that the flow rate assumed higher values when the fluid was in the first channel of loading chamber. The flow rate value started to decrease during the passage from the first channel to the second one.

3.3 Problem with first and second prototype design

The flow rates in first and second design were not stable. It was seen that this problem was not due to PSA used to join together the device's layers, so a more accurate analysis about the centrifugal microfluidic physics was done.

From the theory, the fluidic control on a rotating system occurs through three principal forces (the centrifugal force, Coriolis force and Euler force) that arise from the disc rotation and they are discussed in the Appendix.

The centrifugal force is the force that permits to move the fluid from the center of the disc radially outward. This force depends on the square of angular velocity and on the distance from the center of the disc; keeping the angular velocity constant, centrifugal force increases if the distance from the center of rotation increases. However, it is better to use centrifugal pressure present on a liquid plug than vectorial force. The differential centrifugal pressure (ΔP_w) on a radial column of fluid can be achieved by integrating the magnitude of centrifugal force from radius r_1 to r_2 , where $r_2 - r_1$ is the column fluid radial length [78]:

$$\Delta P_w = \int_{r_1}^{r_2} \rho \omega^2 r dr = \frac{1}{2} \rho \omega^2 (r_2^2 - r_1^2) \quad (2)$$

The differential centrifugal pressure between the loading chamber and waste chamber of first and second design were calculated used equation (2)

First prototype design

In the first design, three channels composed the loading chamber, so the differential pressures between first and waste channel, between second and waste channel and between the third and waste channel were calculated. Each channel had a circular geometry so to calculate the pressure the mean radius of each of them was taken (Figure 3.14).

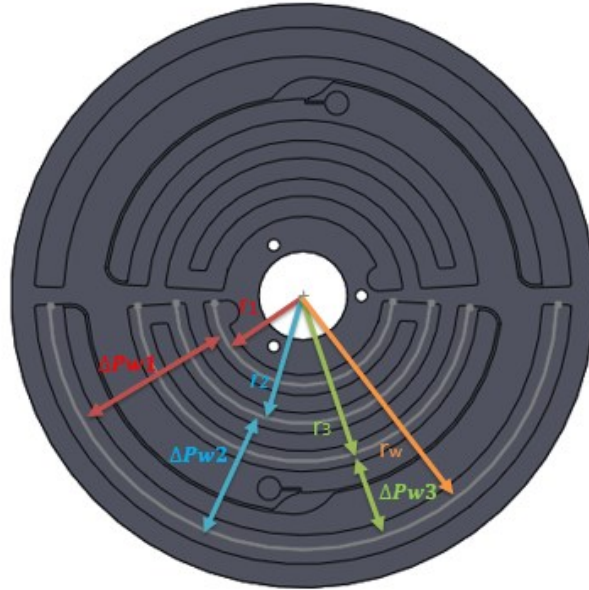


Figure 3.14: CAD design with differential centrifugal pressures.

For the tests a rotational frequency of $f = 1.25 \text{ Hz}$ ($\omega = 2\pi f = 7.85 \text{ rad/s}$) was chosen and water was used ($\rho = 1000 \frac{\text{kg}}{\text{m}^3}$) so:

1. $\Delta P_{w1} = \frac{1}{2} \rho \omega^2 (r_w^2 - r_1^2) = 51.01 \text{ Pa}$
2. $\Delta P_{w2} = \frac{1}{2} \rho \omega^2 (r_w^2 - r_2^2) = 43.55 \text{ Pa}$
3. $\Delta P_{w3} = \frac{1}{2} \rho \omega^2 (r_w^2 - r_3^2) = 33.49 \text{ Pa}$

From the calculations:

$$\Delta P_{w3} < \Delta P_{w2} < \Delta P_1$$

This result shows why the flow rate decreased during the fluidic tests: moving from the first channel to third channel of loading chamber, the differential pressure decreased so also the flow rate reduced its value.

Second prototype design

In the second design, two closer channels composed the loading chamber so the differential centrifugal pressure between each channel and waste chamber was calculated (Figure 3.15).

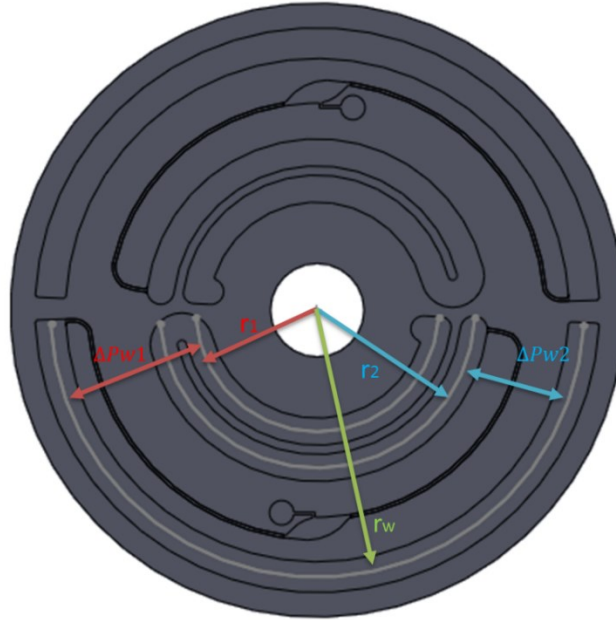


Figure 3.15: CAD design with the differential centrifugal pressures.

For the fluidic test a rotational frequency of 1.5 Hz ($\omega = 2\pi f = 9.42 \text{ rad/s}$) was chosen and water ($\rho = 1000 \text{ kg/m}^3$) was used so:

1. $\Delta P_{w1} = \frac{1}{2} \rho \omega^2 (r_w^2 - r_1^2) = 66.54 \text{ Pa}$
2. $\Delta P_{w2} = \frac{1}{2} \rho \omega^2 (r_w^2 - r_2^2) = 54.63 \text{ Pa}$

From the calculations:

$$\Delta P_{w2} < \Delta P_{w1}$$

This results means that moving from the first channel to second one, the differential pressure decreased and so also the flow rate, indeed, when the liquid was in the first channel the flow rate assumed higher values than those assumed when the liquid was in the second channel of the loading chamber (Figure 3.13). Even if the channels in this case were closer to each other, the pressure difference was still significant when low rotational speeds were used.

3.4 Solution: design on the third prototype

3.4.1 Description of design

To solve the problem of previous designs a third design was realized. It was composed of a single loading chamber, cell culture chamber, waste chamber as well as the micro-channels, inlet and venting holes (Figure 3.16).

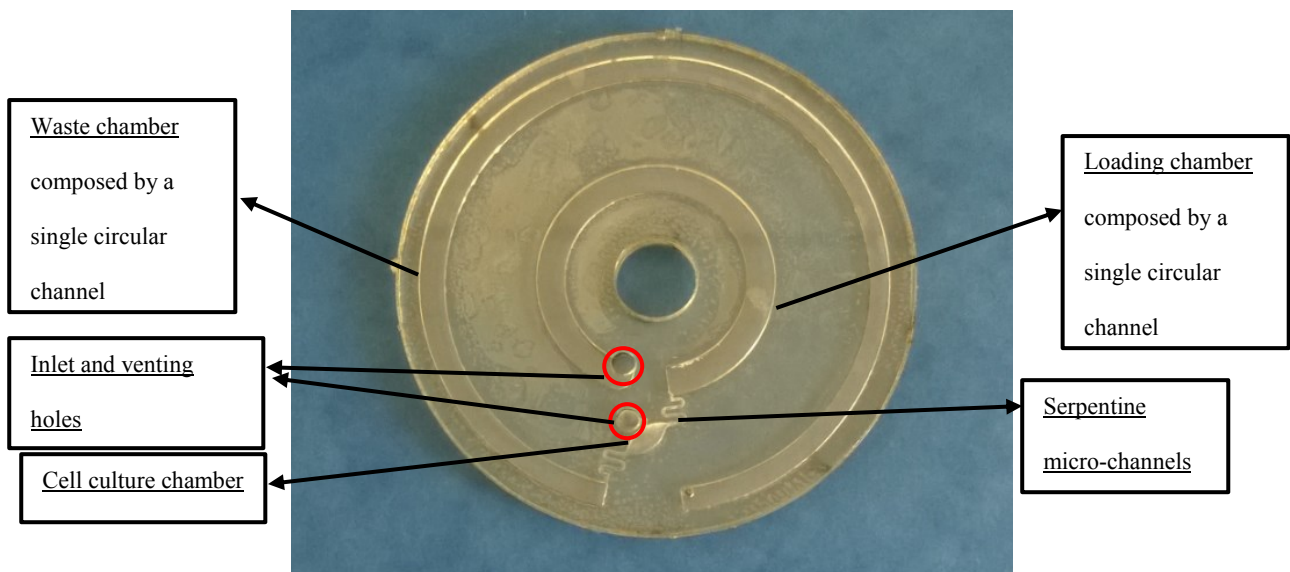


Figure 3.16: Photograph of the third design.

A single circular channel with a width of 5 mm and depth of 2 mm composed the loading chamber. Before to choose a width of 5 mm, three different widths: 8mm, 5.5 mm and 5mm were tested (Figure 3.17 (A), Figure 3.17 (B), Figure 3.17 (C)) in order to verify which value permitted to have a good fluid front during the fluidic test. An example of what means a good fluid front is reported in figure 3.18.

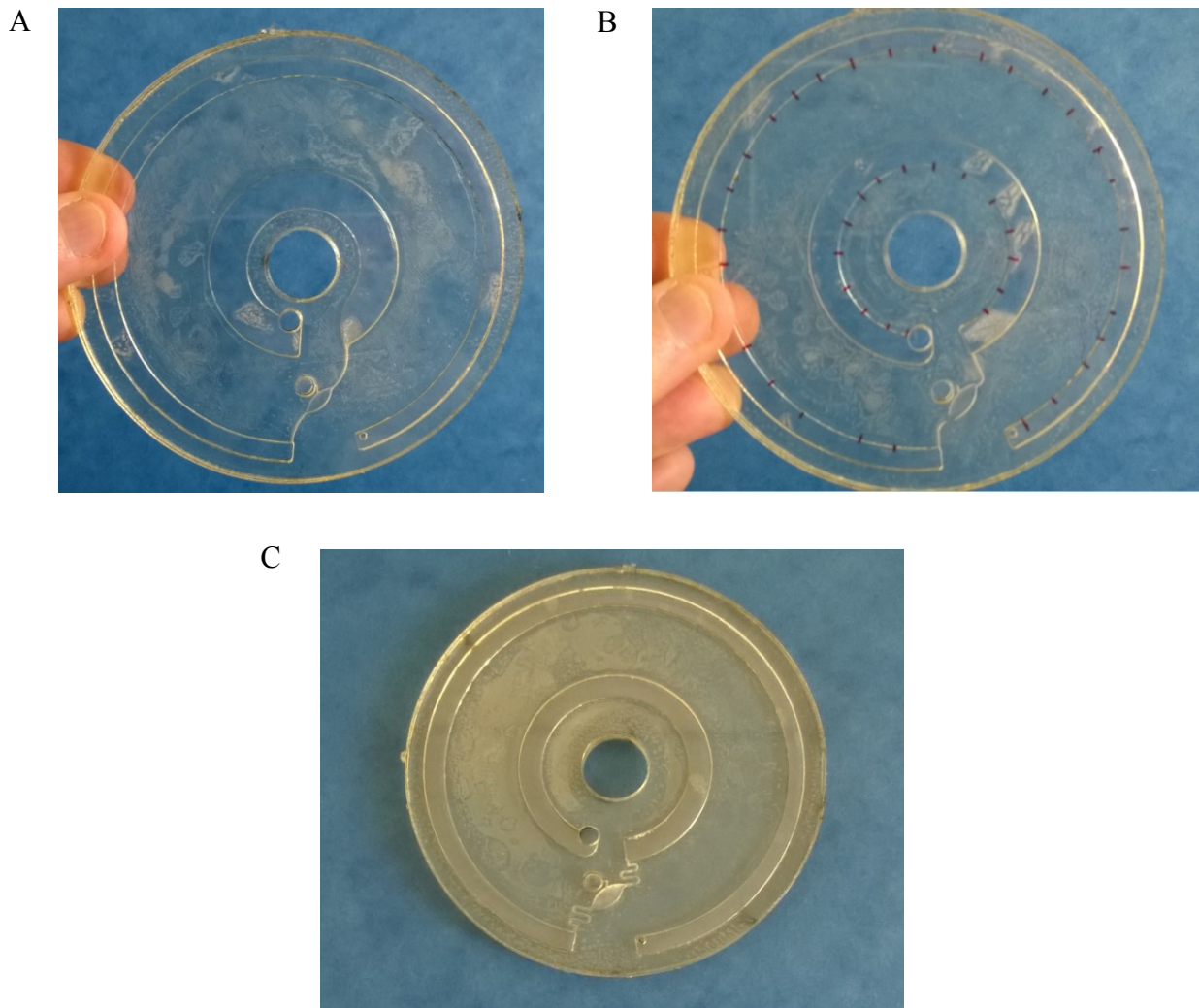


Figure 3.17: (A) The loading channel with a width of 8mm. (B) The loading channel with a width of 5.5 mm. (C) The loading channel with a width of 5mm.

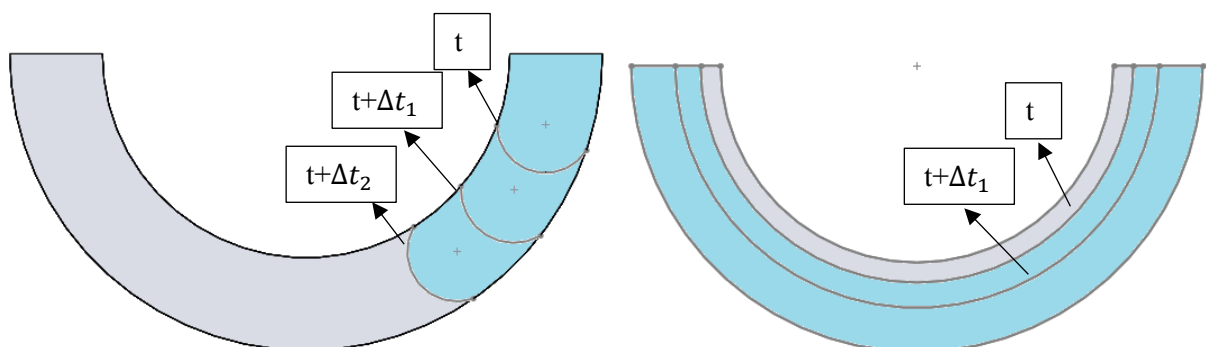


Figure 3.18 A good fluid front (left) can be achieved if the channel has an appropriate width. If the channel is too large the fluid moves as reported on the right side.

It was seen that the channel with a width of 5 mm allowed a good fluid front.

The waste chamber was composed by a single circular channel with a width of 4 mm and a depth of 2 mm. In this way, having a single channel both for loading and waste chamber, the same differential centrifugal pressure between them was always present ($\Delta P_{w1} = \frac{1}{2} \rho \omega^2 (r_w^2 - r_1^2)$) (Figure 3.19)

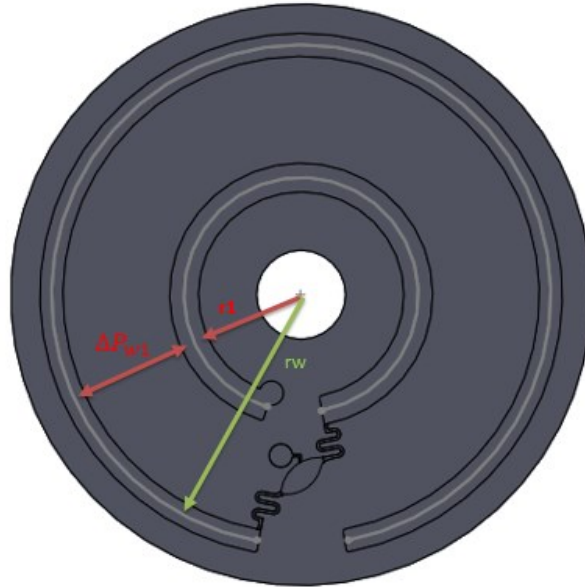


Figure 3.19: CAD drawing of the design with the differential centrifugal pressure between loading and waste chamber.

The cell chamber was not modified, while the two micro-channels, which connected the cell chamber to two reservoirs, were designed with a serpentine shape in order to have low shear stress inside the chamber.

3.4.2 Fabrication technique

At first, the third design was fabricated with the rapid prototyping technique, CO₂ laser ablation, in order to perform initial fluidic tests and evaluate the flow rates.

Five layers composed the disc (Figure 3.20 (A), Figure 3.20(B), Figure 3.20 (C), Figure 3.20 (D), Figure 3.20 (E) and Figure 3.20 (F)).

A. a 2 mm thick PMMA layer with inlet and venting holes,

- B. a 0.150 μm thick PSA layer with inlet and venting holes,
- C. a 2 mm thick PMMA layer with loading, cell culture, waste chambers and micro-channels,
- D. a 0.150 μm thick PSA layer with loading, cell culture and waste chamber,
- E. a 2mm thick PMMA layer used as lid.

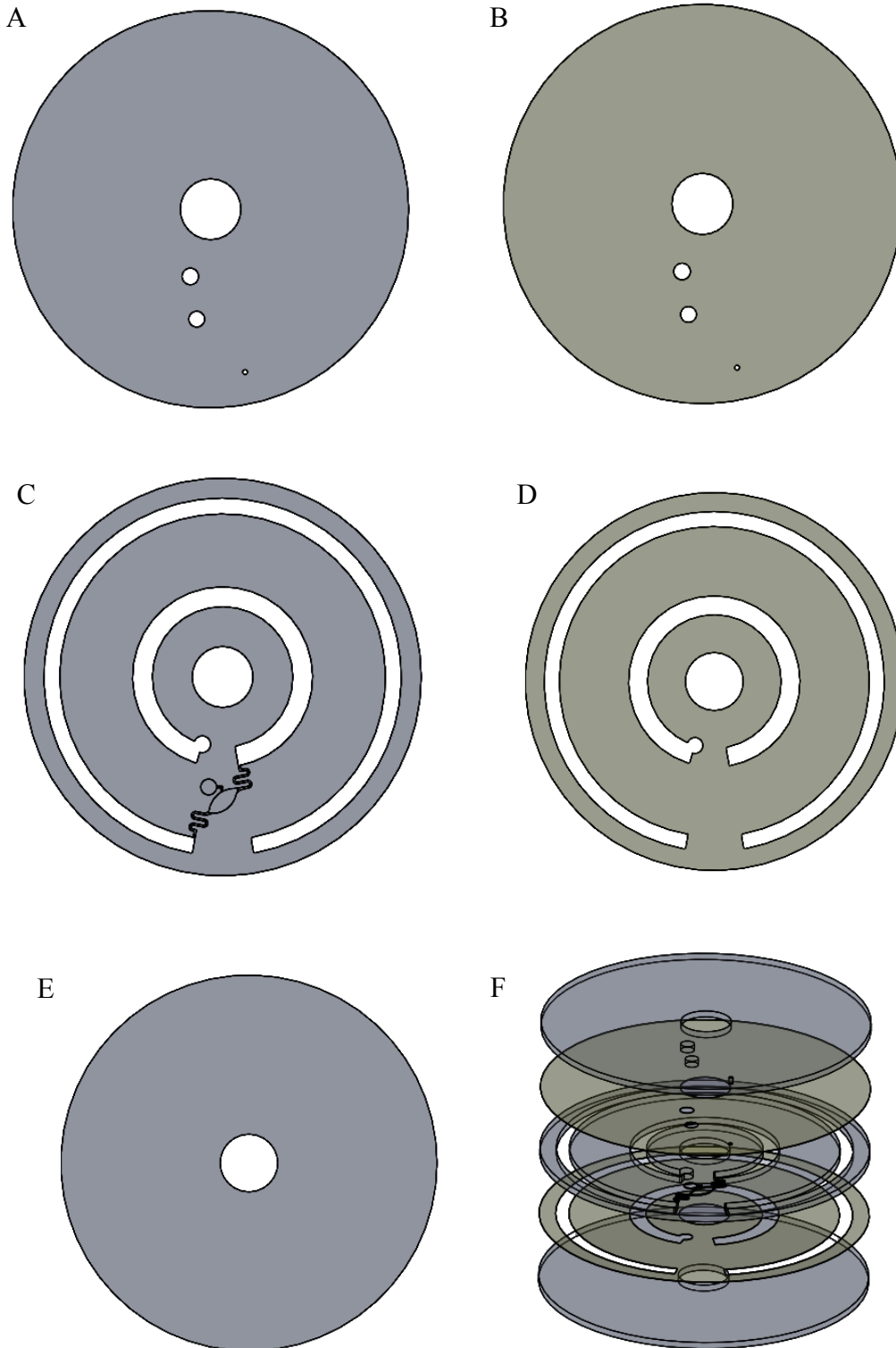


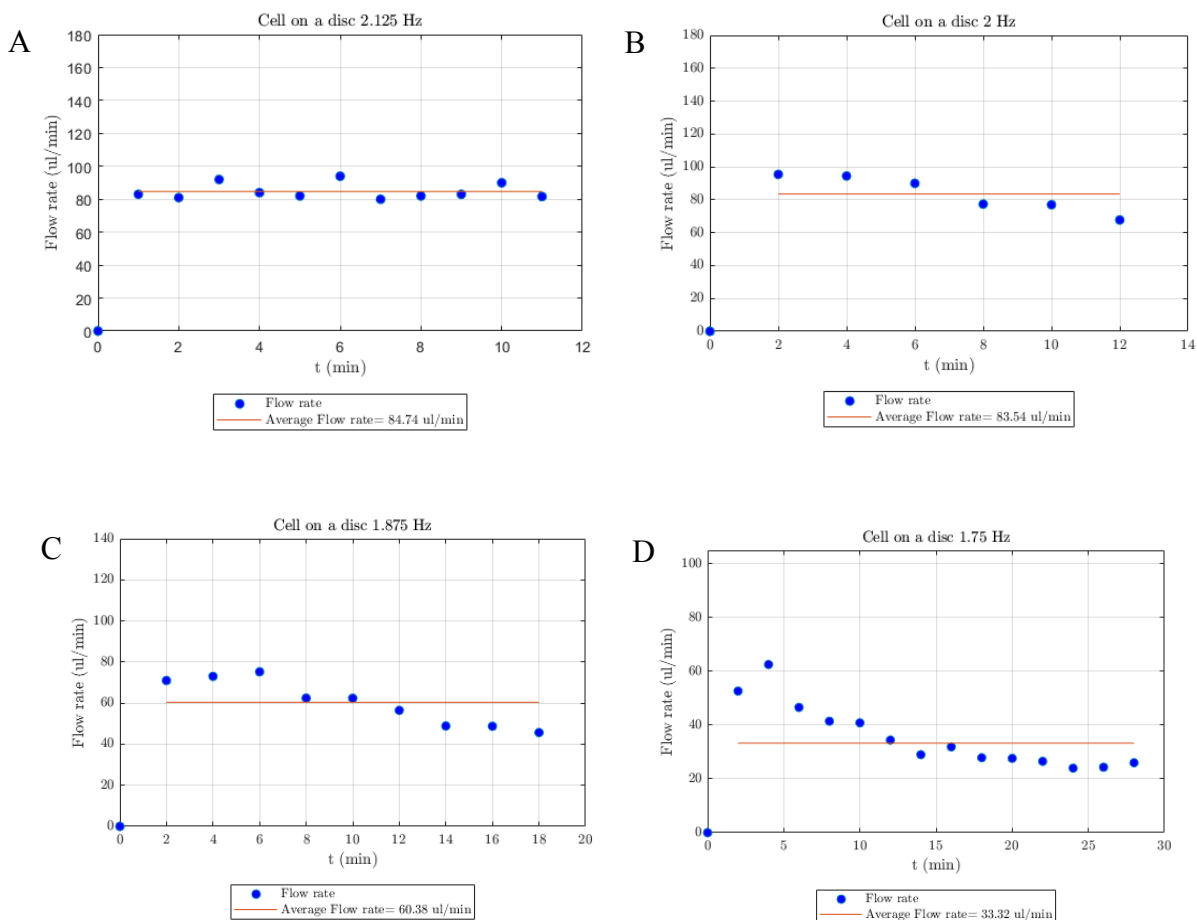
Figure 3.20: (A) top layer with inlet and venting holes. (B) PSA layer with inlet and venting holes. (C) PMMA layer with loading, cell, waste chambers and micro-channels. (D) PSA layer with loading and waste chambers. (E) PMMA layer. (F) Fully assembled fluidic system.

The parameters of CO₂ laser ablation that were used to cut the PMMA and PSA layers and to engrave the structure on PMMA are reported in the second chapter “Materials and methods”. After the fabrication, the different layers were bond together using PSA and pressed with a force of 12 kN, which was applied by bonding press, for five minutes.

3.4.3 Fluidic tests

The disc was tested at different rotational frequencies that ranged from 2.125 Hz to 1.125 Hz, spinning it counterclockwise and using only “ultrapure” water.

The results obtained are reported in Figure 3.21 (A-I)



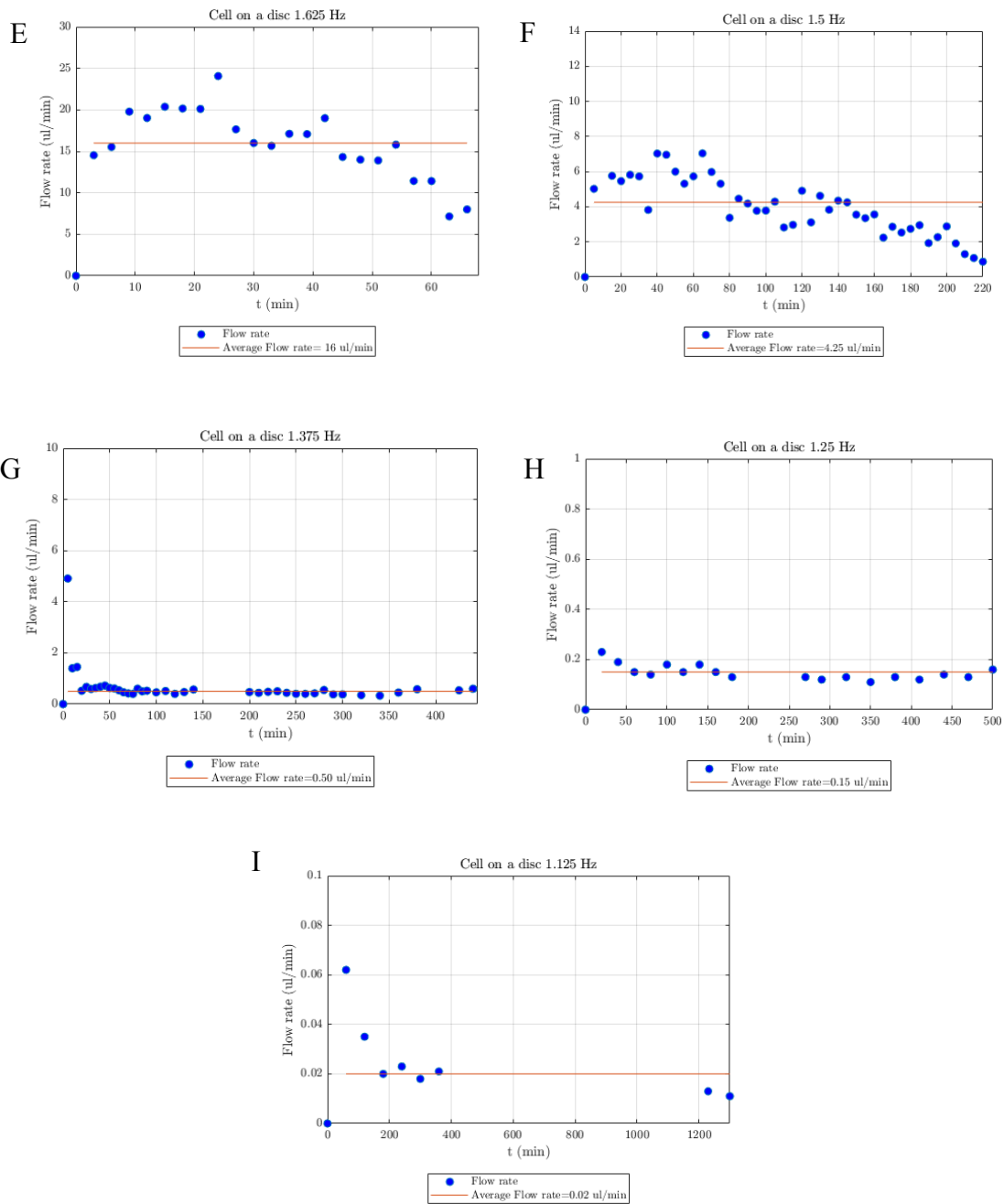


Figure 3.21 (A)-(I): Flow rates and their average values obtained testing the disc at different rotational frequencies

In most experiments, the flow rate was higher at the beginning because the disc was spinned at higher velocity to prime the system. However, the flow rates obtained were more stable than those obtained with previous designs.

Furthermore, the dependency between flow rate and rotational frequency was found (Table 1 and Figure 3.22). The figure 3.22 shows that the dependency can be approximated with a second order polynomial, indeed the velocity \mathbf{u} of liquid plug in a centrifugal microfluidic system depends on the

square of disc's angular velocity ω ($\omega = 2\pi f$ where f is the rotational frequency)[79] hence also the flow rate because it depends from the cross section area and the fluid velocity:

$$Q = A \cdot u \tag{3}$$

Table 1: Average flow rate, standard deviation (STD) and number of samples used to calculate STD for each frequency.

Frequency (Hz)	Flow rate (µl/min)	STD	Number of samples
2.125	84.74	4.96	10
2	83.54	11.26	6
1.875	60.38	11.14	9
1.75	33.32	11.82	13
1.625	16	4.11	21
1.5	4.25	2.29	43
1.375	0.50	0.73	39
1.25	0.15	0.03	17
1.125	0.02	0.016	7

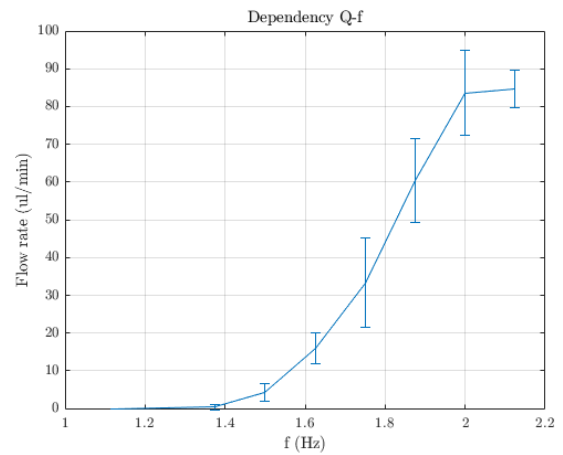


Figure 3.22: Dependency between the flow rate and the rotational frequency

Chapter 4

Lab-on-a-disc for long-term cell culture

The previously presented third design permitted to obtain stable flow rate inside the disc. The next step was to verify if it was possible to increase the volume of loading chamber in order to cultivate bacteria cells for a few days and to achieve the formation of biofilms.

In this chapter, a disc that permits a bacteria cell culture for about five days is presented.

4.1 Design and fabrication

The design of the disc was the third one presented in the previous chapter (Figure 3.20) with the only difference that loading chamber and waste chamber had a depth of 5 mm in order to have a total volume of about 3ml. As mentioned earlier, firstly, the disc was fabricated with a rapid prototyping for the initial tests. However, for bacterial culturing our goal was to create much smoother surfaces than the ones which can be achieved with laser ablation, therefore, the systems presented below were fabricated with micro-milling.

4.1.1 Fabrication with milling machine, CO₂ laser ablation and thermal bonding

In this case, only two layers composed the disc (Figure 4.1 (A), Figure 4.1 (B), Figure 4.1(C)):

- A. a 0.6 mm thick PMMA layer with inlet and venting holes,
- B. a 8 mm thick PMMA layer with loading, cell, waste chambers and micro-channels.

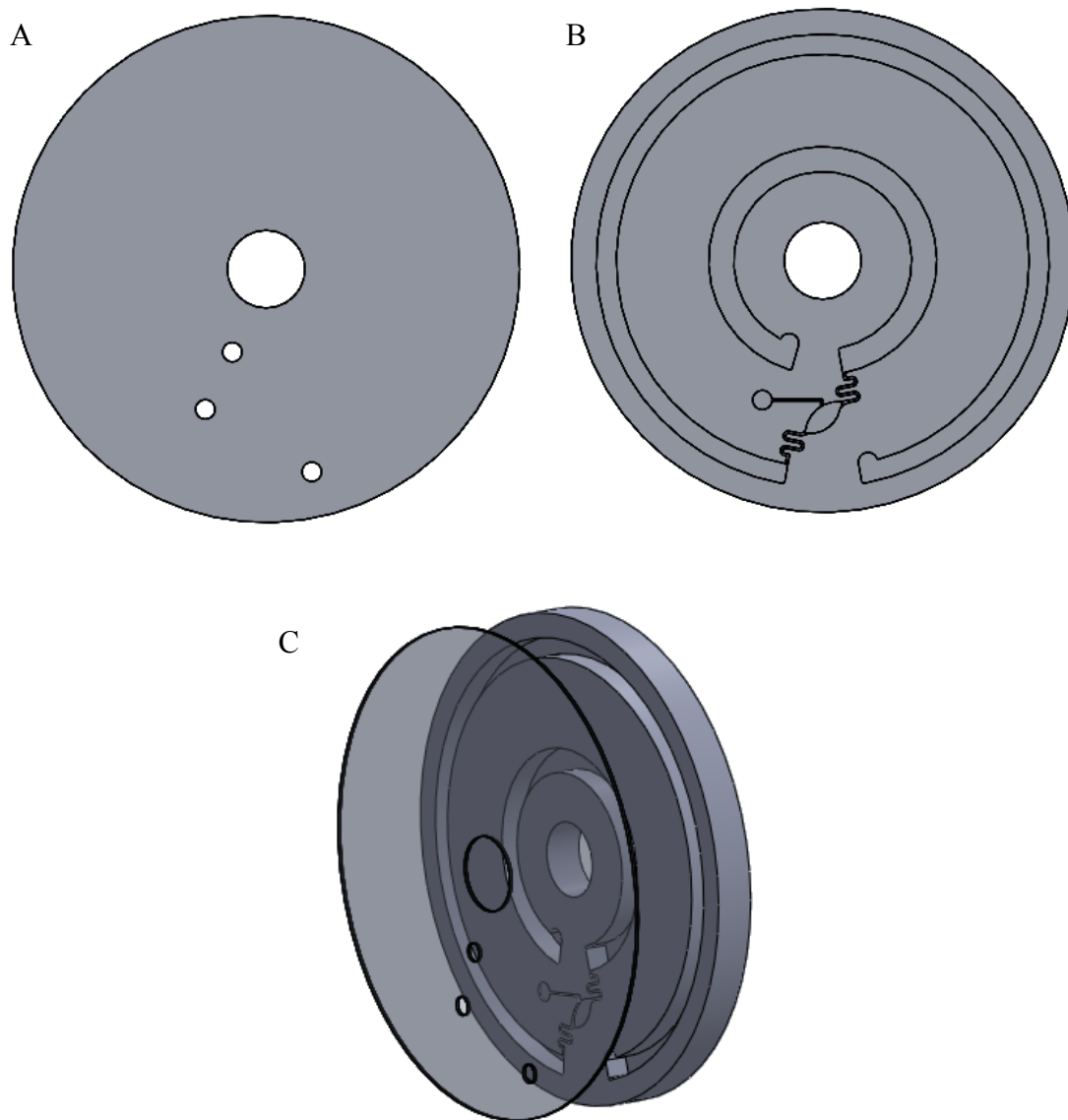


Figure 4.1: (A) CAD drawings of the top PMMA layer with inlet and venting holes. (B) PMMA layer with loading, cell culture, waste chambers. (C) Fully assembled system.

The holes in layer A were realized with CO₂ laser ablation, while the structures in layer B were realized with micro-milling. After the fabrication, the two layers were joined by thermal bonding. The parameters used for milling machine, CO₂ laser and thermal bonding are reported in chapter 2: “Materials and methods”.

4.2 Fluidic tests

As described in the previous section, the disc fabricated with CO₂ laser ablation was tested at different rotational frequencies: 1.375 Hz, 1.25 Hz, 1.125 Hz, 1 Hz, 0.9375 Hz, and 0.875 Hz, spinning it counterclockwise and using only “ultrapure” water.

The results obtained showed that the flow rates were more stable, however still with high variation. The reason for the flow rate instability and variation could be to the effect of the PSA, which can protrude in the channels and partially occlude them. Since in this case we used micro-milling, to achieve smoother and more precise structure and avoid the use of PSA, we expected lower variation in flow rate during the experiments. In addition, the inlet and venting holes were closed with filters in order to verify if they caused changes in fluid flow (Figure 4.2). The usage of filters is needed when performing the bacterial cultures.



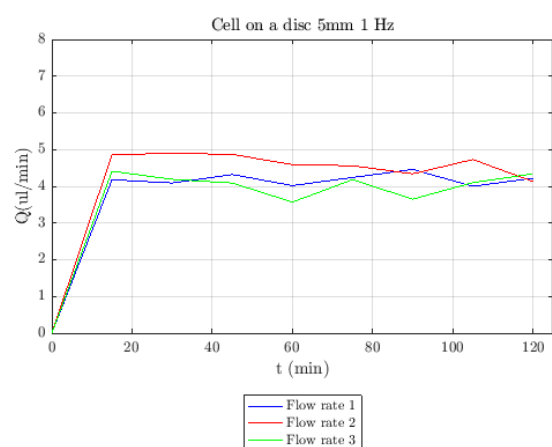
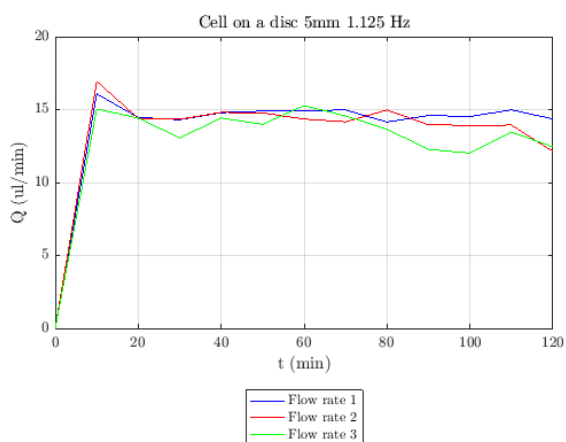
Figure 4.2 Photograph of the disc with filters in the inlet and venting holes.

The filters are important for a cell cultures. They have a diameter of 3mm and a hydrophobic membrane with 0,20 μm pore size that prevented that bacterial culture are contaminated with other undesired cells. [80] (Figure 4.3).



Figure 4.3: Sterile filters.

The disc was tested at different frequencies: 1.125 Hz, 1 Hz, 0.9375 Hz, 0.875 Hz, 0.75 Hz, 0.625 Hz, 0.5 Hz, 0.375 Hz, spinning it counterclockwise and using “ultrapure” water. For each frequency, except for 0.5 Hz and 0.375 Hz, a two hours test was repeated three times in order to evaluate the repeatability of the results. In these tests, higher flow rates than those obtained previously at the same rotational frequencies were expected, based on equations reported in section 4.3, since the loading chamber was deeper. The results obtained (Figure 4.4) show that for each frequency the flow rate was stable and repeatable.



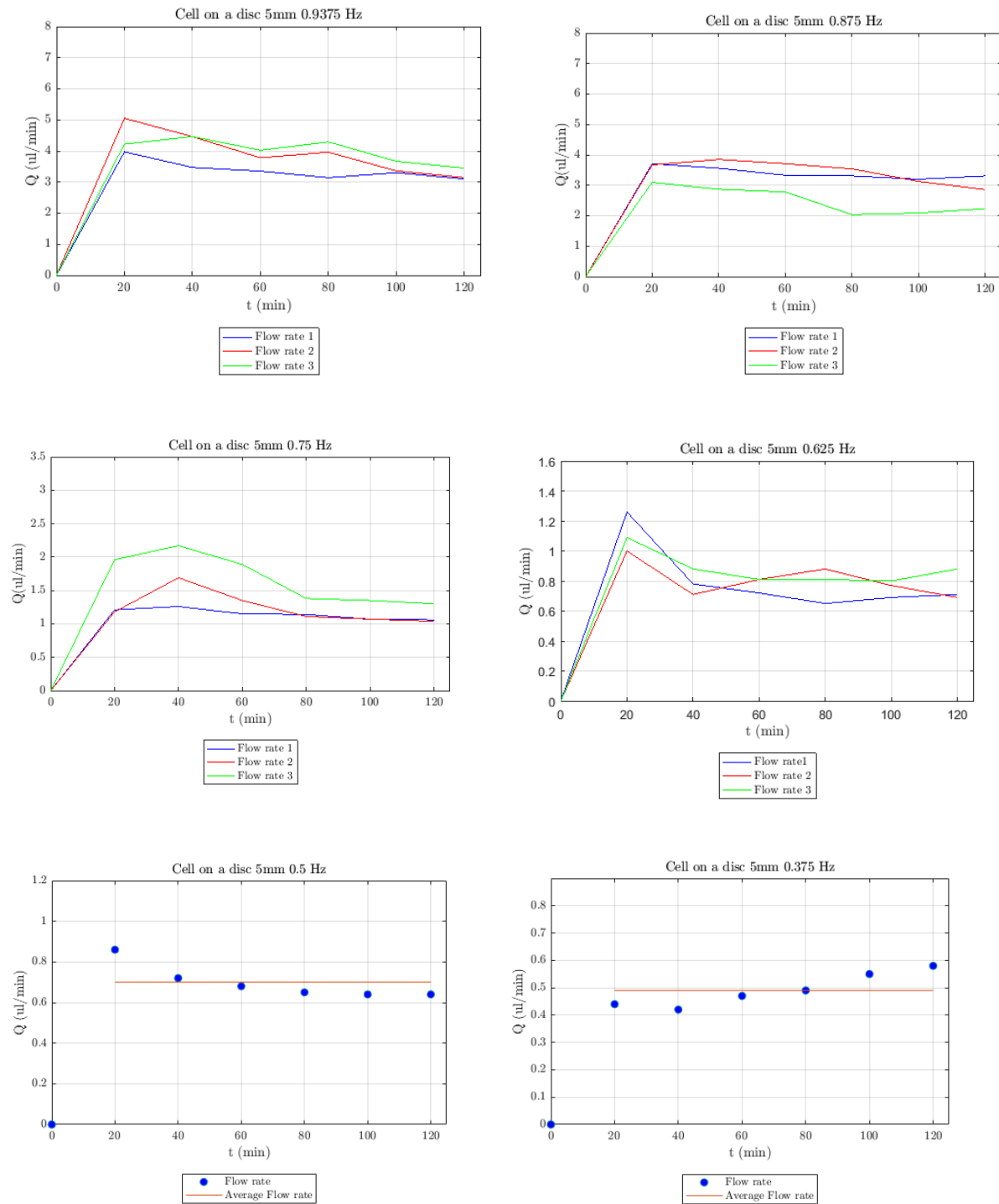


Figure 4.4: Graphs shows the flow rate over time obtained at different rotational frequencies.

Considering the frequencies from 1.125 Hz to 0.625 Hz, the dependency between flow rate and rotational frequency (Table 2) was plotted as presented in Figure 4.5.

Table 2 Average flow rate, STD and number of samples used to calculate STD for each frequency.

Frequency (Hz)	Flow rate ($\mu\text{l}/\text{min}$)	STD	Number of samples
1.125	14.29	0.53	12
1	4.29	0.29	8
0.9375	3.79	0.35	6
0.875	3.13	0.53	6
0.75	1.35	0.28	6
0.625	0.83	0.04	6

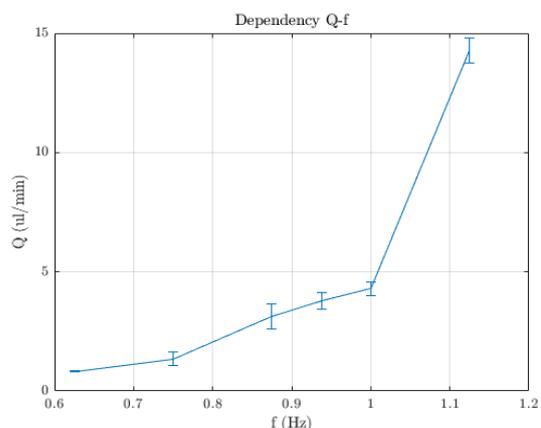


Figure 4.5 Dependency between the flow rate and rotational frequency.

We found that at 0.375 Hz the flow rate was 0.5 $\mu\text{l}/\text{min}$ that is suitable for grow bacterial biofilms in perfusion; therefore we tested the flow rate at this frequency using M9 medium in order to evaluate if the bacterial culture medium effects on flow rate.

M9 is a common medium for bacterial cultures, containing vitamins, salts, glucose, antibiotics and “ultrapure” water. Other components can be added to it to obtain a higher growth rates or to cultivate specific bacterial strains (Table 3) [81].

Table 3:Components of M9 medium.

M9 medium	For 50 mL
10x M9 salts	5 ml
CaCl ₂	5 μl
2000x trace elements	25 μl
100x vitamin solution	0.5 ml
MgSO ₄	100 μl
Glucose	2.5 ml
ITPG	50 μl
Chloramphenicol	68 μl
Spectinomycin	50 μl
MilliQ water	50 ml

The Flow rates test was performed three times with the inlet and venting holes closed with filters. In the first two experiments, the disc was left to spin for two hours and the average flow rates obtained were: 0.73 $\mu\text{l}/\text{min}$ for the first test and 0.67 $\mu\text{l}/\text{min}$ for the second one (Figure 4.6) These values were slightly higher than those obtained with only “ultrapure” water.

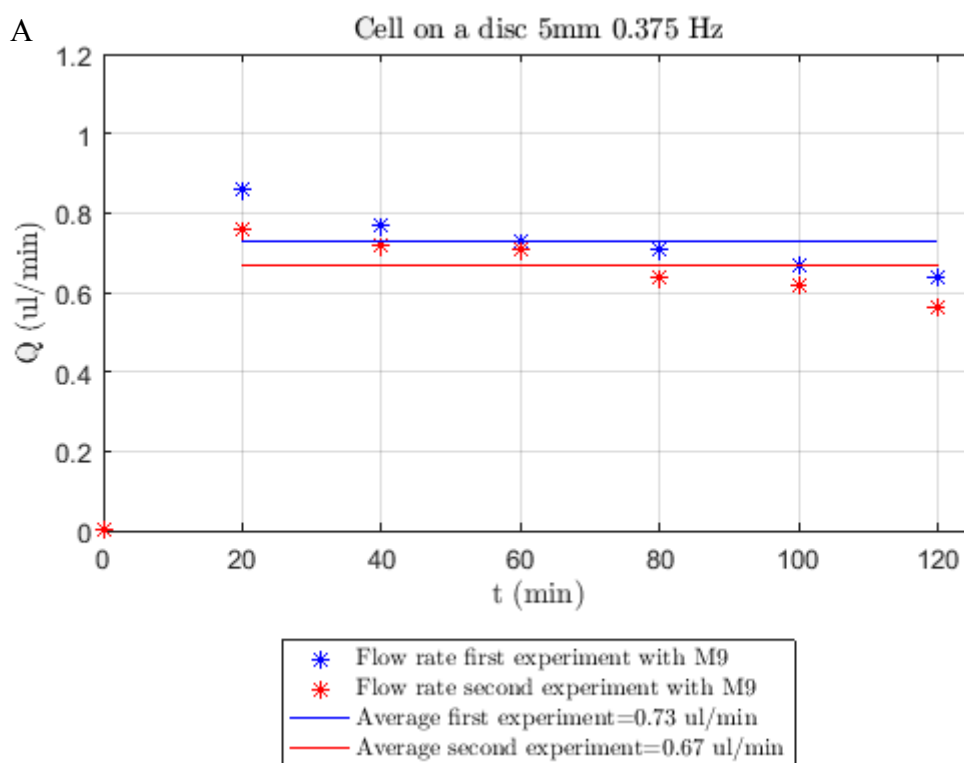


Figure 4.6(A) Flow rate and average value for the first two experiments.

The third flow test was performed for two days and the results obtained (Figure 4.6 (B)) showed that for 40 minutes the flow rate was 0.76 $\mu\text{l}/\text{min}$ and decreased to a stable value of 0.35/0.40 $\mu\text{l}/\text{min}$ over time.

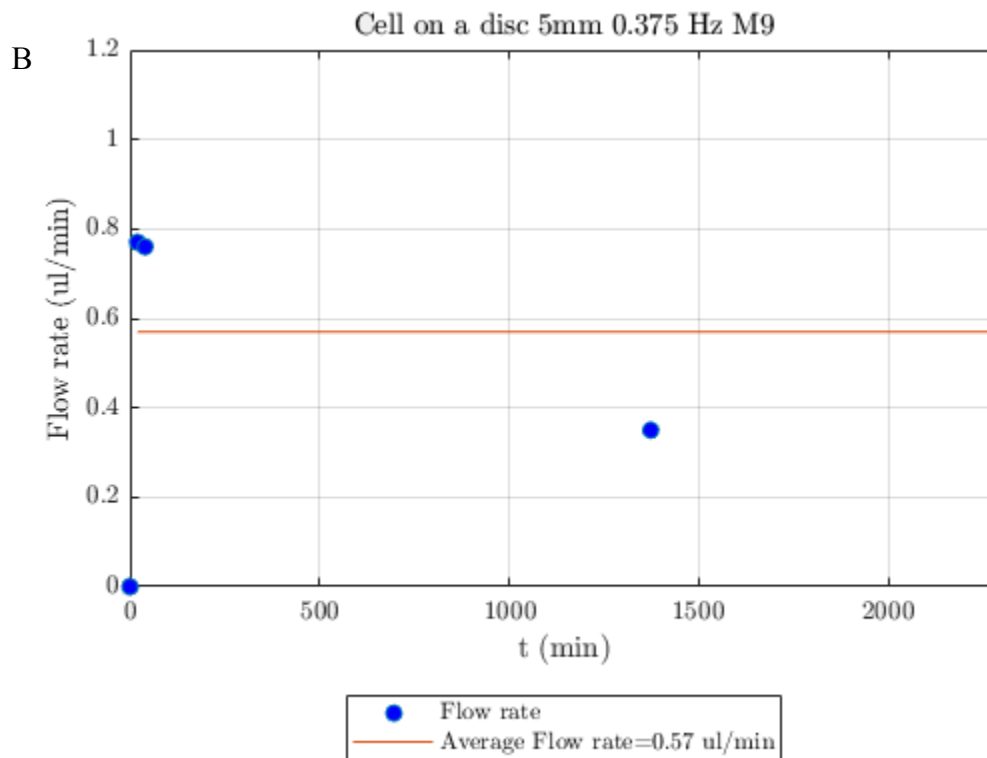


Figure 4.6 (B):Flow rate during the test and its average value in red.

Therefore, another test, always using M9 medium, a rotational frequency of 0.375 Hz and covering the holes with filters was done to verify when the flow rate stabilized at values between 0.35/0.40 $\mu\text{l}/\text{min}$. The graph in Figure 4.7 shows that after four hours the flow rate ranged from 0.36 $\mu\text{l}/\text{min}$ to 0.49 $\mu\text{l}/\text{min}$, reproducing, in this way, the values obtained with “ultrapure” water.

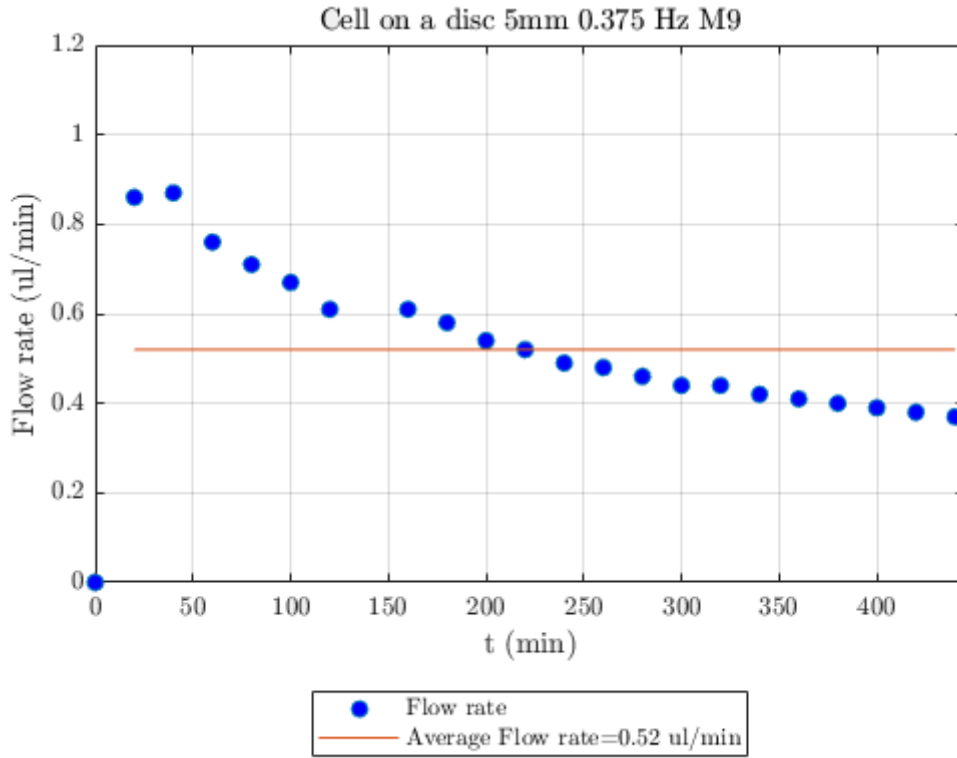


Figure 4.7:Flow rate and its average value in red.

4.3 Theoretical calculations of the flow rates and estimation of shear stress inside the cell culture chamber

The following equations are used to estimate the values of flow rate in the designed centrifugal microfluidic platform. The equations described in this section are valid for laminar flow. A fluid flow is considered laminar when the Reynolds number (Re) is less than 2300. The Reynolds number is given by equation (4), where ρ is the density of the fluid, μ the fluid viscosity, u the velocity of fluid and D_h the hydraulic diameter of the channel [32][82].

$$Re = \frac{\rho u D_h}{\mu} \tag{4}$$

The volumetric flow rate in a microchannel is given by equation (5), where Δp is the pressure drop across the channel and R_{hyd} is the hydraulic resistance of the microchannel [32][82].

$$Q = \frac{\Delta p}{R_{hyd}} \tag{5}$$

The resistance in a rectangular channel can be derived from the Navier-Stokes equations and is given by equation (6) , where L is the length of channel, w is its width and h is its height [32][82].

$$R_{hyd} = \frac{12\mu L}{wh^3} / \left[1 - \frac{h}{w} \left(\frac{192}{\pi^5} \sum_{n=1,3,5}^{\infty} \frac{1}{n^5} \tanh \frac{n\pi w}{2h} \right) \right] \quad (6)$$

If $w = h$ or $w = 2h$ this expression for the resistance can be approximated (equation 7) with an error of 13% or 0.2% respectively [82].

$$R_{hyd} \approx \frac{12\mu L}{wh^3} \left[1 - 0.630 \frac{h}{w} \right]^{-1} \quad (7)$$

In this case, equation (5), which becomes equation (8) replacing the expressions for differential pressure and hydraulic resistance, was used to calculate theoretical flow rates at different rotational frequencies, assuming that the serpentine rectangular micro-channels dominates the hydraulic resistance and that the pressure difference is caused only by the centrifugal force (equation (2)).

$$Q = \frac{wh^3\rho\omega^2(r_2^2-r_1^2)}{24\mu L} \left[1 - 0.630 \frac{h}{w} \right] \quad (8)$$

The parameters and their values used for the calculations are reported in Table 4.

Table 4: Values of parameters used to calculate flow rate with equation.

Parameter	Symbol	Value	Unit
Width of channel	w	0.5	mm
Depth of channel	h	0.3	mm
Length of channel	L	45,4	mm
Inner Radius	r_1	20.18	mm
Outer Radius	r_2	41	mm
Viscosity	μ	0.001	$Pa \cdot s$
Density	ρ	1000	kg/m^3

The theoretical flow rates obtained for each different angular velocity of the disc are reported in Figure 4.8 (A) and Table 5, while in Figure 4.8 (B) theoretical and experimental results are compared.

Table 5 Theoretical values of flow rate for each rotational frequency.

Rotational frequency (Hz)	Theoretical Flow rate ($\mu\text{l}/\text{min}$)
1.125	29.43
1	23.25
0.9375	20.44
0.875	17.80
0.75	13.079
0.625	9.08
0.50	5.81
0.375	3.27

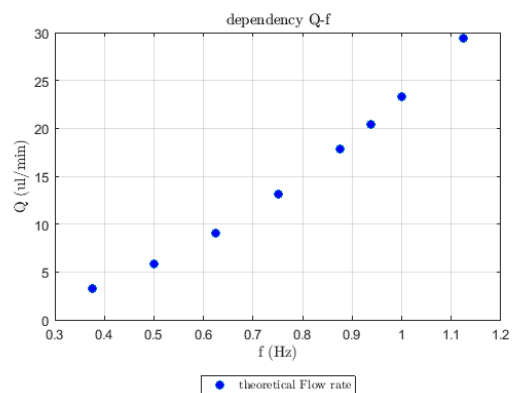


Figure 4.8 (A): Theoretical flow rate

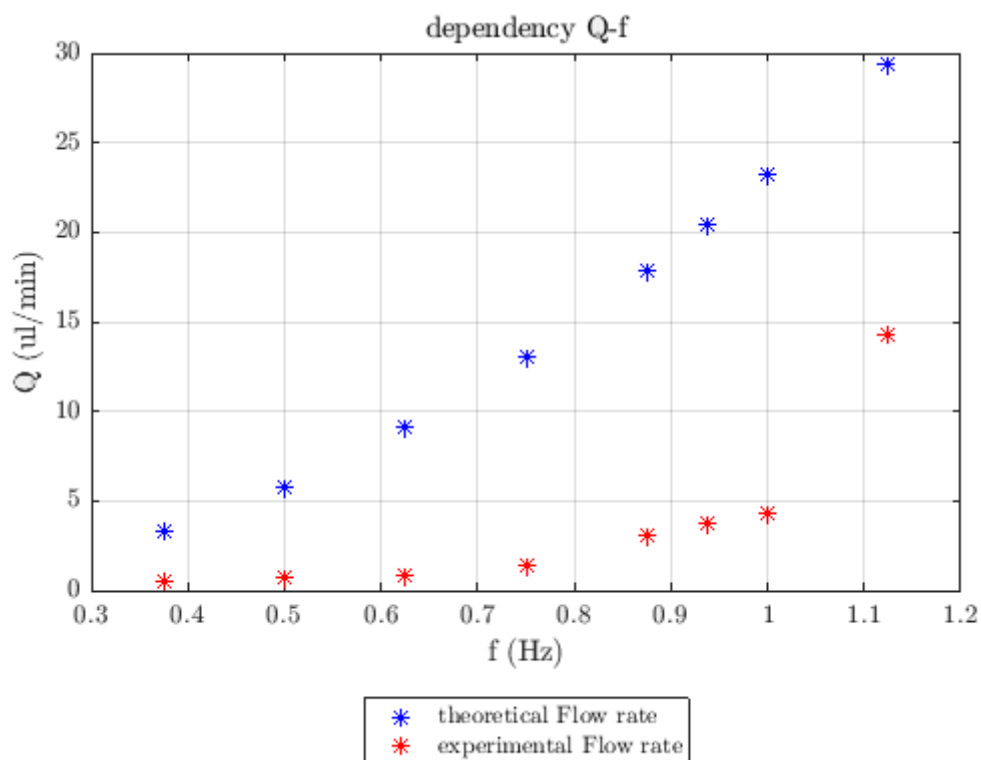


Figure 4.8 (B) Theoretical and experimental flow rate for each rotational frequency.

The values obtained with the equation (8) are only an estimation of flow rates at different frequencies, indeed the only force that was considered was the centrifugal force. In reality, the capillary force,

which was present in the two micro-channels that connected the cell culture chamber to the two reservoirs, opposed to centrifugal force and it could affect the flow rate. This explains why the theoretical values were higher than those obtained experimentally.

As mentioned before, the purpose of this project was not only to have a stable flow rate but also to achieve a value of flow rate that permitted to transport nutrients to bacterial cells without causing high shear stress inside the cell culture chamber. High levels of shear stress could damage the cells, causing their detachment from the surface or their death. Below an estimation of shear stress inside the cell culture chamber is reported, using the expression (9) and the values of parameters reported in Table 6 [83][9]:

$$\tau = \frac{6\mu Q}{wh^2} \quad (9)$$

Table 6: Values of parameters used to estimate the shear stress inside the cell culture chamber

Parameter	Symbol	Value	Unit
Viscosity	μ	0.001	$Pa \cdot s$
Flow rate	Q	$5e - 10$	m^3/s
Width of cell culture chamber	w	0.0043	m
Height of cell culture chamber	h	0.0005	m

The value obtained for the shear stress was $0.0000465 Pa$ which is far lower than that obtained in the study[9], $0.017 Pa$, where *Pseudomonas Aeruginosa* bacterial cells were grown in a microfluidic channel and it was seen that the value of shear stress obtained was not harmful to cells and permitted the formation of biofilm.

4.4 Lab-on-a-disc for long term cell culture, additional optimization

Once we evaluated the flow rates, the inoculation hole was moved further away from cell culture chamber in order to enable microscopic monitoring of the bacterial culture (figure 4.9 (A), Figure 4.9 (B)).

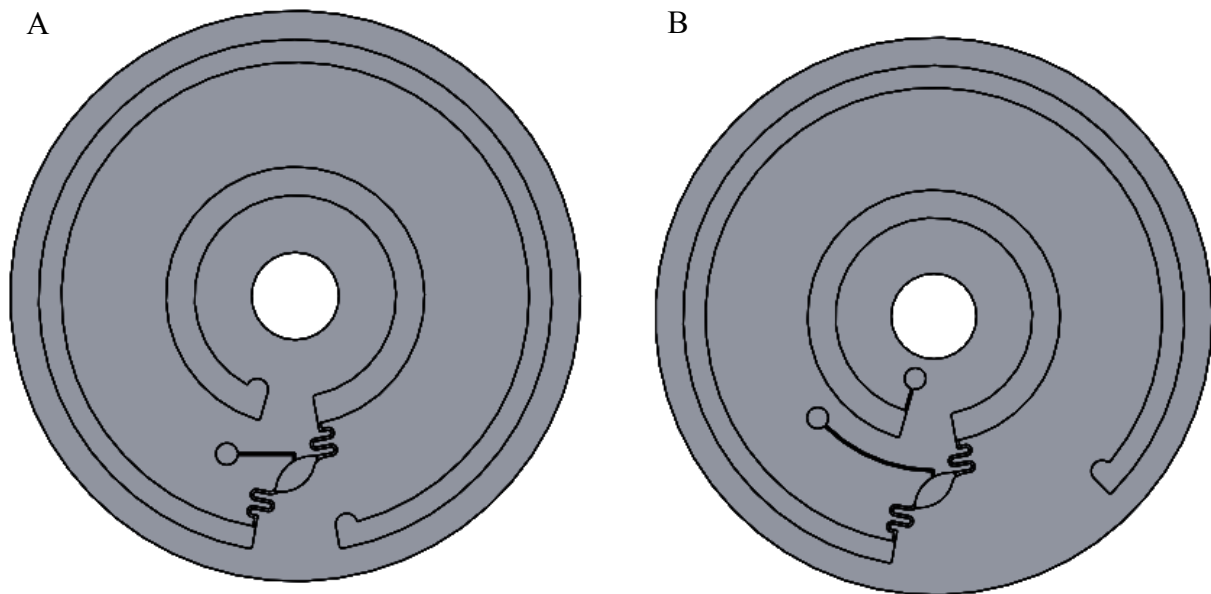


Figure 4.9: (A) CAD drawings of the third prototype. (B) The new positions of inlet and venting holes.

Furthermore, the disc's material was changed. The PMMA is a good material for cell cultures thanks to its biocompatibility but it requires expensive and time consuming methods to be sterilized because of it is sensitive to ethanol and it cannot be sterilized with high temperatures due to its low glass transition temperatures (110°C). For these reasons, the material used to fabricate the disc was polycarbonate (PC). PC is very similar to PMMA but it has a higher glass transition temperature (145°C) and it can be sterilized using both heat steam and ethanol.

The disc was composed by two layers (Figure 4.10 (A), Figure 4.10 (B) and Figure 4.10 (C)):

- A. a 0.6 mm thick PC layer with inlet and venting holes,
- B. a 8 mm thick PC layer with loading, cell culture, waste chambers and micro-channels.

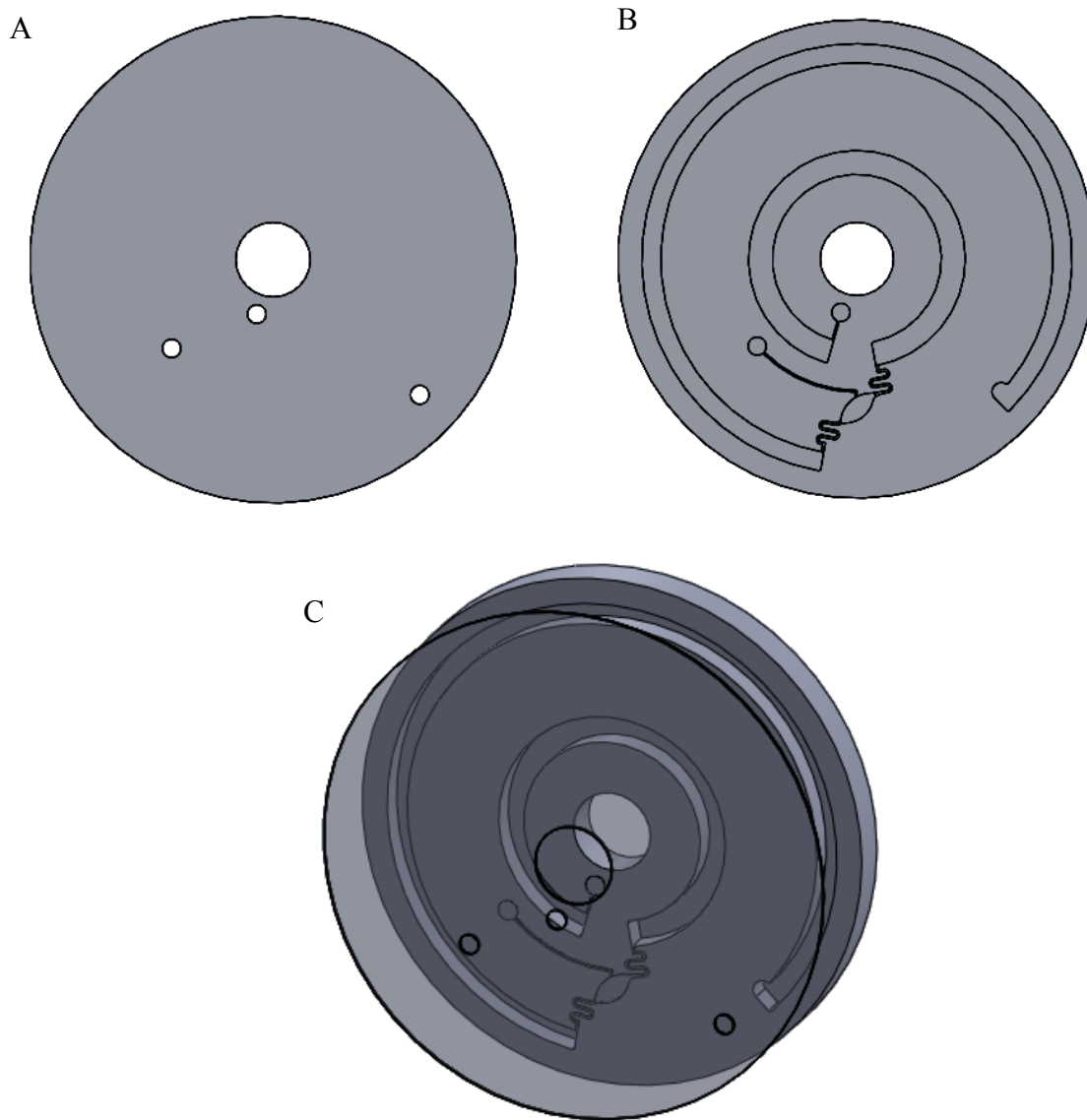


Figure 4.10: (A) CAD drawings of the system with top PC layer with loading and venting holes. (B) PC layer with loading, cell culture and waste chambers. (C) Fully assembled device.

The holes present in layer A were fabricated with a drill and not with CO₂ laser because when the PC meets CO₂ laser's beam, the PC changes its color, losing its transparency (Figure 4.11), while the structures present in layer B were made with micro-milling. Finally, the two layers were joined by thermal bonding. The parameters used for milling machine and thermal bonding are reported in the second chapter "Materials and methods".

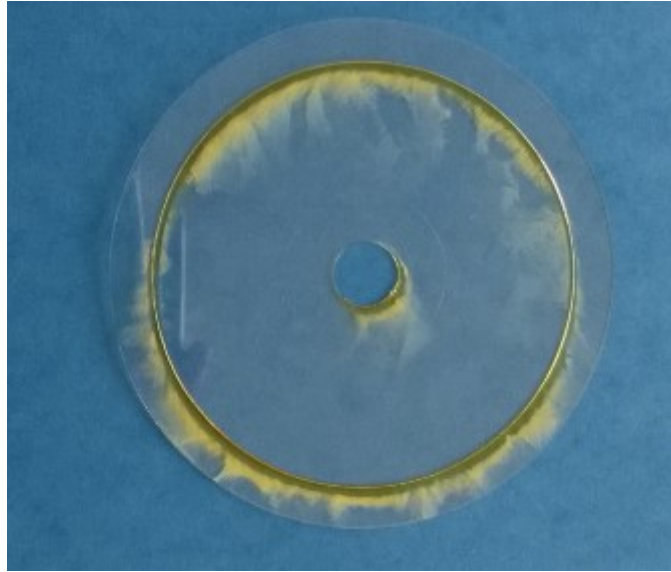


Figure 4.11: Photograph of PC layer cut using CO₂ laser.

4.6 Lab-on-a-disc for long term cell culture: implantation of *Pseudomonas aeruginosa* bacterial cells.

4.6.1 *Pseudomonas aeruginosa* bacterial cells

Pseudomonas aeruginosa are gram-negative, rod shaped bacteria [84].

These bacteria can grow both in terrestrial and aquatic environments and they can cause infections in plants, animals and humans [84][85].

Furthermore, *Pseudomonas aeruginosa* bacteria have the ability to form biofilms with high resistance to antibiotics both on living and non-living surfaces and, for this reasons, they are responsible for the most nosocomial infections and they are considered the first cause of death in patients with Cystic fibrosis [84][85][86].

Unfortunately, the current therapies, based on use of antibiotics, result inefficient in most cases, so new drugs or treatments that for example have effect on communication system (QS) of bacteria cells have to be developed.

4.6.2 *Pseudomonas aeruginosa* culture in the developed lab-on-a-disc device

After finding the right design and the appropriate rotational frequency for bacterial culture, firstly the system was sterilized in autoclave using a heat steam as reported in section 2.4.2 and then it was placed in the incubation room (30°C) at DTU Biosustain where *Pseudomonas aeruginosa* cells was inoculated with insulin syringe inside the disc's cell chamber. The disc was left to spin at a rotational frequency of 0.375 Hz for two days inside an incubator room. The photographs in Figure 4.12 (A and B) were taken with confocal microscope, in the first and second day of the cell culture.

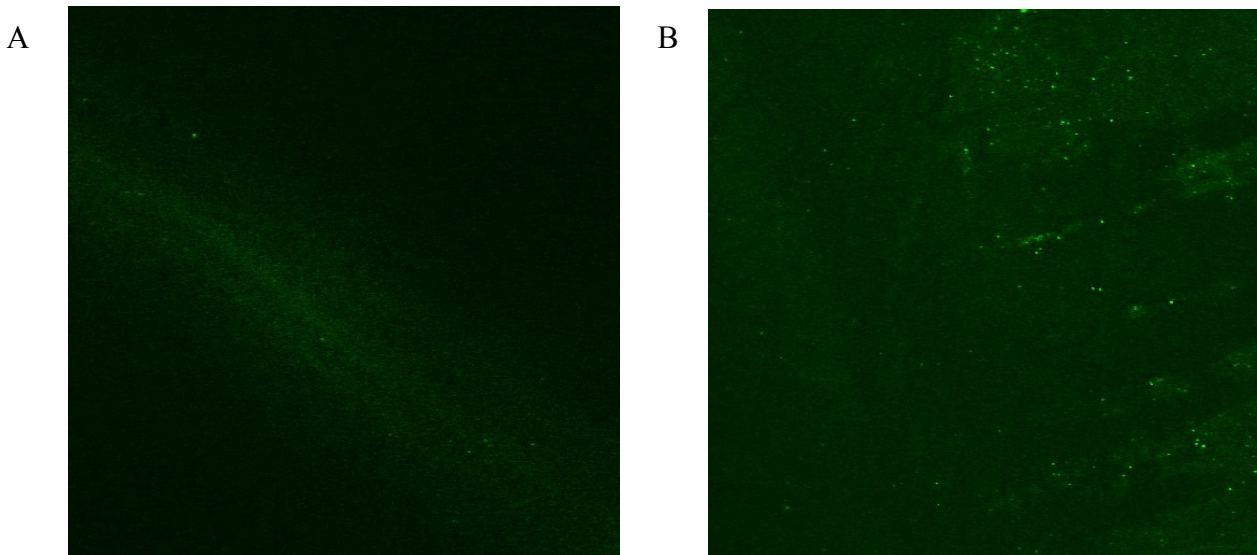


Figure 4.12: (A) Confocal microscopy images of bacterial cells at day 1 (B) and day 2.

As it can be observed from the images only few cells reached the chamber, this was due to the geometry of micro-channel through which the solution was inoculate, so it was decided to change it by enlarging it, in order to enter inside it with the syringe, and doing it closer to cell chamber (Figure 4.13 (A and B) and Figure 4.14

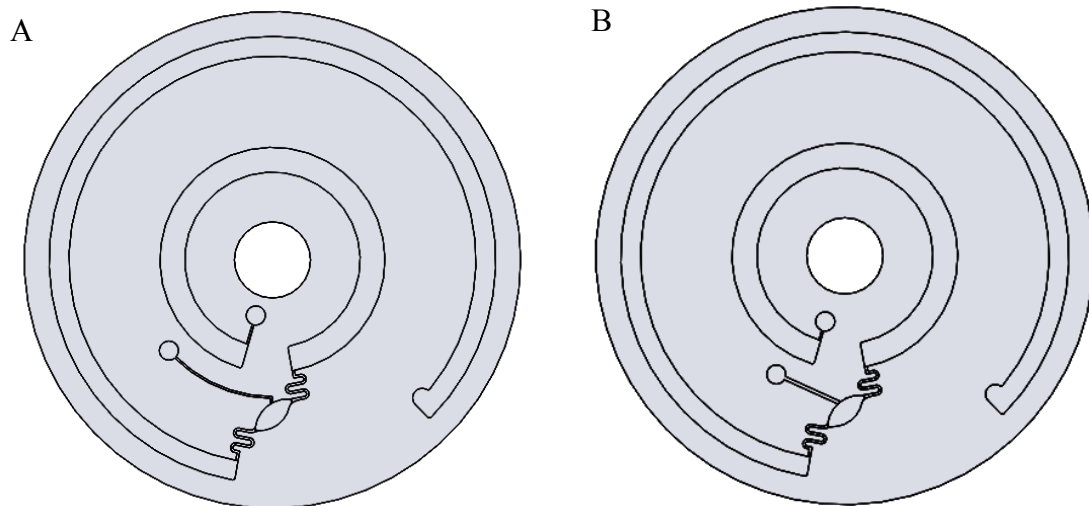


Figure 4.13: (A) CAD drawings of the design used to cultivate *Pseudomonas aeruginosa*. The microchannel had a width of 0.4 mm. (B) CAD drawings of the design with modified micro-channel to inoculate bacterial cells. The micro-channels had a width of 0.7 mm and it was closer to cell chamber.



Figure 4.14: Final design with new micro-channel to inoculate bacterial cells.

Conclusion

This thesis has presented the possibility of creating a centrifugal microfluidic platform for the formation and treatment of bacterial biofilms and the results obtained show that the fabricated design could be suitable for this purpose.

Indeed, the new platform was tested at different rotational frequencies and for each frequency, it was observed that the flow rate was stable and its value was calculated.

At 0.375 Hz a flow rate of few hundreds nl/min was obtained and in according to study[9] this value permits to transport nutrients to cells causing low shear stress that does not damage them.

Furthermore, it was important to use low rotational frequency to have low values of forces that arose from rotation in order to permit the cell attachment and biofilm formation. However, the forces and shear stress are still under calculation in collaboration with DTU compute department.

The next steps for this platform would be the formation of bacterial biofilms inside the cell chamber, the test of antibiotics, the monitoring of the antibiotics' effect and the integration of sensors to be able to perform real-time measurements in order to see how bacterial cells respond to drugs.

Appendix

This section will present the forces that permit the fluid flow and to implement unit operations inside lab on discs.

In general, the forces can be divided in two types [87]:

- extrinsic forces
- intrinsic forces

The extrinsic forces are due to the use of external means, so they were not used in this thesis because an external equipment has not been used.

The intrinsic forces, instead, can be divided in pseudo forces and non-pseudo forces. The pseudo forces arise from the centripetal rotation of the rotor and they include the centrifugal force (F_C), the Coriolis force (F_{CO}) and the Euler force (F_E) (Figure A.1).

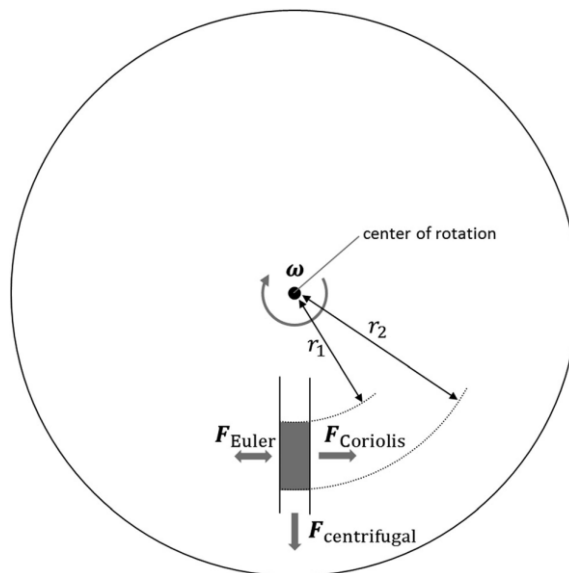


Figure A.1: forces that arise from the disc rotation [87].

The centrifugal force permits the fluid flow from the center of the disc radially outward [87][88]. The expression for this force is:

$$F_C = -\rho\omega \times (\omega \times r) \quad (10)$$

Where ρ is the fluid density, $\boldsymbol{\omega}$ is the angular velocity of the disc and \boldsymbol{r} is the radial position.

The Coriolis force is a tangential force and it is always opposite to the direction of the disc's rotation.

It is used for mixing of samples and for flow switching [38]. The equation for this force is:

$$\boldsymbol{F}_{CO} = -2\rho\boldsymbol{\omega} \times \boldsymbol{v} \quad (11)$$

Where ρ is the fluid density $\boldsymbol{\omega}$ is the angular velocity and \boldsymbol{v} is the velocity of the fluid.

The Euler is another tangential force, as Coriolis force, and its expression is:

$$\boldsymbol{F}_E = -\rho \frac{d\boldsymbol{\omega}}{dt} \times \boldsymbol{r} \quad (12)$$

Where \boldsymbol{r} is the radial position and $\boldsymbol{\omega}$ is the angular velocity.

The non-pseudo forces are present in rotating and non-rotating system [87] and, for example, they include: viscous force, pneumatic force and the capillary force. The capillary force is opposite to the centrifugal force and it is exploited to create passive valves inside a lab-on-a-disc [88].

Acknowledgements

I would like to thank my professor Danilo Demarchi who gave me the possibility to do my project at Technical University of Denmark, my supervisors: Kinga Zòr for her guidance and Laura Serioli who guided me during my project and taught me ‘every secret’ of the job. I would like also to thank Trygvi, Ermes and Max that helped me during that period and all the people that I met at DTU.

Now I would to thank my family and my friends so I am going to write in Italian.

Grazie ai miei genitori che hanno creduto e sempre continueranno a credere in me... grazie perchè mi avete dato tutto e anche ciò che non vi potevate permettere e grazie anche per tutti i traguardi fino ad ora raggiunti perché in fondo sono MERITO VOSTRO.

Grazie ai miei fratelli che sono sempre stati presenti malgrado la lontananza e grazie anche a Daniela e ad Esin.

Grazie a zia Bendetta, a Mario e a Lucy per essermi stati sempre accanto.

Grazie a Francesco che ogni giorno mi spinge a dare il meglio di me e che mi dimostra il suo amore anche nelle piccole cose...grazie per tutti i bei momenti passati insieme fino adesso e per le mille trasferte che ti sei fatto in Danimarca. Grazie anche ai tuoi genitori, alle tue nonne che ogni volta mi fanno sentire a casa.

Grazie a tutti i miei amici e in particolar modo a Fjorda, a Manuela, a Michela, ad Alessandro, a Cecilia e ad Adriana...vi voglio bene.

Grazie ai miei fantastici coinquilini danesi, Margherita e Philip...vi porterò sempre nel cuore.

References

- [1] L. Hall-Stoodley, J. W. Costerton, and P. Stoodley, "Bacterial biofilms: From the natural environment to infectious diseases," *Nat. Rev. Microbiol.*, vol. 2, no. 2, pp. 95–108, 2004.
- [2] B. Biofilm, I. Composition, and R. Human, "Research & Reviews : Journal of Microbiology and Biotechnology," vol. 4, no. 3, pp. 1–14, 2015.
- [3] C. T. Schembri, V. Ostoich, P. J. Lingane, T. L. Burd, and S. N. Buhl, "Portable simultaneous multiple analyte whole-blood analyzer for point-of-care testing," *Clin. Chem.*, vol. 38, no. 9, pp. 1665–1670, 1992.
- [4] S. Haerberle, T. Brenner, R. Zengerle, and J. Ducee, "Centrifugal extraction of plasma from whole blood on a rotating disk," *Lab Chip*, vol. 6, no. 6, pp. 776–781, 2006.
- [5] K. P. Kim *et al.*, "In situ monitoring of antibiotic susceptibility of bacterial biofilms in a microfluidic device," *Lab Chip*, vol. 10, no. 23, p. 3296, 2010.
- [6] N. Høiby, T. Bjarnsholt, M. Givskov, S. Molin, and O. Ciofu, "Antibiotic resistance of bacterial biofilms," *Int. J. Antimicrob. Agents*, vol. 35, no. 4, pp. 322–332, 2010.
- [7] J. Paredes, S. Becerro, and S. Arana, "Comparison of real time impedance monitoring of bacterial biofilm cultures in different experimental setups mimicking real field environments," *Sensors Actuators, B Chem.*, vol. 195, pp. 667–676, 2014.
- [8] M. L. Y. Sin, J. Gao, J. C. Liao, and P. K. Wong, "System Integration - A Major Step toward Lab on a Chip," *J. Biol. Eng.*, vol. 5, no. 1, p. 6, 2011.
- [9] A. Park, H.-H. Jeong, J. Lee, K. P. Kim, and C.-S. Lee, "Effect of shear stress on the formation of bacterial biofilm in a microfluidic channel," *BioChip J.*, vol. 5, no. 3, pp. 236–241, 2011.
- [10] E. P. G. Costerton, J. W. Philip S. Stewart, "Bacterial Biofilms: A Common Cause of

- Persistent Infections,” *Science* (80-.), vol. 284, no. 5418, pp. 1318–1322, 1999.
- [11] E. Hernández-Jiménez *et al.*, “Biofilm vs. planktonic bacterial mode of growth: Which do human macrophages prefer?,” *Biochem. Biophys. Res. Commun.*, vol. 441, no. 4, pp. 947–952, 2013.
- [12] P. Substances, “from *Pseudomonas aeruginosa*,” vol. 336, no. 1973, pp. 302–314, 2001.
- [13] M. V. Zhurina, a. V. Gannesen, E. L. Zdrovenko, and V. K. Plakunov, “Composition and functions of the extracellular polymer matrix of bacterial biofilms,” *Microbiology*, vol. 83, no. 6, pp. 713–722, 2014.
- [14] H. C. Flemming, T. R. Neu, and D. J. Wozniak, “The EPS matrix: The ‘House of Biofilm Cells,’” *J. Bacteriol.*, vol. 189, no. 22, pp. 7945–7947, 2007.
- [15] W. Hu *et al.*, “DNA Builds and Strengthens the Extracellular Matrix in *Myxococcus xanthus* Biofilms by Interacting with Exopolysaccharides,” *PLoS One*, vol. 7, no. 12, pp. 1–12, 2012.
- [16] V. V Vlassov, P. P. Laktionov, and E. Y. Rykova, “Extracellular nucleic acids,” pp. 654–667, 2007.
- [17] A. D. Anno and R. Danovaro, “Extracellular DNA Plays a Key Role,” vol. 309, no. September, 2005.
- [18] S. E. Finkel and R. Kolter, “DNA as a Nutrient : Novel Role for Bacterial Competence Gene Homologs,” vol. 183, no. 21, pp. 6288–6293, 2001.
- [19] J. M. Pretorius, J. Theron, V. S. Bro, and B. Prote, “DNA as an Adhesin : *Bacillus cereus* Requires Extracellular DNA To Form Biofilms □ † Se,” vol. 75, no. 9, pp. 2861–2868, 2009.
- [20] H. Mulcahy, L. Charron-mazenod, and S. Lewenza, “Extracellular DNA Chelates Cations and Induces Antibiotic Resistance in *Pseudomonas aeruginosa* Biofilms,” vol. 4, no. 11, 2008.

- [21] C. Berne, D. T. Kysela, and Y. V Brun, "A bacterial extracellular DNA inhibits settling of motile progeny cells within a biofilm," vol. 77, no. July, pp. 815–829, 2010.
- [22] C. B. Whitchurch, T. Tolker-nielsen, P. C. Ragas, and J. S. Mattick, "Extracellular DNA Required for Bacterial Biofilm Formation."
- [23] S. Andersson, G. Dalhammar, C. J. Land, and G. K. Rajarao, "Characterization of extracellular polymeric substances from denitrifying organism *Comamonas denitrificans*," pp. 535–543, 2009.
- [24] M. R. Parsek, "BACTERIAL BIOFILMS : An Emerging Link to Disease Pathogenesis," pp. 677–701, 2003.
- [25] T. C. Mah and G. A. O. Toole, "Mechanisms of biofilm resistance to antimicrobial agents," vol. 9, no. 1, pp. 34–39, 2001.
- [26] P. S. Stewart and M. J. Franklin, "Physiological heterogeneity in biofilms," vol. 6, no. march, pp. 199–210, 2008.
- [27] Y. Yawata, J. Nguyen, R. Stocker, and R. Rusconi, "Microfluidic studies of biofilm formation in dynamic environments," *J. Bacteriol.*, vol. 198, no. 19, pp. 2589–2595, 2016.
- [28] E. W. K. Young and D. J. Beebe, "NIH Public Access," *Chem Soc Rev*, vol. 39, no. 3, pp. 1036–1048, 2010.
- [29] M. W. Hess, K. Pfaller, H. L. Ebner, B. Beer, D. Hekl, and T. Seppi, *3D versus 2D cell culture. Implications for electron microscopy*, vol. 96, no. C. Elsevier Inc., 2010.
- [30] "www.elveflow.com." .
- [31] Y. Ren, L. M. C. Chow, and W. W. F. Leung, "Cell culture using centrifugal microfluidic platform with demonstration on *Pichia pastoris*," *Biomed. Microdevices*, vol. 15, no. 2, pp. 321–337, 2013.

- [32] D. J. Beebe, G. A. Mensing, and G. M. Walker, "Physics and Applications of Microfluidics in Biology," *Annu. Rev. Biomed. Eng.*, vol. 4, no. 1, pp. 261–286, 2002.
- [33] S. Halldorsson, E. Lucumi, R. Gómez-Sjöberg, and R. M. T. Fleming, "Advantages and challenges of microfluidic cell culture in polydimethylsiloxane devices," *Biosens. Bioelectron.*, vol. 63, pp. 218–231, 2015.
- [34] J. Kim, M. Hegde, S. H. Kim, T. K. Wood, and A. Jayaraman, "A microfluidic device for high throughput bacterial biofilm studies," *Lab Chip*, vol. 12, no. 6, p. 1157, 2012.
- [35] N. J. Cira, J. Y. Ho, M. E. Dueck, and D. B. Weibel, "A self-loading microfluidic device for determining the minimum inhibitory concentration of antibiotics," *Lab Chip*, vol. 12, no. 6, pp. 1052–1059, 2012.
- [36] F. Deiss, M. E. Funes-Huacca, J. Bal, K. F. Tjhung, and R. Derda, "Antimicrobial susceptibility assays in paper-based portable culture devices," *Lab Chip*, vol. 14, no. 1, pp. 167–171, 2014.
- [37] R. Gorkin *et al.*, "Centrifugal microfluidics for biomedical applications," *Lab Chip*, vol. 10, no. 14, p. 1758, 2010.
- [38] S. Hugo, K. Land, M. Madou, and H. Kido, "Centrifugal microfluidic platform for point-of-care diagnostics A centrifugal," *S. Afr. J. Sci.*, vol. 110, no. 12, pp. 1–7, 2014.
- [39] D. C. Duffy, H. L. Gillis, J. Lin, N. F. Sheppard, and G. J. Kellogg, "Microfabricated centrifugal microfluidic systems: Characterization and multiple enzymatic assays," *Anal. Chem.*, vol. 71, no. 20, pp. 4669–4678, 1999.
- [40] J. Kim, S. Hee Jang, G. Jia, J. V. Zoval, N. A. Da Silva, and M. J. Madou, "Cell lysis on a microfluidic CD (compact disc)," *Lab Chip*, vol. 4, no. 5, p. 516, 2004.
- [41] J. Siegrist *et al.*, "Validation of a centrifugal microfluidic sample lysis and homogenization

- platform for nucleic acid extraction with clinical samples,” *Lab Chip*, vol. 10, no. 3, pp. 363–371, 2010.
- [42] T.-H. Kim, J. Park, C.-J. Kim, and Y.-K. Cho, “Fully Integrated Lab-on-a-Disc for Nucleic Acid Analysis of Food-Borne Pathogens,” *Anal. Chem.*, vol. 86, no. 8, pp. 3841–3848, 2014.
- [43] M. Focke *et al.*, “Microstructuring of polymer films for sensitive genotyping by real-time PCR on a centrifugal microfluidic platform,” *Lab Chip*, vol. 10, no. 19, p. 2519, 2010.
- [44] S. Lutz *et al.*, “Microfluidic lab-on-a-foil for nucleic acid analysis based on isothermal recombinase polymerase amplification (RPA),” *Lab Chip*, vol. 10, no. 7, p. 887, 2010.
- [45] S. Lai, S. Wang, J. Luo, L. J. Lee, S. T. Yang, and M. J. Madou, “Design of a Compact Disk-like Microfluidic Platform for Enzyme-Linked Immunosorbent Assay,” *Anal. Chem.*, vol. 76, no. 7, pp. 1832–1837, 2004.
- [46] B. S. Lee *et al.*, “A fully automated immunoassay from whole blood on a disc,” *Lab Chip*, vol. 9, no. 11, p. 1548, 2009.
- [47] J. Park, V. Sunkara, T. H. Kim, H. Hwang, and Y. K. Cho, “Lab-on-a-disc for fully integrated multiplex immunoassays,” *Anal. Chem.*, vol. 84, no. 5, pp. 2133–2140, 2012.
- [48] R. Burger *et al.*, “Centrifugal microfluidics for cell analysis,” *Curr. Opin. Chem. Biol.*, vol. 16, no. 3–4, pp. 409–414, 2012.
- [49] M. Madou, J. Zoval, G. Jia, H. Kido, J. Kim, and N. Kim, “Lab on a Cd,” *Annu. Rev. Biomed. Eng.*, vol. 8, no. 1, pp. 601–628, 2006.
- [50] K. Ren, J. Zhou, and H. Wu, “Materials for microfluidic chip fabrication,” *Acc. Chem. Res.*, vol. 46, no. 11, pp. 2396–2406, 2013.
- [51] J. C. McDonald and G. M. Whitesides, “Poly(dimethylsiloxane) as a material for fabricating microfluidic devices,” *Acc. Chem. Res.*, vol. 35, no. 7, pp. 491–499, 2002.

- [52] P. M. van Midwoud, A. Janse, M. T. Merema, G. M. M. Groothuis, and E. Verpoorte, “Comparison of Biocompatibility and Adsorption Properties of Different Plastics for Advanced Microfluidic Cell and Tissue Culture Models,” *Anal. Chem.*, vol. 84, no. 9, pp. 3938–3944, 2012.
- [53] Y. Chen, L. Zhang, and G. Chen, “Fabrication, modification, and application of poly(methyl methacrylate) microfluidic chips,” *Electrophoresis*, vol. 29, no. 9, pp. 1801–1814, 2008.
- [54] a. M. Jr. *et al.*, “Fabrication of poly(methylmethacrylate) microfluidic chips by atmospheric molding,” *Anal. Chem.*, vol. 76, no. 8, pp. 2290–2297, 2004.
- [55] “medical-applications-polycarbonate @ www.mddionline.com.” .
- [56] Topas, “TOPAS- Cyclic Olefin Copolymers,” p. 4, 2015.
- [57] J. P. Davim, C. Oliveira, N. Barricas, and M. Conceição, “Evaluation of cutting quality of PMMA using CO₂lasers,” *Int. J. Adv. Manuf. Technol.*, vol. 35, no. 9–10, pp. 875–879, 2008.
- [58] T. F. Hong, W. J. Ju, M. C. Wu, C. H. Tai, C. H. Tsai, and L. M. Fu, “Rapid prototyping of PMMA microfluidic chips utilizing a CO₂ laser,” *Microfluid. Nanofluidics*, vol. 9, no. 6, pp. 1125–1133, 2010.
- [59] D. J. Guckenberger, T. E. De Groot, A. M. D. Wan, D. J. Beebe, and E. W. K. Young, “HHS Public Access,” vol. 15, no. 11, pp. 2364–2378, 2015.
- [60] C. T. Æ. D. L. Devoe, “Bonding of thermoplastic polymer microfluidics,” pp. 1–16, 2009.
- [61] Y. C. Leong, L. M. S. Lee, and S. N. Gan, “The Viscoelastic Properties of Natural Rubber Pressure- Sensitive Adhesive Using Acrylic Resin as a Tackifier,” *J. Appl. Polym. Sci.*, vol. 88, pp. 2118–2123, 2003.
- [62] X. Zhu, G. Liu, Y. Guo, and Y. Tian, “Study of PMMA thermal bonding,” *Microsyst.*

Technol., vol. 13, no. 3–4, pp. 403–407, 2007.

- [63] Y. Liu, D. Ganser, A. Schneider, R. Liu, P. Grodzinski, and N. Kroutchinina, “Microfabricated polycarbonate CE devices for DNA analysis,” *Anal. Chem.*, vol. 73, no. 17, pp. 4196–4201, 2001.
- [64] D. Ogończyk, J. Węgrzyn, P. Jankowski, B. Dąbrowski, and P. Garstecki, “Bonding of microfluidic devices fabricated in polycarbonate,” *Lab Chip*, vol. 10, no. 10, p. 1324, 2010.
- [65] R. A. Malloy, *Plastic Part Design for Injection Molding*. 2010.
- [66] B. Ghanbarzadeh and H. Almasi, “World’s largest Science, Technology & Medicine Open Access book publisher,” *RFID Technol. Secur. Vulnerabilities, Countermeas.*, pp. 75–100, 2013.
- [67] R. Gorkin, L. Clime, M. Madou, and H. Kido, “Pneumatic pumping in centrifugal microfluidic platforms,” *Microfluid. Nanofluidics*, vol. 9, no. 2–3, pp. 541–549, 2010.
- [68] W. A. Rutala and D. J. Weber, “Infection control: the role of disinfection and sterilization,” *J. Hosp. Infect.*, vol. 43, no. 1999, pp. S43–S55, 1999.
- [69] M. Silindir and A. Y. Özer, “Sterilization methods and the comparison of E-beam sterilization with gamma radiation sterilization,” *Fabad J. Pharm. Sci.*, vol. 34, no. 1, pp. 43–53, 2009.
- [70] R. Galante, T. J. A. Pinto, R. Colaço, and A. P. Serro, “Sterilization of hydrogels for biomedical applications: A review,” *J. Biomed. Mater. Res. - Part B Appl. Biomater.*, pp. 1–21, 2017.
- [71] M. Ali Behzadfar, S. Mohammadi, M. T. Araghi, R. Shirdam, and H. R. Ghaffari, “Suggestion and feasibility of appropriate treatment methods for the removal of sulfate and organic matter from petrochemical wastewater effluent- A case study,” *Int. J. Pharm.*

Technol., vol. 8, no. 2, pp. 13182–13196, 2016.

- [72] N. G. S. Gopal, “Radiation sterilization of pharmaceuticals and polymers,” *Radiat. Phys. Chem.*, vol. 12, no. 1–2, pp. 35–50, 1978.
- [73] R. E. Baier, A. E. Meyer, C. K. Akers, J. R. Natiella, M. Meenaghan, and J. M. Carter, “Degradative effects of conventional steam sterilization on biomaterial surfaces,” *Biomaterials*, vol. 3, no. 4, pp. 241–245, 1982.
- [74] G. C. C. Mendes, T. R. S. Brandão, and C. L. M. Silva, “Ethylene oxide sterilization of medical devices: A review,” *Am. J. Infect. Control*, vol. 35, no. 9, pp. 574–581, 2007.
- [75] R. Buchalla, C. Schüttler, and K. W. Bögl, “Radiation sterilization of medical devices. Effects of ionizing radiation on ultra-high molecular-weight polyethylene,” *Radiat. Phys. Chem.*, vol. 46, no. 4–6 PART 1, pp. 579–585, 1995.
- [76] D. Kanjickal, S. Lopina, M. M. Evancho-Chapman, S. Schmidt, and D. Donovan, “Effects of sterilization on poly(ethylene glycol) hydrogels,” *J. Biomed. Mater. Res. - Part A*, vol. 87, no. 3, pp. 608–617, 2008.
- [77] “Milli-Q @ en.wikipedia.org.” [Online].<https://en.wikipedia.org/wiki/Milli-Q>.
- [78] D. D. Nolte, “Invited review article: Review of centrifugal microfluidic and bio-optical disks,” *Rev. Sci. Instrum.*, vol. 80, no. 10, 2009.
- [79] J. Ducreé, S. Haeberle, T. Brenner, T. Glatzel, and R. Zengerle, “Patterning of flow and mixing in rotating radial microchannels,” *Microfluid. Nanofluidics*, vol. 2, no. 2, pp. 97–105, 2006.
- [80] “www.sorbtech.com.” .
- [81] “M9_medium @ openwetware.org.” .

- [82] H. Bruus, "Theoretical microfluidics," *Physics (College. Park. Md).*, vol. 18, p. 363, 2008.
- [83] L. Kim, Y.-C. Toh, J. Voldman, and H. Yu, "A practical guide to microfluidic perfusion culture of adherent mammalian cells," *Lab Chip*, vol. 7, no. 6, p. 681, 2007.
- [84] G. Sharma, S. Rao, A. Bansal, S. Dang, S. Gupta, and R. Gabrani, "Pseudomonas aeruginosa biofilm: Potential therapeutic targets," *Biologicals*, vol. 42, no. 1, pp. 1–7, 2014.
- [85] A. Sousa and M. Pereira, "Pseudomonas aeruginosa Diversification during Infection Development in Cystic Fibrosis Lungs—A Review," *Pathogens*, vol. 3, no. 3, pp. 680–703, 2014.
- [86] V. M. I. and K. L. Lawrence R. Mulcahy, "Pseudomonas aeruginosa biofilms in disease," vol. 68, no. 1, pp. 1–12, 2015.
- [87] O. Strohmeier *et al.*, "Centrifugal microfluidic platforms: advanced unit operations and applications," *Chem. Soc. Rev.*, vol. 44, no. 17, pp. 6187–6229, 2015.
- [88] J. Ducreé, S. Haeberle, S. Lutz, S. Pausch, F. Von Stetten, and R. Zengerle, "The centrifugal microfluidic Bio-Disk platform," *J. Micromechanics Microengineering*, vol. 17, no. 7, 2007.